

A Hitchhiker's Guide to the Microtubule

Mechanism and function of +TIP accumualtion

Katharina Drägestein

ISBN: 978-90-8559-364-5

© K. Drägestein (2008)

The research presented in this thesis was performed at the Department of Cell Biology of the Erasmus MC Rotterdam, The Netherlands. Funding was provided by the Nederlandse Organisatie voor Wetenschappelijk Onderzoek (NWO).

Cover: K. Drägestein, “Terschelling in maart”

Thesis lay-out: K. Drägestein

Printing: Optima, www.ogc.nl

A Hitchhiker's Guide to the Microtubule

Mechanism and function of +TIP-accumulation

Een liftershandboek voor de microtubulus

Mechanisme en functie van +TIP-accumulatie

Proefschrift

ter verkrijging van de graad van doctor aan de
Erasmus Universiteit Rotterdam
op gezag van de
rector magnificus

Prof.dr. S.W.J. Lamberts

en volgens besluit van het College voor Promoties

De openbare verdediging zal plaatsvinden op

woensdag 12 maart 2007 om 9:45 uur

door

Katharina Asja Drägestein

geboren te Berlijn, Duitsland



Promotiecommissie

Promotor: Prof.dr. F. G. Grosveld

Overige leden: Prof.dr. M. Dogterom
Dr. A. B. Houtsmuller
Dr. W. Vermeulen

Copromotor: Dr. ir. N. J. Galjart

Bo ja nie ucze największej sztuki życia

Uśmiechać się zawsze i wszędzie

voor Ferd
für meine Eltern

List of abbreviations

CAP-Gly: Cytoskeleton-associated protein, glycine-rich

CLIP: cytoplasmic linker protein

CLASP: cytoplasmic linker protein associated protein

cpm: count per molecule

EB1: end-binding protein 1

FCA: fluorescence cumulant analysis

FCCS: fluorescence cross-correlation spectroscopy

FCS: fluorescence correlation spectroscopy

FRAP: fluorescence recovery after photobleaching

FRET: fluorescence resonance energy transfer

MAPRE: microtubule associated protein, RP/EB family

MEF: mouse embryonic fibroblast

MT: microtubule

MTB: microtubule binding domain

PCH: photon counting histogram

PI-3: phosphatidylinositol-3

PIP3: phosphatidylinositol-3,4,5-triphosphate

s: second

SD: standard deviation

SEM: standard error of the mean

SNR: signal-to-noise ratio

+TIPs: Plus-end-tracking proteins

TOG: tumor over-expressed gene

Content

	Scope of the Thesis	9
Chapter 1	Structure and Function of the Cytoskeleton	11
Chapter 2	Visualization of Proteins and their Dynamics in vivo	35
Chapter 3	Role of CLASP2 in Microtubule Stabilization and the Regulation of Persistent Motility	57
Chapter 4	Dynamic Behavior of GFP-CLIP-170 Reveals Fast Protein Turnover on Microtubule Plus-Ends	79
Chapter 5	General Discussion	107
Chapter 6	Summary/Samenvatting	115
Chapter 7	References	121
	Curriculum vitae	149
	Publications	151
	Dankwoord	153

Scope of the Thesis

The cytoskeleton forms the “backbone” of all eukaryotic cells and consists of microtubules, actin filaments and intermediate filaments. Microtubules have several functions within the context of the cell: among others they form the mitotic spindle, act as rails for long-range motor-driven transport, and help positioning the nucleus. Structurally, microtubules are long hollow polar tubes built from α/β -tubulin dimers. The ends of a microtubule differ in their dynamic properties and intracellular localization/function. In most cells, the less dynamic minus-ends are embedded close to the nucleus, while the more dynamic plus-ends are oriented towards the cell periphery. Plus-end tracking proteins (+TIPs) bind specifically to growing plus-ends, where they have been reported to influence MT dynamics and function, for example in cell migration and division. The aim of my work was to study the mechanisms of plus-end accumulation *in vivo* with the use of fluorescently-tagged +TIPs, and to investigate the role of +TIPs in cell migration. In this thesis I describe the results I obtained and what they signify.

Chapter 1 gives an introduction to the cytoskeleton, microtubules, tubulin isoforms, and posttranslational modifications of tubulin. This provides the background information to describe microtubule associated proteins in general and +TIPs in particular. Subsequently, current theories of +TIP accumulation on microtubule plus-ends are introduced.

Although *in vitro* experiments can give a good idea about the function of an isolated protein, they do not allow studying protein behavior in the cellular context. Therefore **chapter 2** introduces current methods to visualize protein dynamics and protein-protein interactions *in vivo*.

These methods are applied in **chapter 3** to study the function of the +TIP CLASP2 in cell polarization and motility. We investigated the influence of CLASP2 on microtubule dynamics and cell migration, and upstream factors that regulate CLASP2 localization.

Chapter 4 presents results on the mechanism by which CLIP-170, another +TIP, accumulates at growing microtubule plus-ends *in vivo*. This led to the description of a new model, wherein the accumulation of CLIP-170 on plus-ends is much more dynamic than previously postulated.

Finally, the findings on +TIP function and accumulation on microtubule plus-ends are discussed in **chapter 5**.

A grayscale electron micrograph showing a dense network of microtubules. The microtubules are long, thin, and oriented in various directions, creating a complex, woven pattern. They are most prominent in the lower-left and middle-left areas, while the upper-right corner is a lighter, less detailed background.

Chapter 1

Structure and Function of the Cytoskeleton

Although the existence of filamentous structures inside of eukaryotic cells or surrounding them had been debated for more than 100 years (Frixione, 2000), it took until the beginning of the 20th century before the concept of a “cytoskeleton” was widely accepted. This acceptance was mainly based on theoretical considerations. The first clues came from centrifugation experiments with eggs of *Crepidula*. Because these eggs quickly regained their structural identity after centrifugation, a “spongioplasmic network” was postulated (Conklin, 1917). Another consideration were the increasing number of known intracellular enzymatic reactions and their kinetics. As an unstructured cytoplasm would not allow for the observed orchestrated metabolic reactions, Rudolf Peters postulated an “organized network of protein molecules” that serves as structural backbone in or on which enzymes are organized (Peters, 1930).

Visualizing these “networks” proved difficult, because they do not show enough contrast in regular light microscopy. The mitotic spindle had been visualized with polarized light (Schmidt, 1939), but a systematic visualization of the cytoskeleton was only made possible around 1950 with the adaptation of electron microscopy for use with biological specimens. Microtubules were visualized in cilia (Fawcett and Porter, 1954) and consequently in the cytoplasm of all studied cells (Fawcett, 1961). The filamentous nature of muscle fibers was confirmed and myofibers were described (Hall et al., 1946; Rozsa et al., 1950), but it took some time until non-muscle filaments were realized to belong to two distinct groups – microfilaments (actin filaments), which are structurally identical to myofilaments in muscle cells (Pollard and Korn, 1973; Schroeder, 1973), and intermediate filaments (Ishikawa et al., 1968).

All three components of the cytoskeleton – microtubules, actin filaments and intermediate filaments – are linear polymers, but they differ in their mechanical and chemical properties. This translates to their specific functions, although there is also a broad functional overlap, for example all three provide the cell with resistance to mechanical forces.

Microtubules are hollow tubes assembled from α/β -tubulin dimers. Most microtubules consist of 13 protofilaments and have a diameter of 25 nm. They are the most rigid component of the cytoskeleton, with a persistence length (polymer length above which the direction of the two ends is not correlated anymore) exceeding the diameter of cells (Gittes et al., 1993). α/β -tubulin dimers are polarized and because they assemble in a head-to-tail fashion, the resulting microtubule is polarized as well with a so called “plus-end” and “minus-end”. Microtubules are essential for cell division and all long-range motor-driven transport is microtubule mediated.

Actin assembles into a two-stranded helical polymer with a diameter of 5-9 nm, which is known as actin filament or microfilament. The most visual role of actin filaments is in muscle contraction, but they have been consecutively found in nearly all eukaryotic cells, where they play important roles in for example cell-cell contacts, cytokinesis, and maintenance and adaptation of cell morphology. Actin filaments, like microtubules, show polarity as actin monomers assemble head-to-tail. The two ends have been described as barbed and pointed ends, which is based upon their appearance when decorated with the head domain of myosin (a motor

protein described in more detail in chapter 1.2.2.1), which binds asymmetrically to polymerized actin monomers (Huxley, 1963). Actin filaments are the tracks for myosin-mediated short-distance-transport. Single actin filaments are much less stiff than microtubules (Gittes et al., 1993), but accessory proteins (Winder and Ayscough, 2005) facilitate their assembly into bundles and networks so that they can withstand greater forces.

Intermediate filaments differ from actin filaments and microtubules in that they do not have polarity because their building blocks are symmetrical. In contrast to actin filaments and microtubules, intermediate filaments can be formed by a whole family of proteins that form hetero- and/or homo-polymers. In humans, 65 proteins are described to form intermediate filaments (IFs), which can be divided into 5 subfamilies (Oshima, 2007): the heteropolymeric keratins type I and II (found in hair, nails and skin); homopolymeric filament proteins (like vimentin), neuro-filament subunits, and nuclear lamins (which form the nuclear lamina). Although IF proteins have variable C- and N-terminal domains, they share a structurally conserved core domain. Mediated by this core domain, IF proteins assemble into parallel coiled-coiled dimers, which in turn dimerize into antiparallel tetramers. These symmetrical tetramers are packed into a fiber of about 10 nm diameter (Strelkov et al., 2003). Due to their tight packaging, IFs are less bendable than actin filaments and less breakable than microtubules (Kreplak and Fudge, 2007). They can be found mainly in cells that need to resist mechanical strain, like neurons, muscle cells, and the keratinocytes of the skin.

The three components of the cytoskeleton can not be seen as separate entities, but they show a complex structural and functional interplay. Schliwa and van Blerkom suggested already in 1981 that “the cytoskeleton is a highly interconnected unit” (Schliwa and van Blerkom, 1981). They describe that actin filaments, microtubules and intermediate filaments are linked by filamentous structures. These structures might very well be spectraplakins, elongated proteins that have been shown to be able to interact with (at least) two different components of the cytoskeleton (Roper et al., 2002).

Functional interactions between actin filaments and microtubules have been shown for transport of melanosomes in melanophores, which depends on long-range microtubule-based movement and short-ranged actin-based spreading at the cell periphery (Wu et al., 1998). A more complex structural-functional interplay between microtubules and actin filaments was shown to allow microtubules to bear enhanced loads in the cytoplasm without breaking (Brangwynne et al., 2006), because forces are dissipated into the surrounding actin-mesh.

1.1. Microtubules

Microtubules are important for divergent cellular functions. Among others, they form the mitotic spindle that separates chromosomes during cell division, serve as backbone for long-range intracellular transport, and are involved in directed cell movement. Cilia contain specialized microtubules that allow movement of single-cell organisms and fluid displacement in higher-order organisms.

Microtubules are important for divergent cellular functions. Among others, they form the mitotic spindle that separates chromosomes during cell division, serve as

backbone for long-range intracellular transport, and are involved in directed cell movement. Cilia contain specialized microtubules that allow movement of single-cell organisms and fluid displacement in higher-order organisms.

Microtubules are polarized hollow tubes assembled of protofilaments of α/β -tubulin dimers. The two ends of a microtubule are structurally different. In most cell types, the minus-ends of microtubules are embedded in the microtubule organizing center (MTOC) (Kellogg et al., 1994; Schiebel, 2000), which in many cell types is located in a dent of the nuclear membrane (Huslpas et al., 1994). The plus-ends radiate into the cytoplasm and switch between episodes of growth and shrinkage, a process called dynamic instability (Fig. 1-1). The transition to growth is called MT rescue, and the transition to shrinkage MT catastrophe. Dynamic instability was first described *in vitro* (Mitchison and Kirschner, 1984) and subsequently confirmed in living cells (Cassimeris et al., 1988; Sammak and Borisy, 1988; Schulze and Kirschner, 1988). Dynamic instability results in a wider spread of microtubule length and a faster turnover of MTs than expected for passive polymerization (Howard, 2001). This allows the cell to constantly probe the cytoplasm and to quickly adapt to a changing environment. The functional implications of dynamic instability and the underlying structural details on the molecular and macromolecular level have been studied extensively and will be introduced in more detail.

1.1.1. Microtubule structure

α/β -tubulin dimers assemble head-to tail into linear protofilaments, which in turn assemble laterally to form hollow microtubules with a diameter of about 25 nm. The number of protofilaments per microtubule is tightly regulated and most microtubules grown *in vivo* consist of 13 protofilaments, while most microtubules grown *in vitro* consist of 14 protofilaments.

EM experiments of microtubules have shown patterns that could be explained by two possible tubulin lattices (Erickson, 1974) – The A-type lattice where lateral bonds are formed between α - and β - tubulins of adjacent protofilaments, or the B-type lattice where lateral bonds are formed between two α -tubulins and two β -tubulins, each of adjacent protofilaments. Consecutive experiments have excluded

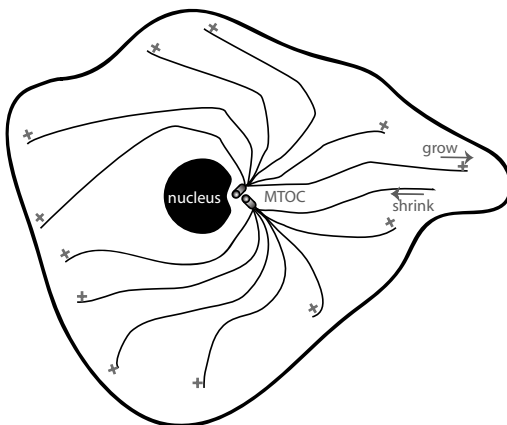


Figure 1-1: MT cytoskeleton

Schematic drawing of a fibroblast, including the MTOC and the dynamic microtubule network

the A-type lattice and confirmed that the B-type lattice is the natural occurring tubulin arrangement. In a B-type lattice protofilaments are slightly staggered, resulting in a left-handed 3-star helix with 12 nm pitch, in which lateral bonds between adjacent protofilaments are formed between the same tubulin subunits (Mandelkow et al., 1986; Song and Mandelkow, 1993). This could be confirmed by computational experiments (Sept et al., 2003).

One helical turn in a B-type lattice corresponds to a shift of 1.5 tubulin dimers, because they are 8 nm long. This implies that microtubules have a “seam” where α - and β -tubulin subunits from adjacent protofilaments form lateral bonds (Kikkawa et al., 1994). The distinct structure of the seam has been proposed as a binding surface for microtubule associated proteins (MAPs). This could be confirmed for the MAP Mal3 in yeast (Sandblad et al., 2006).

Free tubulin dimers bind two GTP molecules – one at the nonexchangeable N-site of α -tubulin and one at the exchangeable E-site of β -tubulin. Incorporation of tubulin into growing microtubules results in interactions between consecutively incorporated tubulin dimers that trap the GTP in the E-site and trigger its hydrolysis to GDP. Therefore, β -tubulin along the length of a microtubule is bound to GDP, while the plus-end is capped by a layer of GTP-bound β -tubulin (Carlier, 1982). GTP-bound tubulin is relatively straight and favours polymerization, while GDP-bound tubulin favors a curved conformation. Lateral and longitudinal bonds between adjacent tubulin dimers prevent that GDP-tubulin adopts the curved conformation that is energetically favourable for free GDP-tubulin. Computer simulations show that the interaction forces, which keep GDP-tubulin in the MT-lattice straight, are weaker close to the end of the microtubule (Janosi et al., 2002). To prevent depolymerization, the top-layer of GDP-tubulin needs to be protected by a “cap”. The cap might be formed by a terminal tubulin sheet that has not yet closed into a tubule, but the most favoured view is a terminal layer of GTP-tubulins that form strong lateral bonds. Dependent on the nature of the MT-cap, different events lead to MT catastrophe and disassembly: 1) closure of the tubulin sheet up to the MT end or 2) slowed MT assembly that allows GTP-hydrolysis to catch up with GTP-tubulin polymerization and expose GDP-tubulin at the MT end.

The “infamous GTP cap” (as it was dubbed by an anonymus reviewer) has been the focus of many studies over the last 25 years, but as of today, no consensus could be reached about the size and precise function of this cap. Several groups have reported that a single layer of GTP-bound tubulin is enough to stabilize microtubules (Caplow and Shanks, 1996; Panda et al., 2002) but newer studies cast serious doubt on these results (Caplow and Fee, 2003; Molodtsov et al., 2005). A model that describes dynamic MT behaviour assuming first-order reaction kinetics for GTP-hydrolysis is able to mirror dynamic instability (Margolin et al., 2006; VanBuren et al., 2002). Simulations based on this model predict that individual protofilaments can shorten without provoking a catastrophe even when the microtubule as a whole is in a growth phase. Tracking microtubule growth with optical tweezers confirmed these simulations (Schek et al., 2007). These experiments show that the speed of tubulin incorporation is highly variable at the molecular level, and that this is not due to the incorporation of tubulin oligomers of variable length. These findings are in contrast to reports that show the incorporation of tubulin oligom-

ers (Kerssemakers et al., 2006). Even though further experiments are needed to confirm the exact nature of incorporated tubulin entities, both studies agree on a less straight front of tubulin growth than a “GTP-cap” would imply.

The structure of tubulin dimers assembled *in vitro* into zinc-induced sheets has been solved at 3.5 Å resolution (Lowe et al., 2001; Nogales et al., 1998). “Docking” this tubulin structure into a lower-resolution structure of microtubules as obtained by EM resolved the microtubule-structure with 8 Å resolution (Li et al., 2002a). Together with the recently reported structure of GDP-bound tubulin (Wang and Nogales, 2005), this allows for a more structural description of intermediate states during microtubule polymerization and depolymerization (Nogales and Wang, 2006).

The energy stored in GTP-bound β -tubulin is released in several steps during the “tubulin-lifecycle” (reviewed in Desai and Mitchison, 1997), making it possible for the microtubule to exert pushing forces during assembly and pulling forces during disassembly (Dogterom et al., 2005; Nogales and Wang, 2006).

1.1.2. Dynamic instability

Initial attempts to describe polymerization of tubulin and actin led to the development of the classical polymerization theory (Oosawa, 1970). It is based on the assumption that microtubules are polymers in equilibrium, and that their length fluctuation thus only depends on the concentration of free tubulin, the affinity of tubulin for microtubules, and the dissociation rate with which tubulin is lost from microtubule ends. Applying the classical polymerization theory to MT dynamics results in very limited length fluctuations for any given MT. It would take a year for a 15 μm long MT to fluctuate to zero length at equilibrium conditions (Mitchison and Kirschner, 1984).

MT length *in vitro* has been shown to fluctuate much more than can be explained by the classical polymerization theory. Individual MTs were shown to either shrink or grow with infrequent transitions between the two states. This non-equilibrium behavior has been termed “dynamic instability” (Mitchison and Kirschner, 1984). MTs in living cells also show dynamic instability (Cassimeris et al., 1988; Sammak and Borisy, 1988), as seen by the rapid incorporation of microinjected fluorescently labeled tubulin into the microtubule array of interphase cells (Saxton et al., 1984).

Dynamic instability requires an energy source, which is the hydrolysis of tubulin-bound GTP after polymerization. Hydrolysis releases chemical energy that is stored as mechanical strain in the microtubule lattice as GDP-bound tubulin dimers prefer a curved conformation but are kept straight in the microtubule lattice. When microtubules undergo catastrophe and switch from growth to shrinkage, this strain is released, and individual curved protofilaments peel outwards, resulting in rapid depolymerization. When new GTP-bound tubulin dimers are incorporated, the shrinking microtubule is rescued and starts polymerizing again. Dynamic instability can be described by four parameters: elongation rate, shortening rate, rescue frequency and catastrophe frequency. Microtubules can also pause in a metastable state in which the microtubule neither grows nor shrinks (Janosi et al., 2002).

If microtubules were classical polymers at equilibrium, it would take years for a cell to reorganize its microtubule array in order to progress from interphase to

mitosis. Obviously, this exceeds the lifespan of many organisms. Therefore dynamic instability is crucial for cells to migrate and progress through the cell cycle, and for the attachment of kinetochores to spindle microtubules ("search-and-capture", Holy and Leibler, 1994). Both polymerization and depolymerization can generate forces, which are comparable to forces generated by motor proteins (Howard, 2001) and can be used to push vesicles or cell membranes, pull chromosomes apart during mitosis and stabilize the nucleus in the cell center.

MT polymerization rate *in vivo* is about 5-10 times higher than *in vitro* (Cassimeris, 1993). Unexpectedly, the catastrophe frequency is also increased *in vivo*. This points towards the existence of factors that independently modulate polymerization rate and catastrophe frequency (Cassimeris, 1993). It has long been known that MT dynamics are tightly regulated during the cell cycle and at cell differentiation (Bulinski and Gundersen, 1991) with the most obvious changes at the transition from interphase to mitosis (McNally, 1996). The spatial regulation of dynamic instability could also be shown, with increased MT turnover at the cell periphery (Komarova et al., 2002b) and local stabilization of microtubules during cell polarization (Gundersen and Bulinski, 1988). Using known parameters of dynamic instability during interphase and mitosis, the observed changes in microtubule dynamics at the progression into mitosis could be simulated (Gliksman et al., 1993).

Microtubule dynamics might be regulated through several mechanisms: 1) influencing the pool of free tubulin dimers, 2) modulating the mechanical strain of GDP-tubulin through interactions along the microtubule lattice, 3) changing the structure of growing/shrinking MT ends and 4) severing MTs and inducing depolymerization of the new uncapped ends. Mechanisms 2) and 3) require proteins that bind MTs or the MT end and will be discussed in more detail in chapter 1.2 and 1.3.

The mean length of MTs increases very steeply with increasing tubulin concentration (Howard, 2001). Therefore, proteins like Stathmin/Op18 that can sequester tubulin monomers (reviewed in Cassimeris, 2002) are expected to influence MT dynamics. Stathmin activity is phosphorylation-dependent, and phosphorylation of stathmin in turn has been shown to be spatio-temporally regulated (Niethammer et al., 2004), which emphasizes the tight regulation of microtubule dynamics.

Several microtubule severing enzymes have been described, which work together to control spindle length (McNally et al., 2006), move chromosomes during mitosis (Zhang et al., 2007), and regulate axonal outgrowth (Wood et al., 2006).

1.1.3. Tubulin isoforms and their posttranslational modifications

For quite some time after the discovery of tubulin as building block of microtubules, the only known isoforms were α - and β -tubulin. A screen for proteins that interact with β -tubulin in *Aspergillus nidulans* led to the discovery of γ -tubulin (Oakley and Oakley, 1989). γ -tubulin is an essential protein of all eukaryotic cells that is involved in microtubule assembly through γ -tubulin ring complexes (reviewed in Schiebel, 2000). It has been suggested that γ -tubulin not only has a role in microtubule nucleation, but also in the regulation of microtubule dynamics, although the underlying mechanisms still need to be elucidated (Raynaud-Messina and Merdes, 2007). Over the last 15-20 years, additional isoforms of tubulin have been

discovered that are less ubiquitously expressed than the core tubulin repertoire of α -, β - and γ -tubulin and function in the assembly of axonemes and basal bodies (reviewed in Dutcher, 2001).

The variety of microtubule functions and the existence of subsets of microtubules that differ in their stability and resistance to proteolytic enzymes led to the postulation of the existence of several forms of tubulin (Behnke and Forer, 1967) even before the discovery of the heterodimeric nature of tubulin (Bryan and Wilson, 1971; Feit et al., 1971). This was consequently elaborated as the “multitubulin hypothesis” (Fulton and Simpson, 1976). The existence of different tubulins could be confirmed with the sequencing of several isotypes of α - and β -tubulin in animals, plants, fungi and some protists (compiled by Luduena, 1993; Luduena, 1998). Mice for example express 6 isotypes of α -tubulin and 7 isotypes of β -tubulin. Their expression is tissue-specific and regulated during development, but most cells express an overlapping set of isotypes.

Sequence differences between isotypes have been conserved between species, pointing towards conserved specific functions of different isotypes (Luduena, 1998). Microtubules normally contain several isoforms and these can be readily interchanged. Even a chimera of chicken- and yeast- β -tubulin transfected into 3T3-cells gets readily incorporated into all microtubules (Bond et al., 1986). This global interchangeability might mask smaller, more subtle differences in structure or dynamic behavior. For example, the touch-receptor neurons of *C. elegans* contain specialized MTs with a particular isotype of β -tubulin (MEC-7) and an increased number of protofilaments. MEC-7 null mutants lack these specialized MTs and show no touch sensitivity (Hamelin et al., 1992; Savage et al., 1994). Budding yeast (*S. cerevisiae*) contains only two isotypes of α -tubulin and a single β -tubulin. Mutants lacking one of the α -tubulins are viable, but tubulin isolated from these mutant strains assembles into MTs with different dynamic behavior in vitro (Bode et al., 2003). This is supported by isotype-dependent assembly dynamics of bovine β -tubulin in vitro (Lu and Luduena, 1994; Panda et al., 1994). Microtubules assembled from α/β_{III} -tubulin are more dynamic, with faster assembly and disassembly rates and less time spent in the pause state. β_{III} -tubulin is mainly expressed in the brain, but it is also found in a variety of tumors, even if the original tissue did not express β_{III} -tubulin (Katsetos et al., 2003). β_{III} -tubulin is less susceptible to taxol-induced MT stability, which might explain taxol-resistance in many types of cancer cells (Kavallaris et al., 1999).

Most variability between tubulin-isotypes is found in the C-terminal regions. This relatively unstructured region seems to be located at the surface of the MT. Some distinct “hot spots” of variability have been found in the N-terminus of β -tubulin as well. They differ between isotypes but not between species, and have been proposed to interact with the C-terminus in the tertiary structure (Burns and Surridge, 1990).

The importance of the C-terminus in the specification of tubulin-function is enhanced by possible posttranslational modifications (PTMs) of tubulin. A broad range of modifications have been described, of which most affect C-terminal residues: detyrosination, removal of the last 2 amino acids of α -tubulin ($\Delta 2$), polyglycylation and polyglutamylation. Only phosphorylation and acetylation affect residues

in the “N-terminal core”. All modifications except the $\Delta 2$ -truncation are reversible. In light of the variety and variability of PTMs, Verhey and Gaertig (2007) proposed a “tubulin code” that regulates MT function in analogy to the “histone code” that regulates gene transcription.

1.1.3.1. Acetylation

Nearly all α -tubulins can be acetylated at a conserved lysine at position 40 (L'Hernault and Rosenbaum, 1985). The enzyme responsible for acetylation has not yet been identified, but HDAC6 and SIR2 (North et al., 2003) have been shown to catalyze deacetylation (Hubbert et al., 2002; Zhang et al., 2003b). Acetylation seems to be a modification that a subset of long-lived microtubules (for example axonemal MTs) acquires over time. These microtubules are more resistant to depolymerization by the MT destabilizing agent nocodazole, but they are not protected from depolymerization by cold treatment (Piperno et al., 1987). Mutating lysine-40 in tetrahymena resulted in complete loss of acetylation (Gaertig et al., 1995) but had no detectable phenotype. In contrast, acetylation influences the migration of NIH-3T3 cells, as overexpression of HDAC6 increased cell motility while depletion of HDAC6 inhibited cell migration (Tran et al., 2007). Down-regulation of SIR2 in granular cells resulted in increased levels of acetylated microtubules and mediated protection from axonal degeneration (Suzuki and Koike, 2007).

GLFND (also known as MIR1 (Stein et al., 2002) and FSD1 (Carim-Todd et al., 2001)) specifically localizes to acetylated MTs, and an excess of GLFND increases the number of acetylated MTs in cells (Manabe et al., 2002). Anterograde transport of JIP-1 containing vesicles is facilitated in neurites containing acetylated tubulin (Reed et al., 2006), therefore acetylation is the first post-translational modification that has been shown to mediate spatial selectivity of transport in asymmetric cells (Bulinski, 2007).

1.1.3.2. Tyrosination/ $\Delta 2$ -truncation

Most mammalian α -tubulins have a C-terminal tyrosine, which can be removed by a tubulin tyrosine carboxypeptidase (TTCP) and added back by tubulin-tyrosine ligase (TTL). TTL has been cloned and studied extensively (Erck et al., 2000; Erck et al., 2003; Trichet et al., 2000), but TTCP escaped detection, although recent studies point in the direction of a Nna1-like metallocarboxypeptidase (Fonrose et al., 2007; Kalinina et al., 2007; de la Vega et al., 2007). TTCP and TTL differ in their substrate preference: TTCP preferentially detyrosinates assembled microtubules, while TTL readily tyrosinates free tubulin dimers. As a result, detyrosination might be used as a marker of microtubule lifetime, but does not stabilize microtubules itself. The relation between detyrosination and microtubule lifetime is not reflected by an increase of detyrosination towards the microtubule minus-end (Geuens et al., 1986).

Polarization of cells is linked to the extensive detyrosination of a subset of microtubules that is oriented towards the direction of cell migration (Gundersen and Bulinski, 1988). In some cell types the stabilization of microtubules (and the detyrosination that is linked to this modification) may depend on signaling via lysophosphatidic acid (Nagasaki and Gundersen, 1996). Regulated detyrosination

is necessary for proper myogenic differentiation (Chang et al., 2002). Protrusions containing detyrosinated tubulin have been found to mediate cell-cell and cell-matrix contacts in mammary epithelial cells (Whipple et al., 2007).

Targeted deletion of the TTL-encoding gene in mice has been shown to be lethal, due to neuronal problems (Erck et al., 2005). While a pool of tyrosinated tubulin remains in dividing cells (through tubulin synthesis), no tyrosinated tubulin remains in differentiated cells. This seems to be especially detrimental to neuronal cells, as they fail to develop and migrate properly. Cultured TTL null neurons have an altered timecourse of neurite outgrowth and their axons differentiate prematurely. It was speculated that this was due to the loss of CLIP-170, a microtubule associated protein that binds microtubules via its CAP-Gly domains, from neurite outgrowth and growth cones in TTL null neurons. However, mice in which the gene encoding CLIP-170 was deleted, have no overt neuronal phenotype (Akhmanova et al., 2005).

Removal of the last residue in detyrosinated α -tubulin results in $\Delta 2$ -tubulin that can no longer be tyrosinated. $\Delta 2$ -tubulin can mostly be found in neurons with very long-lived microtubules, but not much is known about its function.

1.1.3.3. Phosphorylation

Phosphorylation of tubulin was the first modification to be described (Eipper, 1972). Although phosphorylation has now been reported for several tubulins from turkey to carrots (reviewed in Luduena, 1998), it remains a less common modification. This might be due to the fact that tubulin itself is already negatively charged and addition of a negative phosphate-group might not have a big impact (Westermann and Weber, 2003). It remains partly unclear which enzymes catalyze tubulin phosphorylation in vivo, although casein kinase II appears to mimic phosphorylation in vitro (Serrano et al., 1987), and a microtubule-associated casein kinase-like kinase has been reported (Crute and Van Buskirk, 1992).

Removal of phosphate from β_{III} -tubulin does not affect microtubule assembly in vitro (Khan and Luduena, 1996). More recently, opposing effects of tubulin phosphorylation on microtubule integrity have been described. Banan et al. (2004) describe the disruption of the MT cytoskeleton in Caco-2 cells that have a decreased concentration of active PKC- θ , which they show to correlate with a decreased level of phosphorylated tubulin. Tubulin phosphorylation in Caco-2 cells on the other hand appears to promote its incorporation into MTs. The opposite seems to be the case in HeLa cells at the transition from interphase to mitosis. There, Cdk1 is phosphorylating β -tubulin, and phosphorylated tubulin is not incorporated into the MT array (Fourest-Lieuvin et al., 2006).

1.1.3.4. Polyglutamylation/Polyglycylation

Polyglutamate and polyglycine can be covalently attached to conserved glutamate residues in the C-terminus of α - and β -tubulin. Several glutamates in the same tubulin molecule can be modified, and single sidechains can contain more than 30 glycines or 20 glutamates. Both modifications are predominantly found in long-lived microtubules, for example in sperm, neurons, and cilia. The majority of enzymes that catalyze polyglycylation and polyglutamylation and their reverse reactions are

still unknown, but a family of TTL-like proteins responsible for polyglutamylation has been described (Janke et al., 2005). Members of this protein family differ in their substrate specificity (α - vs. β -tubulin) and in the catalyzed reaction (side-chain formation vs. elongation) (van Dijk et al., 2007).

Polyglutamylation and polyglycylation are important for cilia formation (Thazhath et al., 2002) and influence the binding of microtubule associated proteins and motor proteins to microtubules (Bonnet et al., 2001). The side-chain length at which optimal binding is observed seems to be dependent on the binding protein (Bonnet et al., 2001). Defects in polyglutamylation reduce the MT-binding of several motor proteins *in vitro* and alter the subcellular distribution of motor proteins *in vivo* (Ikegami et al., 2007).

1.2. Microtubule associated proteins

Many proteins can bind microtubules. They can be divided into three groups:

1. Microtubule associated proteins (MAPs) that bind along the microtubule lattice. They were discovered due to their cosedimentation with microtubules assembled *in vitro* (Borisy and Olmsted, 1972; Murphy and Borisy, 1975; Runge et al., 1979).
2. Motor proteins, which use energy from ATP-hydrolysis to move along the microtubule.
3. Plus-end tracking proteins (+TIPs) that specifically accumulate at the plus-end of growing microtubules. The first member of this group, CLIP-170, was described almost a decade ago (Perez et al., 1999).

Obviously the division described above is imperfect. For example, +TIPs have been shown to localize to minus-ends of microtubules, to the microtubule lattice, and/or to associate with tubulin (Akhmanova and Hoogenraad, 2005). Furthermore, members of the kinesin motor protein family specifically depolymerize microtubules from the plus-end using ATP hydrolysis, but have been described to reach the microtubule end independent of motor activity (Blaineau et al., 2007; Helenius et al., 2006).

1.2.1. Classical MAPs

Tubulin can be selectively enriched from brain lysate by repeated cycles of polymerization and depolymerization, with the purified protein being able to form microtubules *in vitro* (Shelanski et al., 1973; Weisenberg, 1972). Although most impurities are removed by the repeated polymerization cycles, several proteins were shown to get enriched together with tubulin (Murphy and Borisy, 1975; Runge et al., 1979). These proteins were termed MAPs (microtubule associated proteins), and more family-members have been described (reviewed in Amos and Schlieper, 2005; Maccioni and Cambiasso, 1995).

MAPs tend to be elongated proteins that contain several microtubule binding domains, enabling them to bind several tubulin dimers at the same time. This might explain how MAPs stabilize MTs (Sloboda and Rosenbaum, 1979), and promote MT assembly *in vitro* (Hirokawa, 1994; Itoh and Hotani, 1994; Matus, 1990). The affinity of MAPs for microtubules is tightly regulated by kinases and phosphatases (Cassimeris and Spittle, 2001).

MAPs are predominantly found in neurons, but more ubiquitously expressed MAPs have also been cloned (for example MAP4). Neuronal MAPs have been linked to neuro-degenerative disorders (Fischer et al., 2007; Lace et al., 2007), putting them into the spotlight of research. Although tau and MAP2 are expressed in the same cell and are both MAPs, they show a mutual exclusive distribution in nearly all cells – tau is constrained to the axon, while MAP2 localizes to dendrites and the cell body. Contrasting, the distribution of MAP1, another neuronal MAP, is not restricted to one or the other compartment.

1.2.2. Motor proteins

Motor proteins transform the chemical energy released through ATP-hydrolysis into mechanical energy to move along actin filaments or microtubules. The microtubule-based motors are dynein, which moves towards the –end, and the kinesins, of which most move towards the +end. Organelles often move bi-directionally, requiring the attachment and activity of minus- and plus-end directed motors to be coordinated and tightly regulated (Gross, 2003; Welte, 2004).

1.2.2.1. Kinesin

Kinesins transport a variety of cargo, ranging from membranous structures and protein complexes to viruses, chromosomes and mRNA. Kinesins form a large protein family, with 14 subfamilies distinguished thus far (Lawrence et al., 2004). They can be grouped according to the position of their head domain. N-terminal kinesins (all of which are +end directed motors) are most abundant. C-terminal kinesins form a small group of -end directed kinesins. The destabilizing I-kinesins contain an internal domain and do not move cargo along microtubules, but use the energy from ATP-hydrolysis to promote MT depolymerization.

Kinesins share a common globular motor domain (also referred to as head domain) that binds to microtubules and hydrolyses ATP. Adjacent domains determine structure and cargo-specificity, and bind accessory proteins. “Conventional” kinesin (KIF5) contains an N-terminal motor domain, a central α -helical homodimerization domain and a C-terminal tail domain that can bind KAR3, a kinesin light chain that mediates cargo-binding (see Mandelkow and Mandelkow, 2002). Conventional kinesin is a processive motor that keeps at least one head attached to the microtubule at all times, which allows it to move hundreds of steps without falling off the microtubule. The two motor domains of a KIF5-dimer “walk” in an asymmetric hand-over-hand fashion with 8 nm step length – the length of a tubulin dimer (reviewed in Asbury, 2005).

Cell division depends at several stages on the proper function of N-terminal kinesins (reviewed in Wozniak et al., 2004). For example, members of the Eg5 family, which are homotetrameric, cross-link microtubules from both poles and help to form a bipolar spindle (Kwok and Kapoor, 2007). Furthermore, CENP-E supports bipolar attachment of kinetochores to microtubules. In addition, a diverse group of kinesins can bind to DNA and is involved in the alignment of chromosomes at the metaphase plate. Finally, kinesins of the MKLP1 family organize the microtubules during cytokinesis.

Another group of kinesins involved in mitosis are the depolymerizing kinesins of the kinesin-13 subfamily – MCAK and KIP2. Motile kinesins preferentially bind to the straight microtubule lattice, while depolymerizing kinesins preferentially bind to curved MT protofilaments at MT ends. They use energy from ATP-hydrolysis to induce a bent conformation of protofilaments that facilitates depolymerization (Kinoshita et al., 2006; Moore and Wordeman, 2004; Ovechkina and Wordeman, 2003; Sharp et al., 2005; Wordeman, 2005).

Defects in kinesin mediated long-range transport have been linked to neuro-degenerative diseases like ALS and Alzheimer's, to cause failure of cilia-function leading to polycystic kidney disease or hearing loss, and mutations in depolymerizing kinesins can lead to mitotic defects (Chevalier-Larsen and Holzbaur, 2006; Hirokawa and Takemura, 2003; Mandelkow and Mandelkow, 2002).

1.2.2.2. Dynein/dynactin

Dyneins are –end directed motor proteins. They can be divided into 2 groups (Hook and Vallye, 2006) – axonemal dyneins that couple microtubules in cilia and are responsible for ciliary movement, and cytoplasmic dyneins that transport cargo along microtubules. In contrast to what its name implies, cytoplasmic dynein 2 is found in cilia where it mediates retrograde traffic. The only dynein found in the cytoplasm is cytoplasmic dynein 1, on which the following description will focus.

Cytoplasmic dynein 1 is a multisubunit protein of 1.2 MDa. It contains a dimer of dynein heavy chains, which form the core motor domain, and intermediate and light chains, which determine cargo specificity. Each heavy chain folds into a ring structure of 6 AAA (ATPase Associated with diverse cellular Activities) domains and an additional non-ATPase domain. From this ring emerges a stem that connects dynein to the microtubule and a stalk that folds over the ring and stabilizes it. This stalk is necessary for cargo attachment (Burgess et al., 2003; Samso and Koonce, 2004). Like kinesins, dynein uses energy from ATP-hydrolysis to move along the microtubule. Upon ATP hydrolysis, a small structural change in the AAA domains, which is amplified through the stem (Serohijos et al., 2006), causes dynein to step along the microtubule.

Dynein is not very efficient in cargo binding on its own (Karki and Holzbaur, 1999), but makes use of dynactin, a heteromultimeric protein complex, to tether cargo (Gill et al., 1991), which is especially important for long-range neuronal transport (Waterman-Storer et al., 1997). Over the years, the components of the dynactin-complex and their function have been untangled (Schroer, 2004). The largest subunit of the dynactin-complex is p150(glued), a protein that can bind to microtubules on its own and thereby might improve dynein processivity (Culver-Hanlon et al., 2006). As p150(glued) also functions as a +TIP, it will be described in more detail in chapter 1.3.2.2. Furthermore, it should be noted that dynactin was recently shown to associate with kinesin and is therefore likely to be involved in coordinating motors of opposite polarity (Gross, 2003).

As a motor protein, dynein is involved in many cellular functions, among which are vesicle movement, maintenance of Golgi integrity and the positioning of the nucleus (Martin et al., 2004). It is also important during mitosis (Karki and Holz-

baur, 1999) and many viruses reach the nucleus via dynein-mediated transport (Greber and Way, 2006).

1.3. +TIPs

The term “plus-end-tracking protein” (+TIP) was coined by Schuyler and Pellman in 2001 to describe an emerging family of proteins that specifically localize to the growing +ends of microtubules (Schuyler and Pellman, 2001). Dynamic plus-end-tracking was first described for CLIP-170, based on a GFP-fusion protein of CLIP-170 that was visible as “cellular fireworks” of comet-like fluorescent dashes moving mostly from the cell center to the periphery (Perez et al., 1999).

The family of +TIPs has been growing since its initial description, and new family members are described every year. Several reviews have focussed on the function of +TIPs and the mechanisms that mediate +end specificity (Akhmanova and Hoogenraad, 2005; Carvalho et al., 2003; Galjart, 2005; Galjart and Perez, 2003; Lansbergen and Akhmanova, 2006; Mimori-Kiyosue and Tsukita, 2003; Morrison, 2007; Vaughan, 2004).

Numerous functions have been linked to +TIPs:

1. They influence MT dynamic instability (Komarova et al., 2002a).
2. They link MTs to other cellular structures like vesicles, the cell membrane, and components of the cytoskeleton (Vaughan et al., 2002).
3. They might act as chaperones to promote MT assembly (Slep and Vale, 2007).
4. They might function in mechanotransduction (D’Addario et al., 2003).
5. They play a role in signal transduction (Zhou et al., 2004).
6. They are essential in mitosis, as they modulate MT dynamics and guarantee proper kinetochore-attachment (Pereira et al., 2006).

Although +TIPs share the ability to track growing MT +ends *in vivo*, they do not share a common microtubule binding domain (MTB) (Slep and Vale, 2007). +TIPs can be grouped based on their MTB (see Fig. 1-3).

For example, CLIP-170, its homologue CLIP-115, and p150(glued) contain CAP-Gly (Cytoskeleton-associated protein glycine-rich) MTBs. The crystal structures of several CAP-Gly domains have been solved (Honnappa et al., 2006; Li et al., 2002b; Mishima et al., 2007; Weisbrich et al., 2007) and provide insight into their structure-function relationship. CAP-Gly domains contain a highly conserved groove that binds the C-terminus of α -tubulin and of EB1-like family members. Furthermore, the Cap-Gly domain of p150(glued) was shown to bind to a conserved coiled-coil region of EB1, termed the “EB-domain”.

Proteins of the EB1-family in turn bind MTs via their calponin homology (CH) domain. CH domains are found in a large group of proteins, most of which interact with actin (Korenbaum and Rivero, 2002). The crystal structure of the CH-domain of EB1 led to the hypothesis that EBs bind to MTs primarily via electrostatic and hydrophobic interactions (Hayashi and Ikura, 2003).

Members of the XMAP215-family contain several TOG (tumor over-expressed gene) domains, of which representative structures have been solved (Al-Bassam et al., 2007; Slep and Vale, 2007). CLASPs contain a single TOG domain and several TOG-like domains, which might classify them as distant members of the XMAP215-

family (Slep and Vale, 2007). Finally, the recently discovered Navigators contain a conserved domain that mediates microtubule binding but lacks homology with other known MTBs (Martinez-Lopez et al., 2005). Although the four MTB domains described here do not represent all plus-end binding regions, the examples show that a wide variety of structures can associate with the MT end.

1.3.1. Theories of +end specificity

Not only do +TIPs differ in their MTB, but also in the way they accumulate at +ends. Since the first description of CLIP-170 as a +TIP, the mechanisms that lead to +end specificity have been studied, and several theories have been proposed (Fig. 1-2). These can be divided into mechanisms that describe +end specificity as dependent on the +TIP and tubulin/microtubules alone, and those that involve a third factor. The first group of theories encompasses treadmilling, co-polymerization and 1-dimensional diffusion; the second group encompasses motor-mediated delivery of +TIPs and “hitchhiking” on another +TIP. Much effort has been put into understanding +end specificity, and the emerging picture is a complex one. The mechanisms may vary between orthologues of the same +TIP (i.e. CLIP-170, which is proposed to co-polymerize in mammals (Folker et al., 2005) and to be motor-delivered in yeast (Maekawa and Schiebel, 2004)). In addition, even a single +TIP might accumulate through different mechanisms, depending on the position in the cell and the cell cycle (i.e. APC, which can accumulate in EB-dependent and -independent manners, Kita et al., 2006).

1.3.1.1. Treadmilling

Treadmilling microtubules are simultaneously polymerizing at one end (the +end) and depolymerizing at the other (the -end). When Perez et al. described GFP-CLIP-170 to move in fluorescent comets from the nucleus to the cell periphery, they envi-

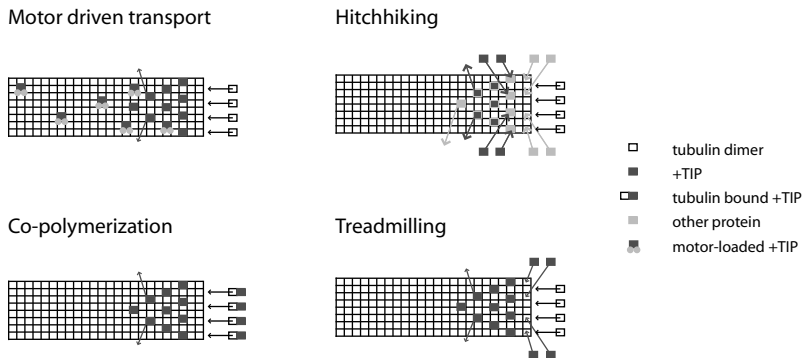


Figure 1-2 Current theories of +end accumulation

For the description of +end accumulation, copolymerization and treadmilling only depend on the MT end and the +TIP. They differ in the way the +TIP reaches the +end (either together with tubulin dimers or after the incorporation of tubulin). In motor driven transport, a +TIP is transported along the MT towards the +end. In the case of hitchhiking, the localization of one +TIP to the MT end depends on the +end localization of another +TIP.

sioned a comparable mechanism underlying this movement (Perez et al., 1999). Fluorescence speckle microscopy (see chapter 2.3.3) indicated that CLIP-170 binds to the polymerizing MT end and dissociates after some time without sliding along the microtubule (Perez et al., 1999). Two questions need to be answered to understand the mechanisms underlying treadmilling: How does a +TIP specifically accumulate on the +end? And what triggers its subsequent dissociation?

+TIPs can localize to the +end either through co-polymerization with tubulin, a mechanism that will be dealt with in chapter 1.3.1.2, or through recognition of a specific conformation of the microtubule tip. Dissociation can be triggered either by conformational changes of the microtubule, or by modifications and/or conformational changes of the +TIP itself.

Conformational differences between the microtubule lattice and the plus-end have been described (see chapter 1.1.2). Polymerizing microtubule ends adopt a sheet-like conformation, which can extend for up to 2 μm in vitro before closing into a tube (Chretien et al., 1995). The corresponding mean sheet-length is 0.3 μm . Conformational changes also occur on a smaller level as tubulin dimers adopt a slightly curved conformation upon GTP-hydrolysis.

Binding of CLIP-170 to microtubules has been shown to be inhibited by phosphorylation (Rickard and Kreis, 1991). Kinase-activity is preferentially located at the microtubule, while phosphatase-activity seems cytoplasmic. A phosphorylation-cycle therefore might regulate the treadmilling of CLIP-170, but a study by Choi et al. (2002) shows that different phosphatases and kinases can influence MT-binding of CLIP-170 differently. They report that rapamycin can phosphorylate CLIP-170 through FRAP/mTOR (FKBP12-rapamycin-associated protein). This rapamycin-sensitive phosphorylation of CLIP-170 can overrule the inhibition of MT-binding upon rapamycin-insensitive phosphorylation of CLIP-170 (Choi et al., 2002).

1.3.1.2. Co-polymerization

Microtubules elongate through polymerization of tubulin dimers. If a +TIP is bound to the incorporating tubulin and co-polymerizes with it, it will localize to growing +ends. Obviously, this requires that the +TIP has affinity for free tubulin dimers. A lower affinity for tubulin incorporated into the microtubule lattice results in dissociation of the +TIP from the MT. Co-polymerization has been hypothesized to be the mechanism underlying in vitro accumulation of CLIP-170 at +ends (Arnal et al., 2004; Folker et al., 2005). Addition of CLIP-170 to MTs in vitro increases the rescue frequency and induces the formation of curved tubulin-oligomers that might function as “prefab”-elements to rescue shrinking MTs (Arnal et al., 2004). This is supported by a much higher affinity of a CLIP-170 fragment for free GTP-bound tubulin ($K_d=0.037 \mu\text{M}$) than for MTs mimicking a GTP-bound (0.12 μM) or a GDP-bound conformation (0.23 μM) (Folker et al., 2005). This interaction of CLIP-170 with tubulin depends on the C-terminal tyrosine of α -tubulin (Mishima et al., 2007).

1.3.1.3. Motor-driven transport

Motor-driven transport to the MT end requires a +end directed kinesin. The yeast homologues of CLIP-170, Bik1p in budding yeast (Lin et al., 2001), and Tip1p in

fission yeast (Brunner and Nurse, 2000), have been shown to depend on a kinesin to accumulate at the +end. The kinesins are Kip2p in budding yeast (Carvalho et al., 2004) and Tea2p in fission yeast (Busch et al., 2004). NUDM, the orthologue of p150(glued) in *Aspergillus nidulans*, also requires a kinesin for +end accumulation (Zhang et al., 2003a), as does APC in mammalian cells (Cui et al., 2002; Mimori-Kiyosue et al., 2000).

Motor-driven transport does not automatically result in accumulation of a protein at the MT +end. If the kinesin would just “walk along the microtubule” and fall off at the +end taking the +TIP with it, the +TIP would be distributed all along the microtubule with a linear gradient towards the +end, but it would not result in a comet-like appearance of the +TIP at the MT end with (nearly) no staining along the microtubule lattice. In order to achieve +end accumulation, +TIPs need to be retained when they reach the +end (Galjart and Perez, 2003). This might explain, why APC that lacks the MTB can still bind the kinesin adaptor protein Kap3 but fails to accumulate at +ends (reviewed in Nathke, 2004).

If the processes that accumulate motor-delivered +TIPs at the MT end can not distinguish between MT +end conformations, “+TIPs” can remain bound to the ends of pausing and/or shrinking microtubules, as has been shown for APC (Langford et al., 2006).

1.3.1.4. Hitchhiking

Most +TIPs described so far can bind to growing MTs directly (Morrison, 2007), even though they might depend on each other for increased binding (Komarova et al., 2005). Another group of +TIPs can interact indirectly with the +end by binding to the core group of directly interacting +TIPs, a phenomenon dubbed “hitchhiking” (Carvalho et al., 2003). As hitchhiking +TIPs depend on core +TIPs for +end accumulation, the maximum time they stay accumulated is limited by the disappearance of the core +TIPs.

APC and Kar9, the yeast homologue of APC, have been described to depend on EB1 for +TIP accumulation (Nakamura et al., 2001). Another hitchhiking protein is the dynein heavy chain 2 (dyn2) in *S. cerevisiae*, which requires the LIS1-homologue Pac1 for +end accumulation (Lee et al., 2003). More recently, the dependence of melanophilin and myosinVa on EB1 for +end tracking has been shown (Wu et al., 2005). In *Drosophila*, the spectraplakine Shot normally localizes to the MT +end but fails to do so in cells depleted of DmEB1 (Slep et al., 2005). Most hitchhiking +TIPs can bind to EB-proteins directly and depend on EBs for localization to the +end. Interestingly, although the staining patterns of DmEB1 and Shot on +ends partly overlap, Shot accumulates along a longer stretch of MT than DmEB1 (Slep et al., 2005), hinting at an EB-independent mechanism of Shot-retention on the +end.

1.3.1.5. 1D-diffusion

Decreasing the dimensions in which a molecule can diffuse decreases the time it takes for this molecule to reach a specific target. The “reduction in dimensionality” has first been proposed for proteins binding a specific target-sequence of DNA (von Hippel and Berg, 1989). A similar mechanism might facilitate the accumulation of proteins at the MT +ends. The possibility of a microtubule binding protein to diffuse

along a microtubule has been shown for flagellar dynein. In the presence of ATP, a partly dissociated outer arm flagellar dynein complex (containing the β -heavy chain and an intermediate chain) translocated unidirectionally along a microtubule in vitro. Unexpectedly, the same complex lost directionality after inhibition of ATPases, but continued diffusing in 1D along the microtubule (Vale et al., 1989).

More recent papers propose 1D diffusion for the depolymerizing kinesin MCAK (Helenius et al., 2006) and a basic MT-binding domain of p150(glued) (Culver-Hanlon et al., 2006). This basic domain can move processively along MTs in vitro, and increases the processivity of dynein, while the CAP-Gly domain of p150(glued) inhibits dynein motility. 1D-diffusion along the MT increases the speed with which MCAK targets to microtubule ends (Helenius et al., 2006).

1.3.2. +TIP families

Although +TIPs can be grouped according to the mechanisms by which they accumulate at MT +ends, these mechanisms are not easily discernible, can vary between orthologues of the same +TIP, could co-exist, and might be subject to scientific debate. With protein-sequences easily available, a more obvious classification of +TIPs is based on sequence homologies (Fig. 1-3).

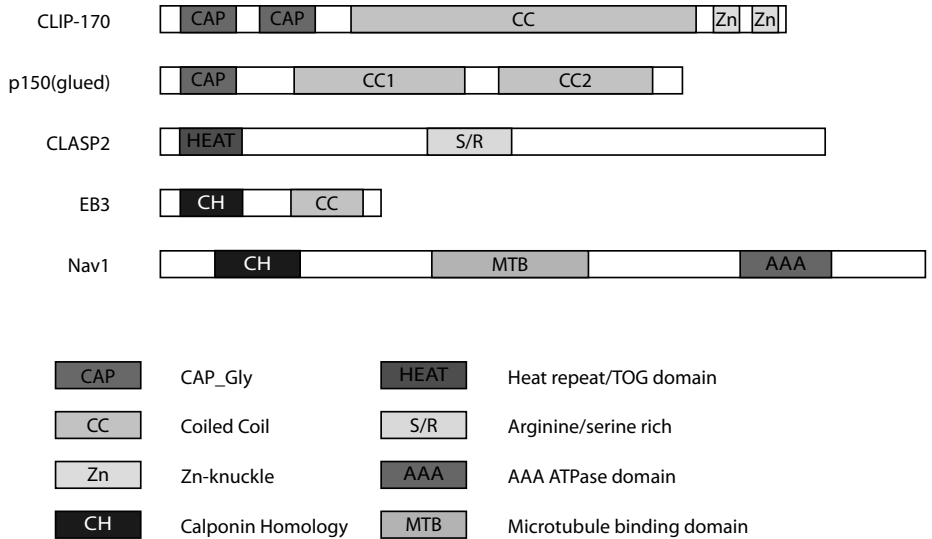


Figure 1-3: Schematic representation of +TIP sequences

CLIP-170 and p150(glued) bind +ends through their CAP_Gly domains. The central domain of CLASP2, containing an arginine/serine rich region is thought to mediate MT binding, although the N-terminal HEAT repeat is homologue to the HEAT repeats mediating MT-association of XMAP-215. The calponine homology domain of EB proteins mediates their interaction with +ends. The MTB region of Navigator proteins differs from known microtubule binding domains, but has not been further characterized yet.

1.3.2.1. Cytoplasmic linker proteins (CLIPs)

In a screen for nucleotide-sensitive microtubule-binding proteins in HeLa cells, Rickard and Kreis found a protein with a molecular mass of 170 kDa (initially termed pp170, now known as CLIP-170) that associates with microtubules in vitro and accumulates at the ends of a subset of microtubules in vivo (Rickard and Kreis, 1990). Subsequent experiments showed that these accumulations colocalize with newly polymerized microtubule +ends (Diamantopoulos et al., 1999) and that a GFP-CLIP-170 fusion protein tracks polymerizing +ends (Perez et al., 1999). CLIP-170 is considered the prototype +TIP, because it was the first protein described to exhibit this dynamic microtubule-association. Homologues of CLIP-170 have been described in many eukaryotes.

CLIP-170 can bind to MTs through its N-terminus, which contains two CAP-Gly domains (Riehemann and Sorg, 1993). Two Zn-knuckles in the C-terminus are important for protein-interactions. These two interaction-domains are linked by a long coiled-coil that forms a rod-shaped dimerisation domain (Pierre et al., 1992). The coiled-coil region contains two “kinks” (Scheel et al., 1999) at which the rod might bend to allow intramolecular interactions of the N-terminal CAP-Gly domains with the C-terminal Zn-knuckles (Lansbergen et al., 2004). CLIP-170 is ubiquitously expressed and shows highest expression levels in muscle, testis, liver and brain (Akhmanova et al., 2005). Several isoforms have been described that differ in their expression profile (Akhmanova et al., 2001; Akhmanova et al., 2005; Bilbe et al., 1992; Griparic and Keller, 1998; Scheel et al., 1999). The closest homologue of CLIP-170 in vertebrates is CLIP-115, which is mainly expressed in the brain, lacks the C-terminal Zn-knuckles (De Zeeuw et al., 1997), and localizes to growing MT +ends as well (Hoogenraad et al., 2000). The phenotype of knock out mice for CLIP-115 resembles the symptoms of patients with Williams Syndrome (Hoogenraad et al., 2002), a neurodegenerative disorder that is caused by the hemizygous deletion of a chromosomal region containing the gene encoding CLIP-115.

Members of the CLIP-family influence MT dynamics: mammalian CLIP-170 promotes rescue of shrinking MTs (Komarova et al., 2002a), while Tip1p, the homologue in fission yeast, is an anti-catastrophe factor (Brunner and Nurse, 2000). The interaction of CLIP-170 with MTs seems to be regulated on several levels: 1) Interaction of CLIP-170 and CLIP-115 with MTs is phosphorylation-dependent (Hoogenraad et al., 2000; Rickard and Kreis, 1991) and a CLIP-170 kinase has been described (Choi et al., 2002); 2) the C- and N-terminal domains of CLIP-170 can interact and overexpression of the C-terminus abolishes accumulation of CLIP-170 on +ends (Lansbergen et al., 2004); 3) accumulation on +ends is reduced in the absence of EB1 and EB3 (Komarova et al., 2005); 4) CLIP-170 can not localize to +ends in cells lacking TTL (Peris et al., 2006).

CLIP-170 has been linked to cell polarization through its interaction with IQGAP1 (Fukata et al., 2002), which is an integrator that influences cytoskeletal function (Briggs and Sacks, 2003). Other binding partners of CLIP-170 are LIS1 (Coquelle et al., 2002), p150(glued) (Goodson et al., 2003), EBs (Komarova et al., 2005) and CLASPs (Akhmanova et al., 2001).

1.3.2.2. *p150(glued)*

The dynein complex links cargo to the dynein motor complex. One component of the dynein complex, p150(glued), associates with microtubules and colocalizes with CLIP-170 at the +end (Vaughan et al., 1999). The +end accumulation of p150(glued) depends on +end localization of CLIP-170 (Watson and Stephens, 2006), although it can bind to microtubules directly (Vaughan et al., 2002). The CAP-Gly domain of p150(glued) is necessary for p150(glued) binding to CLIP-170, and a recently described basic microtubule binding domain might be responsible for the non-CLIP-170-mediated microtubule binding (Culver-Hanlon et al., 2006).

A pointmutation (G59S) in the CAP-Gly domain of p150(glued) perturbs its binding to EB1 and +ends, in (motor neuron like) MN1 cells, leading to aggregates of the protein and increased cell death (Levy et al., 2006), which might explain neuronal defects in patients with this mutation.

1.3.2.3. *Cytoplasmic linker protein associated proteins (CLASPs)*

Mammalian CLASPs were first described as common interaction partners of CLIP-115 and CLIP-170 (Akhmanova et al., 2001). CLASPs are homologues of *Drosophila* Orbit/MAST (Inoue et al., 2000; Kline-Smith and Walczak, 2000; Lemos et al., 2000), which are conserved throughout evolution. The two mammalian paralogues, CLASP1 and CLASP2, are spliced into several isoforms of 140 to 170 kDa. CLASP1 α and CLASP2 α share about 77% sequence homology. All isoforms share a C-terminal domain that mediates interactions with CLIP-115, CLIP-170 and other proteins (Efimov et al., 2007; Lansbergen et al., 2006), and a central region that interacts with MTs and EBs (Mimori-Kiyosue et al., 2005), while the very N-terminus is isoform-specific. The expression patterns differ between the two paralogues and their isoforms, with CLASP2 being enriched in the brain and CLASP2 β being brain-specific. Endogenous CLASP localizes to the Golgi apparatus, centrosomes, kinetochores and microtubule +ends (Akhmanova et al., 2001).

CLASPs play a role in mitosis and cell migration. Their importance for proper mitosis has been evolutionary conserved: Stu1p is an essential component of the mitotic spindle in *S. pombe* (Yin et al., 2002), deletion of Orbit/MAST in *Drosophila* leads to mitotic defects and abnormal spindles (Inoue et al., 2000; Lemos et al., 2000), *cls-2* is essential for mitosis in *C. elegans* (Gonczy et al., 2000), and the *Xenopus*-homologue Xorbit/CLASP plays a role in mitosis (Hannak and Heald, 2006). In mammalian cells, both CLASP1 and CLASP2 are important for proper mitotic progression, with defunct kinetochore attachment in cells lacking CLASP1 (Maiato et al., 2003) and prolonged mitosis in CLASP2 knock out cells (Maiato et al., 2003; Pereira et al., 2006). These defects can partly be rescued by overexpression of the other CLASP paralogue.

The dynamics of CLASPs differ between the cell interior and the cell edges. Throughout the cytoplasm, CLASPs act as +TIPs that can be regulated by phosphorylation (Akhmanova et al., 2001). At the cell cortex of HeLa cells, CLASPs get transiently immobilized (Mimori-Kiyosue et al., 2005) through interactions with LL5 β and ELKS (Lansbergen et al., 2006). Interestingly, CLASP2 can switch to a MAP-like behavior in the lamellopodia of migrating PtK1 cells (Wittmann and Waterman-

Storer, 2005), but can also associate with actin along stress-fibers (Tsvetkov et al., 2007), where it might facilitate guidance of microtubules along actin filaments.

In migrating cells, the Golgi network gets reoriented towards the leading edge, more microtubules are growing towards the leading edge, and a fraction of these gets stabilized (Gundersen and Bulinski, 1988). Tracking growing microtubules in human epithelial cells led to the unexpected observation that most microtubules are not growing from the centrosome (thought to be the MTOC), but nucleate at the transgolgi network (Efimov et al., 2007). The transgolgi-nucleated microtubules depend on CLASP2 expression (Efimov et al., 2007), which gives a functional role to CLASP2 localization at the Golgi network (Akhmanova et al., 2001).

1.3.2.4. End binding proteins (EBs)

The MAPRE family of genes encodes 3 mammalian proteins: EB1, EB2 (and its splice variant RP1), and EB3/EBF3 (and its splice variant RP3) (Su and Qi, 2001). EB1 was first described as an interaction partner of APC (Su et al., 1995), hence its name “end-binding” protein. EB1 and EB3 are ubiquitously expressed, while the expression levels of EB2 vary between cell lines (Su and Qi, 2001). EB3 is especially abundant in the central nervous system, where it binds to the brainspecific form of APC (Nakagawa et al., 2000), and in muscles.

EBs bind microtubules and tubulin *in vitro* and accumulate *in vivo* at centrosomes and growing MT +ends (Berrueta et al., 1998; Bu and Su, 2001; Juwana et al., 1999). Overexpressed EBs lose their +end specificity and bind along the whole microtubule, where EB1 and EB3 - but not EB2 - induce the formation of MT bundles (Bu and Su, 2001). Interestingly, the centrosomal localization of EBs is not dependent on their MT-binding domain, but is linked to the centrosomal proteins CAP350 and FOP (Louie et al., 2004; Yan et al., 2006).

EB-proteins contain three conserved domains. The N-terminal CH-domain mediates MT-interactions, whereas the coiled-coil domain located at the C-terminus (also termed the “EB-like domain”) is responsible for homodimerization. The EB-like domain interacts with APC, MACF and other binding partners (Bu and Su, 2003; Slep et al., 2005). The last few aminoacids of EB1 are highly homologous to the C-terminus of tyrosinated α -tubulins and CLIP-170. This allows for a whole set of interactions between CAP-Gly domains on one hand and EB-like domains on the other hand (Hayashi et al., 2007; Mishima et al., 2007). The crystal structure of the C-terminus of EB1 together with the CAP-Gly domain of p150(glued) revealed specific interactions between both the “EB-like domain” and the extreme C-terminus of EB1 with the Cap-Gly domain of p150(glued) (Honnappa et al., 2006).

It is intriguing that every +TIP found so far can interact with members of the EB family, which led to the view of EBs as a “spider in the web” (Lansbergen and Akhmanova, 2006; Morrison, 2007). The proper localization of many +TIPs to the microtubule end can be influenced by knock down of EBs (Komarova et al., 2005) or overexpression of a truncated EB-construct (Askham et al., 2002). Members of the EB-family are involved in interaction/signaling networks at the cell cortex in all species investigated (Lansbergen and Akhmanova, 2006). The importance of EBs during mitosis (Tirnauer and Bierer, 2000) is stressed by spindle assembly defects in the absence of DmEB1 in *Drosophila* (Rogers et al., 2002).

1.3.2.5. *Adenomatous polyposis coli (APC)*

Adenomatous polyposis coli (APC) is an extensively studied large multidomain protein that is mutated in most colorectal cancers (reviewed in Nathke, 2004). It is believed to act as a scaffold in the Wnt-signaling pathway (Bienz, 2002), but many more functions have been described over the last years (comprehensively reviewed by Hanson and Miller, 2005). These include cell migration, cell-cell-contacts, spindle assembly, MT stabilization and neuronal differentiation.

APC contains a basic domain that binds to MTs and an EB1-binding C-terminal domain, but requires kinesins to localize to the +end (Cui et al., 2002; Jimbo et al., 2002). In migrating cells, endogenous APC mainly associates with +ends in cell protrusion, where it induces MT growth and remains attached to shrinking MTs (Kita et al., 2006). This association does not depend on EB1. Lack of APC decreases cell migration without compromising cell polarity (Kroboth et al., 2007).

Besides being located to MT +ends, APC can localize to the plasmamembrane (Grohmann et al., 2007), to the actin cytoskeleton at cell-cell contacts (Langford et al., 2006), and to the nucleus (Henderson, 2000).

1.3.2.6. *Neuron Navigators (NAVs)*

Neuron navigator 1 (NAV1) is a recently described protein that can localize to growing +ends in vivo (Martinez-Lopez et al., 2005). Localization to the +end depends on its microtubule binding domain, which is also conserved in the paralogues NAV2 and NAV3. Navigators are large proteins of about 250 kDa, which are homologues of unc-53 in *C. elegans*, a protein playing crucial roles in cell migration and axonal guidance. They share a C-terminal AAA ATPase domain of unknown function. NAV2 and NAV3 contain an N-terminal CH-domain that is also present in unc-53 (Peeters et al., 2004). Several splice isoforms and alternative start codons have been described (Maes et al., 2002). An alternatively spliced exon of Nav1 contains a putative nuclear localization signal (NLS) (Peeters et al., 2004). This putative NLS is interesting in light of earlier reports that describe a cytoplasmic as well as nuclear localization of NAV2 (Ishiguro et al., 2002; Merrill et al., 2002). NAV1 is mainly expressed in the heart and skeletal muscle, NAV2 is quite ubiquitously expressed, and NAV3 is (mostly) brain-specific (Coy et al., 2002; Maes et al., 2002; Peeters et al., 2004).

Decreased expression of NAV2 was observed in dorsal root ganglia of vitamin A-deficient embryos. Severe vitamin-A deficiency during development resulted in morphological changes and even total lack of these ganglia, which contain the cell-bodies of bipolar sensory neurons (Merrill et al., 2002). In line with these findings are severe sensory deficits of mice hypomorphic for NAV2 (Peeters et al., 2004).

Chapter 2

Visualization of Proteins and their Dynamics in vivo

The goal of modern cell biology is to understand protein behavior not only in an artificial system, but in the cellular context. During fixation of cells, all information about protein dynamics is lost, making it impossible to distinguish protein molecules that are permanently immobilized on a scaffold from transiently bound ones. It is therefore important to study protein dynamics in vivo in order to comprehend protein function.

In this chapter, I first outline the main determinants of protein dynamics in relationship to function, and then continue to describe how fluorescence-based methods can be used to measure protein behaviour in living cells.

2.1. Determinants of protein dynamics and function

The intracellular pool of a given protein can be described by several parameters, the most important of which are concentration, localization, diffusion and binding behavior of the protein. Together with the sequence and structure of the protein and information about its stability, they grant insight into protein function.

Localization of a protein is partly determined by specific targeting domains in its sequence. For example, a nuclear import signal allows active transport into the nucleus of a cell. However, while the overall localization of a protein often remains constant, single molecules are diffusing freely and binding transiently to varying interaction partners. Obviously, the amount of protein molecules bound to these partners not only depends on binding affinities, but also on the overall concentration of protein and binding partners.

2.1.1. Concentration

Structural proteins like histones, actin or tubulin are very abundant and each comprise several percent of the total protein pool, corresponding to millions of molecules per cell. The other extreme are proteins that act in signaling cascades, where few copies might suffice. Protein concentration is regulated by gene expression and RNA stability and translation on the one hand, and protein degradation on the other hand. Proteins can be expressed cell type specific (for example hemoglobin in erythrocyte progenitors), and the contribution of a given protein to the total protein pool is cell type dependent. Tubulin constitutes about 3% of the total protein content in 3T3 cells and neuroblastoma cells (Chafouleas et al., 1981; Hiller and Weber, 1978; Olmsted, 1981), but up to 20% in neurons (Hiller and Weber, 1978). Protein concentration is not only cell type dependent, but can also be regulated during the cell cycle or upon signaling (Wang et al., 2006).

2.1.2. Localization

Subcellular domains vary greatly in their properties (like structure, pH value, molecular composition). Therefore, the localization of a protein depends on its function - and the functionality of a protein in turn depends on its localization. For example, most receptors for extracellular signals are located at the plasma membrane, while proteins involved in DNA replication and translation reside in the nucleus. The intracellular localization of a protein can therefore provide first clues towards understanding its function. Protein localization can change during the cell cycle or upon signaling. Several mutations in tumor suppressor genes that

facilitate cancer development have been shown to involve protein mislocalization (Fabbro and Henderson, 2003).

2.1.3. Diffusion and transport

The overall distribution of a protein pool might remain constant over time, but this does not necessarily reflect single molecule behavior. Individual protein molecules can passively diffuse through the cell, or be actively transported. The more mobile a given protein, the faster its overall distribution pattern can change.

Uniform distribution of a molecule is energetically most favorable. If an external disturbance (like a concentration gradient) is applied, the system relaxes into the most favorable state by relocalization of molecules. This process depends on the concentration gradient and the mobility of the protein, and can be described by Fick's second law of diffusion,

$$\frac{\partial}{\partial t} c(\bar{x}, t) = D \nabla^2 c(\bar{x}, t) \quad (\text{Eq. 2.1})$$

where ∇ is the nabla operator that denotes the derivative of a function in all spatial dimensions, $c(\bar{x}, t)$ the concentration at position \bar{x} , and D the diffusion coefficient. Assuming that all diffusing molecules M were localized to a single plane/line/spot (1-/2-/3- dimensional diffusion, $r = 0$) at $t = 0$, the solution to (Eq. 2.1) is

$$c(r, t) = \frac{M}{(4\pi Dt)^{d/2}} e^{-\frac{r^2}{4Dt}} \quad (\text{Eq. 2.2})$$

where r denotes the distance from the initial source and d the dimensionality of diffusion (1/ 2/ 3D). The initially infinitively concentrated source spreads into a Gaussian distribution with a spread of $\sqrt{2Dt}$ at full width half maximum. The spread of diffusing molecules is independent of the dimensionality of diffusion, whereas the drop of concentration at $r = 0$ increases exponentially with dimensionality.

The diffusion coefficient of a given molecule depends on the temperature T (in Kelvin), the viscosity η of the solvent and the hydrodynamic radius r_h of the molecule,

$$D = \frac{k T}{6 \pi \eta r_h} \quad (\text{Eq. 2.3})$$

Ultracentrifugation of a purified protein in a buffer of known viscosity has long been used to determine the protein diffusion coefficient and thus its hydrodynamic radius. The hydrodynamic radius provides some insight into the shape of a protein and its incorporation in protein complexes. Turning this relationship around, the diffusion coefficient of a molecule of known hydrodynamic radius can be exploited to gain information about the viscosity of the surrounding medium. This technique was for example used to show that the viscosity of the cytoplasm does not differ from that of the nucleus (Seksek et al., 1997), and to reveal a drop in viscosity upon activation of *Dictyostelium* cells (Potma et al., 2001).

Eukaryotic cells mainly contain water, but the high concentration of proteins and other macromolecules, and the subdivision of the cytoplasm by intersecting membranes. This has hardly any influences on the mobility of small molecules like water, but can hamper the diffusion of larger protein molecules, a phenomenon known as anomalous diffusion (Banks and Fradin, 2005). Anomalous diffusion leads to a time-dependent decrease of the observed diffusion constant $D(t) = \Gamma t^\alpha$, dependent on the parameter α describing the degree of anomaly, and the constant Γ , for 3D-diffusion leading to a rewritten relationship between the mean square displacement (MSD), $\langle r^2(t) \rangle$, and the diffusion coefficient D :

$$\underbrace{\langle r^2(t) \rangle = 6Dt}_{\text{normal}} \rightarrow \underbrace{\langle r^2(t) \rangle = 6\Gamma t^\alpha}_{\text{anomalous}} \quad (\text{Eq. 2.4})$$

Diffusion is a passive process that is fast over short distances, but gets very slow over long distances, for example in axons. Energy dependent active transport via motor proteins greatly increases displacement rates. Active transport of a protein can be suspected, if its MSD increases more rapidly than linear with time.

2.1.4. Binding behavior

Hardly any proteins are chemically so inert that they do not interact with other macromolecules in the cell, and their function and dynamic behavior are at least partly determined by their reversible interaction with other proteins, DNA, RNA or membranes.

The reversible binding of a protein P to a scaffold S ,



can be described by two rate constants: the rate of binding k_{on} and the rate of dissociation k_{off} . At equilibrium, the binding and dissociation reactions are balanced:

$$k_{on} [P][S] = k_{off} [PS] \quad (\text{Eq. 2.6})$$

k_{on} and k_{off} can be combined into the equilibrium constant K_{eq} and its reciprocal, the dissociation constant K_D (in mole), which is a measure for the affinity of P for S .

$$K_{eq} = \frac{k_{on}}{k_{off}} = \frac{[PS]}{[P][S]} \rightarrow K_D = \frac{k_{off}}{k_{on}} \quad (\text{Eq. 2.7})$$

The half-life of an “inert” interaction (affinities are constant) is linked to the dissociation constant by

$$t_{1/2} = \frac{\ln(2)}{k_{off}} \quad (\text{Eq. 2.8})$$

which allows one to calculate k_{off} from measured half-lives of association. The half-life can range from milliseconds for weak interactions to hours for the interaction between histones and DNA (Kimura and Cook, 2001).

The interaction between a protein and its binding partners can be regulated by numerous means:

1. Most scaffolds contain several binding sites for a given protein, which can influence one another. If the binding is cooperative, a bound molecule facilitates the binding of consecutive molecules. This leads to the local accumulation of a protein, as can be seen for single strand binding protein (SSB) along DNA (Ferrari et al., 1994). If the binding is anti-cooperative, a bound molecule inhibits the binding of consecutive molecules.
2. When several proteins share the same binding partner to which they bind mutually exclusively, they compete. Then binding depends not only on the concentration of protein P_1 and its affinity for S , but also on the relative concentration of the competing protein P_2 and its affinity for S .
3. Proteins can be part of mutually exclusive complexes with different function, often regulated by external signals or during the cell cycle.
4. Many proteins can bind to themselves or other copies of the same protein, which can influence protein behavior. Intramolecular binding can result in the masking of an interaction domain, and effectively sequester the protein as can be seen for the autoinhibition of CLIP-170 (Lansbergen et al., 2004). On the other hand, intermolecular binding that does not mask the interaction domain might increase the local concentration of binding domains, thereby facilitating binding. This might explain why most +TIPs need at least two MT-binding domains to bind microtubules efficiently (Slep and Vale, 2007).
5. Proteins that are overexpressed tend to accumulate in aggregates. Aggregated proteins are often inaccessible for interacting proteins and lose their binding abilities.
6. The most striking naturally occurring multimerization is the polymerization of cytoskeletal proteins – obviously tubulin and microtubules differ greatly in their ability to bind other proteins.

Traditionally, binding of proteins is assessed by *in vitro* assays. However, this does not conserve the local environment encountered by a protein *in vivo*, which could change binding properties. To understand protein function, it is therefore necessary to determine its localization, mobility and binding partners in the cellular context.

2.2. Using fluorescence to visualize proteins

Single cells are far too small to be seen by the human eye. Visualization of plant and eukaryotic cells and bacteria only became possible with the invention of light microscopy in the 17th century, and its subsequent improvement. In conventional light microscopy, light passing through the specimen gets absorbed, generating contrast. Most eukaryotic cells contain proteins, nucleic acids, and membranes that, unlike the cell walls of plants, hardly absorb light of visible wavelengths. Therefore, although the resolution became high enough to be able to visualize single cells and their internal structure, lack of contrast prevented this in untreated samples.

Several approaches were taken towards improving the visualization of cellular structures. Initial ideas were based on using dyes that bind to membranes, DNA, or

specific proteins. Having to fix cells before staining remained a problem, as fixation itself can alter cellular structures (Hoetelmans et al., 2001) and precludes visualization of any dynamic processes.

Searching for other possibilities to generate contrast from cells led to the development of differential interference contrast (DIC) microscopy in the 1950s (Pluta, 1994). Differences in refractive indices result in a phase-shift of polarized light. DIC uses interference between those phase-shifted wave-fronts to generate contrast. In cells, differences in refractive indices are found between membranes and aqueous solutions, but not inside the cytoplasm, enabling the visualization of all membrane enclosed structures but leaving the cytoplasm without contrast differences.

Colored dyes that specifically stain DNA, membranes or some proteins have been known for a long time, but not all dyes can be combined, and they are only available for a small percentage of proteins. The discovery of small fluorescent dyes like Cy5 or rhodamine, which can be covalently bound to proteins, in combination with the broader availability of antibodies made specific visualization possible for most proteins against which antibodies are available (Silverstein, 2004). Antibody-based visualization requires fixed cells, only allowing a static image of protein localization and introducing fixation and other artifacts.

In order to visualize proteins in vivo, the purified protein of interest can be covalently linked to a small dye and subsequently reintroduced into a single cell by microinjection. This technique is laborious, which has stimulated the development of visualization methods that require neither fixation nor microinjection of cells. The most widely known approach is the use of fluorescent proteins, where an autofluorescent protein (often green fluorescent protein, GFP) is fused to the protein of interest by genetic means.

One should realize that fluorescent proteins are large tags (25-30 kDa), which can impair the function of fusion proteins. EB3 for example can still bind to microtubule ends as EB3-GFP fusion protein but is impaired in its binding to CLIP-170, while GFP-EB3 still binds to CLIP-170 but is largely impaired in its binding to microtubule ends. To circumvent these possible problems, the FAsH/ReAsH-system was developed (Griffin et al., 1998). It consists of a 6 aminoacid tag that can even be inserted into a helix-sequences, and an arsenic dye that can penetrate the cell membrane and only fluoresces when it is bound to the specific tag sequence (Adams et al., 2002). Despite its advantageous size, the FAsH/ReAsH tag is not broadly used, possibly because of its toxicity and the low signal-to-noise ratio (SNR) that can be obtained with a single tag (Miller and Cornish, 2005).

2.2.1. Green Fluorescent Protein (GFP)

Green fluorescent protein (GFP) was discovered by Shimomura et al. (1962) when they were isolating the blue luminescent protein Aequorin from *Aequorea victoria* jellyfish and found another protein that fluoresced green when excited with UV-light, but it took another 30 years before the gene sequence of GFP was identified (Prasher et al., 1992).

Fluorescence of GFP is intrinsic and does not require external cofactors. Introducing DNA coding for GFP into prokaryotic or eukaryotic cells results in the production of fully functional fluorescent protein (Chalfie et al., 1994). Introducing

point mutations has improved the maturation speed and photostability of GFP (Yang et al., 1996). Mutation of amino acids around the fluorophore generated fluorescent proteins with shifted absorption and emission spectra. Yellow fluorescent protein (YFP) and cyan fluorescent protein (CFP) (Miller et al., 1999) are now widely used, for example in FRET experiments (see chapter 2.5.3).

Fluorescent proteins have also been discovered in other species (Matz et al., 1999). Tetrameric red fluorescent DsRed from *Discosoma striata* (Fradkov et al., 2000) has been mutated into the monomeric mRFP (Campbell et al., 2002), making it more suitable for *in vivo* applications. The mRFP-derived family of mFruits (Shaner et al., 2004) has further expanded the fluorescence spectrum with which proteins can be visualized. Recently, the brighter far-red proteins Katushka (Shcherbo et al., 2007) and its monomeric mutant mKate (Merzlyak et al., 2007) have been reported.

Mutants of GFP have been engineered that either remain non-fluorescent until activated with a shorter wavelength laser pulse, or change their absorption and emission spectrum upon activation. These mutants are well suited to study protein transport and to test if subcellular domains are connected (Lippincott-Schwartz and Patterson, 2003).

The photophysical properties of GFP have been studied extensively, which improves the interpretation of experiments with GFP-fusion proteins. An electron is lifted from the ground state S_0 to the higher energetic state S_1 upon absorption of a photon by a fluorescent molecule. Relaxation back into S_0 is coupled to the emission of a photon with a longer wavelength than the exciting photon (due to the Stoke's shift). The excited electron can also enter a so-called triplet state where it changes its spin, which prohibits relaxation into the ground state. A GFP-molecule is trapped in the non-fluorescent triplet-state for on average 5-25 μ s. The precise value depends on the GFP variants studied and the measurement method used (Visser and Hink, 1999; Widengren et al., 1999).

GFP can also "blink" into a longer lived non-fluorescent state in addition to the transition into the triplet state. The average lifetime of this off-state was reported to be 1.6 s *in vitro* (Garcia-Parajo et al., 2000) and 2.3 s for a H2B-GFP fusion protein *in vivo* (Ibrahim, 2006), which is independent of the excitation laser power. The frequency with which individual GFP-molecules "blink" into the darkstate increases with used laser power, and the maximum emission intensity is reached at 1.5 kW/cm², above which the increase in excitation intensity is counteracted by an increase in "blink" frequency (Garcia-Parajo et al., 2000).

2.3. Fluorescence as a tool to measure protein dynamics

The advent of GFP not only revolutionized cell biology (Tsien, 1998), but also the study of protein dynamics (reviewed by Lippincott-Schwartz et al., 2001). Techniques that make use of fluorescence to study protein behavior can be divided into four groups:

1. single molecule techniques that track individual fluorescent molecules in time and space;
2. ensemble techniques that look at the average behavior of a protein (for example FRAP);

3. single molecule techniques that do not reveal spatial information (for example FCS);
4. attempts to simultaneously track all fluorescent molecules in time and space.

2.3.1. Laser Scanning Microscopy (LSM)

Conventional epifluorescent microscopy does not block out-of-focus light, which results in blurry images with low resolution in the z-axis. To eliminate out-of-focus light, a pinhole is introduced in the beam path in confocal microscopy, which reduces the imaged area to a diffraction limited spot. Moving the laserbeam with mirrors across the sample in X- and Y- direction generates a two-dimensional image. In the early days of confocal microscopy (the 1950s), the introduction of a pinhole blocked most of the emitted fluorescence, and high excitation intensities were therefore needed to generate a reasonable fluorescent signal, resulting in fast photobleaching. Advent of computer systems, improved detectors, and introduction of laser technology to the field of bio-imaging in the 1980s helped to overcome this drawback. In confocal laser scanning microscopy (CLSM), a laser beam is focused through an objective onto the specimen. The emitted fluorescence passes through the objective and the pinhole onto a detector. The detector used in most commercially available systems is a photo-multiplier tube that registers about 10% of the incoming photons.

The laser beam used in CLSM can be deflected by mirrors in X- and Y-direction to generate a two-dimensional image. Three-dimensional images are achieved by moving the focal plane (or sample) in Z-direction and repeating X-Y-scans. The laser dwell time at a given X-Y-Z-position determines on the one hand imaging speed and on the other hand image intensity. As temporal resolution comes at the expense of spatial resolution and vice versa, image size and sampling rate need to be optimized for every application, especially when following dynamic processes.

Excitation of fluorophores can also destroy them. The rate with which fluorophores are bleached (destroyed) depends on their photostability and the excitation power. When imaging cells expressing low amounts of fluorescent protein, increasing the laser power might therefore not improve image quality. Photobleaching needs to be reduced as much as possible in time-lapse imaging, so that the image quality does not degrade too much over time. Destroyed fluorophores often contain free radicals that are cytotoxic, but the barrel-structure of GFP protects the cell from most toxic effects of photodestroyed GFP molecules.

2.3.2. Fluorescence Speckle Microscopy (FSM)

Microtubules in cells that contain a small fraction of fluorescently labeled tubulin molecules incorporate these randomly and appear speckled. These speckles can be followed over time, tracking their movement, appearance and disappearance (reviewed in Danuser and Waterman-Storer, 2006). The signal-to-noise ratio and number of traceable speckles is low if individual speckles are due to the absence/presence of a single fluorescent molecule in a diffraction limited spot. More information can be gathered from cells with higher labeling ratio, where speckles arise

from statistical variations in protein number and each contain several fluorescent molecules (Danuser and Waterman-Storer, 2006).

FSM is often used in so-called “kymograph” analyses to study microtubule dynamics or protein turnover along a microtubule, but more sophisticated analysis of FSM images enables probing actin cytoskeleton dynamics (Danuser and Waterman-Storer, 2006).

2.3.3. Fluorescence Correlation Spectroscopy (FCS)

All molecules move randomly, a process called Brownian motion. In addition to this stochastic variation in their location, fluorescent molecules also switch between fluorescent and non-fluorescent states (as described for GFP in chapter 2.2.1). This leads to fluctuations in the amount of fluorescence that can be detected from a single molecule at a given position. Most of these fluctuations cancel each other out in classical fluorescence microscopy, which visualizes the sum of fluorescence emitted from many molecules. The remaining fluctuations are encountered as noise that worsens the signal-to-noise ratio (SNR). These fluctuations, however, contain hidden information about the dynamics of the system.

First applications of fluctuation spectroscopy were described at the beginning of the 20th century by Svedberg and Inouye (1911), who investigated light scattering of colloidal gold particles. Fluorescence correlation spectroscopy (FCS), which uses fluctuations in fluorescence intensity to gather information about molecule behavior, was introduced in the 1970s (Elson and Magde, 1974; Magde et al., 1972; Magde et al., 1974). Confocal optics (Qian and Elson, 1991) and improvements of the signal to noise ratio and sensitivity facilitated single molecule detection (reviewed in Maiti et al., 1997).

Extensive descriptions of the theoretical basics of fluorescence correlation spectroscopy have been published (Elson and Magde, 1974; Thompson, 1991). The key concept in fluorescence correlation spectroscopy (and other fluctuation-based methods) is the autocorrelation function $G(\tau)$, which describes the average self-similarity of the intensity I for increasing time-intervals τ .

$$G(\tau) = \frac{\langle I(t)I(t+\tau) \rangle}{\langle I \rangle^2} = 1 + \frac{\langle \delta I(t)\delta I(t+\tau) \rangle}{\langle I \rangle^2} \quad (\text{Eq. 2.9})$$

The deviation of the intensity from the average, $\delta I(t)$, obviously depends on the deviation in the concentration of fluorescent particles δC , but also on their position r in the excitation and detection volume, because excitation and detection efficiency are position-dependent:

$$\delta I(t) = \eta \int_V W(r) \delta C(t, r) \quad (\text{Eq. 2.10})$$

where η is the molecular brightness, expressed as the count rate per molecule and second. In confocal microscopy, the detection efficiency $W(r)$ can be approximated with a 3D Gaussian curve where ω_{xy} and ω_z describe the distance in lateral and axial direction at which the intensity I decays to $I = I_0 \cdot e^{-2}$ (Rigler et al., 1993):

$$W(r) = e^{-2 \frac{x^2 + y^2}{\omega_{xy}^2}} \cdot e^{-\frac{z^2}{\omega_z^2}} \quad (\text{Eq. 2.11})$$

The autocorrelation function (Eq. 2.9) can be solved for i independent species of freely diffusing molecules by inserting equations (Eq. 2.2), (Eq. 2.10) and (Eq. 2.11).

$$G(\tau) = 1 + \frac{1}{\langle N \rangle} \cdot \sum_i \frac{1}{\left(1 + \frac{\tau}{\tau_{dif,i}}\right) \sqrt{1 + \left(\frac{\omega_{xy}}{\omega_z}\right)^2 \frac{\tau}{\tau_{dif,i}}}} \quad (\text{Eq. 2.12})$$

The average concentration of fluorescent particles is denoted by $\langle N \rangle$, and $\tau_{dif,i}$ the average time a molecule of species i remains in the observation volume, depends on its diffusion coefficient:

$$D_{tran} = \frac{\omega_{xy}^2}{4 \tau_{dif}} \quad (\text{Eq. 2.13})$$

The average number of fluorescent molecules in the observation volume can easily be calculated from the amplitude of the autocorrelation function ($\tau = 0$):

$$G(0) = 1 + \frac{1}{\langle N \rangle} \quad (\text{Eq. 2.14})$$

The solution for the autocorrelation function described in (Eq. 2.12.) is based on the assumption that the molecular brightness η of a fluorophore remains constant. This does not hold for most fluorophores at commonly used excitation powers, because fluorophore transition into the triplet state (see chapter 2.2.1) often causes fluorescent “flickering”. If fluorescence fluctuations arising from inter- and intramolecular reactions (like transition into the triplet state) are much faster than fluctuations caused by molecular movement, the two dynamics can be separated:

$$G_{total}(\tau) = X_{kinetics}(\tau) \cdot G_{motion}(\tau) \quad (\text{Eq. 2.15})$$

Triplet kinetics can be described with a simple exponential decay, which depends on the fraction T of molecules in triplet state and the average time $\tau_{triplet}$ a molecule remains in the triplet state

$$X_{triplet}(\tau) = 1 - T + T \cdot e^{-\frac{\tau}{\tau_T}} \quad (\text{Eq. 2.16})$$

Inserting equations (Eq. 2.16) and (Eq. 2.12) into equation (Eq. 2.15) yields the most widely used description of 3D diffusion in the presence of a non-fluorescent triplet-state (Widengren et al., 1995).

$$G(\tau) = 1 + \frac{1}{\langle N \rangle} \cdot \frac{1 - T + T e^{-\tau/\tau_T}}{(1 - T)} \cdot \sum_i \frac{1}{\left(1 + \frac{\tau}{\tau_{dif,i}}\right) \sqrt{1 + \left(\frac{\omega_{xy}}{\omega_z}\right)^2} \frac{\tau}{\tau_{dif,i}}} \quad (\text{Eq. 2.17})$$

Usually, a theoretical autocorrelation curve is fitted to experimentally obtained data by a Levenberg-Marquardt non-linear least square fitting algorithm.

The autocorrelation curve has also been solved for other dynamic processes like two-dimensional diffusion (for example in membranes), directed transport, and anomalous diffusion, broadening the applicability of FCS in addressing biological questions. Several reviews in recent years describe the broad range of biological questions addressed with FCS (Gosch and Rigler, 2005; Kim and Schwille, 2003; Medina and Schwille, 2002; Thompson et al., 2002; Vukojevic et al., 2005), that range from intracellular protein concentrations and ligand-receptor interactions to gene expression and the formation of protein complexes.

Much of modern cell biology is based on GFP-fusion proteins. In order to better understand results from these experiments, the behavior of GFP has been studied extensively, mostly using FCS. Intracellular GFP is relatively inert and does not bind to other macromolecules. Measuring the diffusive behavior of GFP in subcellular compartments therefore relates to their viscosity. Studies of Chen et al. (Chen et al., 2002) show, that the effective viscosity encountered by GFP in the cytoplasm ($D_{tran} = 25 \mu m^2/s$) and the nucleus ($D_{tran} = 23.5 \mu m^2/s$) is about three times higher than in aqueous solutions ($D_{tran} = 78 \mu m^2/s$). These findings are in line with a four-fold decrease of D in the cytoplasm and nucleus compared to an aqueous solution (Seksek et al., 1997).

The SNR in FCS experiments depends on the collection efficiency of the detector, the molecular brightness, and inversely on the number of molecules in the measurement volume. Confocal optics reduce the effective volume of standard FCS setups to less than 0.5 fl, with $\omega_{xy} \approx 0.25 \mu m$ and $\omega_z \approx 1.5 \mu m$ (Gao et al., 2007). Avalanche photodiodes (APDs) used as detectors in most FCS set-ups have a detection efficiency of about 80%, which is much higher than the PMTs used in CLSM set-ups.

A theoretical study by (Enderlein et al., 2005) shows, that diffusion coefficients and concentrations calculated from autocorrelation curves critically depend on the set-up of the experiment. Most FCS experiments are based on the measurement of a standard of known concentration and diffusion coefficient as a reference for the evaluation of the samples of interest, which eliminates most sources of errors (Enderlein et al., 2005). Autofluorescence in biological samples is another factor that can influence the interpretation of FCS experiments, especially when autofluorescence arises not from many dim sources, but from few bright sources that generate an autocorrelated signal (Brock et al., 1998). In contrast to plant cells, autofluorescence is only a minor problem in most cultured mammalian cells, as long as they are not subject to stressors (like prolonged visualization under the microscope).

2.3.4. Fluorescence Recovery After Photobleaching (FRAP)

FCS looks at small fluctuations around the average concentration with the aim not to disturb the system (although the continuously focussed laser beam locally heats the sample). A different approach is chosen in FRAP (Fluorescence Recovery After Photobleaching), where a fraction of intracellular fluorophores is deliberately rendered non-fluorescent through bleaching with high laser power, and the subsequent relaxation of the system to equilibrium is monitored (Houtsmuller and Vermeulen, 2001; Reits and Neefjes, 2001).

Like FCS, FRAP was developed in the 1970's. It was initially used to measure recovery of fluorescence after a round spot in the plasma membrane had been bleached (Axelrod et al., 1976). Under these circumstances, 50% of initial fluorescence has recovered after τ_{dif} , which depends on the apparent diffusion coefficient D , the correction factor γ that depends on the shape of the laser beam and the fraction of initially bleached molecules, and the width of the laser beam ω at which the laser intensity has dropped to $I = I_0 \cdot e^{-2}$.

$$\tau_{dif} = \frac{\omega^2 \gamma}{4D} \quad (\text{Eq. 2.18})$$

In the presence of an immobile fraction, which does not exchange with the surrounding unbleached molecules over the timecourse of the experiment, a mobile fraction R can be defined, which depends on the fluorescence intensity before bleaching F_i , the remaining fluorescence intensity F_0 directly after the bleach, and the maximum regained fluorescence intensity F_∞ .

$$R = \frac{F_\infty - F_0}{F_i - F_0} \quad (\text{Eq. 2.19})$$

For favorable bleach geometries and fluorescent molecules that purely recover due to their diffusion, the FRAP recovery curve can be described analytically. This gets more complicated if other processes than diffusion influence fluorescence recovery or if the bleach geometry is not favorable. Two approaches to the interpretation of more complex FRAP data have been developed. The first one uses evermore complicated formulas that try to encompass all the processes leading to the observed recovery. The second approach gathers as much data about the protein studied (concentration, unobstructed diffusion behavior) and tries to emulate measured FRAP recoveries by varying dynamic parameters in computer simulations (Farla et al., 2004; van den Boom et al., 2007; Sadegh Zadeh et al., 2007; Xouri et al., 2007). Most approaches that use computer simulations have been focused on nuclear proteins.

Sprague et al. (2004) have provided the most extensive evaluation of fluorescence recovery in a round bleached spot in the presence of diffusion and binding events. They assume 1) that the system is at equilibrium before bleaching, so that the total number of free binding sites, free molecules and bound molecules remains constant over the timecourse of the FRAP experiment, 2) that the fraction of bleached molecules is negligible compared to the total pool of fluorescent molecules, and 3) that bound molecules do not diffuse. This simplifies the functions that describe the system and enables an analytical description of FRAP recovery

for a single diffusing species in the presence of binding reactions. The average of the Laplace transform of the fluorescence intensity in the bleached spot is given by

$$\overline{frap}(p) = \frac{1}{p} - \frac{F_{eq}}{p} \left(1 - 2K_1(qw)I_1(qw)\right) \times \left(1 + \frac{k_{on}^*}{p + k_{off}}\right) - \frac{C_{eq}}{p + k_{off}} \quad (\text{Eq. 2.20})$$

This function contains Bessel functions of the first and second kind, and depends on the variables k_{on} , k_{off} , C_{eq} , F_{eq} , S_{eq} and D_{tran} , which demonstrates the complexity of numerical solutions to FRAP recovery curves. Sprague et al. demonstrate that can be simplified for recoveries that are dominated by either reaction kinetics or diffusion, and evaluate for which range of k_{on} and k_{off} these simplifications are applicable.

In nearly all interpretations of FRAP data, the concentration of immobile binding sites is assumed to remain constant over the time course of the experiment. This holds true for proteins that bind to DNA or along the microtubule lattice, but some focal adhesion proteins tend to turn over with comparable rates as the focal adhesions themselves. A theoretical framework has been described that allows to determine kinetic rates under conditions where the number of binding sites decays or grows exponentially (Lele and Ingber, 2006). This equation is even more complex than (Eq. 2.20), containing four exponential terms and several variables, making its usefulness for real applications doubtful.

Most fitting functions derived so far assume that bleaching is instantaneous, and the first post-bleach image is acquired immediately. This ensures that the bleach geometry can be described precisely and that all molecular movement can be followed in the FRAP curve. Modern confocal microscopes can image areas of about $10 \mu\text{m}^2$ with 10 Hz, making it tempting to approximate that molecules indeed remain static during the bleach. Most real applications on the other hand require several bleach iterations to achieve enough bleach depth and deal with molecules whose displacement between the bleach and acquisition of the first post-bleach image is not negligible, which might lead to the gross underestimation of diffusion coefficients and the misinterpretation of binding behavior (Weiss, 2004). Other factors that influence the measurement of FRAP and the quality of fitted parameters have been described concisely (Klonis et al., 2002).

In most interpretations of FRAP experiments, the only variable is the recovery of fluorescence intensity averaged over the bleached area. This neglects any spatial information that could be gathered from the experiment. A different approach is proposed by Seiffert and Oppermann (2005) who bleach a spot or strip and follow the fluorescence intensity over time perpendicular to the bleached area. This yields a Gaussian curve that slowly flattens and broadens. Neglecting any binding reaction, this can be treated as diffusion of bleached molecules according to (Eq. 2.1) and (Eq. 2.2). The intensity $I(r, t)$ at a given timepoint and position is dependent on the pre-bleach intensity I_0 and M , the amount of fluorescence lost during bleaching.

$$I(r, t) = I_0 - \frac{M}{(4\pi Dt)^{d/2}} \cdot e^{\frac{-r^2}{4Dt}} = I_0 - A(t) \cdot e^{\frac{-r^2}{2\omega^2}} \quad (\text{Eq. 2.21})$$

The spread of bleached molecules can also be described by a Gaussian distribution with amplitude $A(t)$ and the full width of half maximum ω (Seiffert and Oppermann, 2005). Comparing the two sides of (Eq. 2.21) reveals that the diffusion coefficient can be determined from a linear plot of ω^2 vs. t , based on

$$\omega^2 = 2Dt \quad (\text{Eq. 2.22})$$

Based on (Eq. 2.21), the dimensionality of diffusion d can be determined from a plot of $\log A$ vs. $\log t$, as can be appreciated by rewriting

$$A(t) = \frac{M}{(4\pi D)^{d/2}} \cdot t^{-d/2} \quad (\text{Eq. 2.23})$$

in logarithmic form:

$$\log A = -\frac{d}{2} \log t + \log \frac{M}{(4\pi D)^{d/2}} = -\frac{d}{2} \log t + K \quad (\text{Eq. 2.24})$$

FRAP experiments reveal the diffusion coefficient D of a given protein and its mobile fraction (the fraction of unbleached molecules exchanging with bleached ones over the timecourse of the experiment), but the processes that lead to the observed diffusion coefficient remain unresolved. Slower diffusion can be due to a more viscous environment, but also to transient binding to an immobile scaffold. A complementary technique to FRAP is FLIP (fluorescence loss in photobleaching), where a region of the cell is bleached repeatedly, and fluorescence intensity in other regions of the cell is followed. If the studied protein were restricted to the bleached area (i.e. trapped in a vesicle or specific patch on the plasma membrane), no loss of fluorescence in other regions of the cell is to be expected. If the protein were completely free diffusing, one would expect a uniform loss of fluorescence all over the cell. This technique has been used to study protein behavior in the nucleus (Hoogstraten et al., 2002; Phair and Misteli, 2000; Wachsmuth et al., 2003), nucleo-cytoplasmic shutteling (Koster et al., 2005), and the continuity of cell compartments. It is also useful in identifying regions of protein binding, as these will remain as fluorescent spots in an otherwise bleached cell.

2.4. Time-lapse imaging

The advent of computer systems that could store image data in real time led to a revolution in imaging and image processing. Before the wide availability of computer systems to store and process image data, extraction of image features was a very laborious task. Following few particles over time or analyzing the structural features of several images was therefore the limit of feasibility. Modern computer systems have automated most steps of image acquisitions and analysis, generating

much more datapoints and enabling sound statistic analysis of the results. Broad availability of imaging software, and their (relative) ease of use made time-lapse microscopy one of the most widely used research techniques. The broad scope of commercial imaging software on the other hand also limits its suitability, as it lacks specialized algorithms that are able to solve specific research questions.

Addressing a research question with time-lapse analysis can be divided into four steps that can be optimized: 1) image acquisition, 2) image preprocessing, 3) feature extraction, and 4) feature analysis (Meijering et al., 2008).

2.4.1. Image Acquisition

The ultimate goal of optimizing image acquisition is to generate images as fast as possible that are as good as possible with as little damage to the cells as possible. Obviously, these three goals are not to be seen independently of one another. Increasing the laser or lamp power will improve image quality - at the expense of photobleaching and phototoxicity; and increasing the frame rate will improve the time resolution - at the expense of image quality.

Still, many optimizations can be made that benefit both image quality and image speed. Fluorophores vary greatly in their photostability and phototoxicity, and their suitability might depend on the available imaging system. The optical path of the microscope (including filters and beamsplitters) needs to be adjusted to maximize detection efficiency, which is obviously influenced by the quality and settings of the photodetector.

Although cells are three-dimensional, it might be beneficial to image them in 2D to improve imaging speed, but one needs to first determine if the resulting loss of spatial information influences the data interpretation.

2.4.2. Image Preprocessing

The purpose of image preprocessing is to reduce artifacts of image generation and enhance image features without altering the image content. The most commonly encountered artifact is photobleaching during time-lapse imaging, which may disguise subtle changes in local intensities. Small movements of the stage or of cells might mask or enhance intracellular movements. Image registration (the alignment of all images in a time-series so that an immobile feature remains immobile) can correct for this (Goobic et al., 2005). In confocal microscopy, the point-spread-function (PSF) is elongated along the z-axis, which convolutes the images and reduces their z-resolution. Deconvolution can improve z-resolution, and several algorithms that either assume knowledge about the PSF or not have been described (Meijering et al., 2008).

Apart from these techniques that aim at counteracting imaging artifacts, image features can also be enhanced by background subtraction or contrast enhancement. More demanding is the proper application of filters to reduce noise and enhance image features without changing the image content (Meijering et al., 2008). Filtering algorithms can be divided into two groups: linear filters that reduce noise but also blur relevant features, and non-linear filters. Non-linear filters cause less blur, and range from simple median filtering to much more sophisticated ones that need careful fine-tuning to not alter image features.

2.4.3. Feature extraction/ tracking

Time-lapse imaging generates more information than can be analyzed manually, which led to the advent of computer-aided tracking in the 1980s (Berns and Berns, 1982). Since then, many tracking-algorithms have been published that differ in their complexity, and in their suitability for either cell-tracking or particle-tracking (reviewed in Meijering et al., 2006). Images of small particles are often diffraction limited, and the challenge of tracking them is to detect them. In contrast to small particles whose shape remains (relatively) constant over time, cells change their shape constantly, especially while migrating. The challenge in cell-tracking is to find a given cell back in consecutive frames even when its shape changed between frames.

2.4.3.1. Classical tracking algorithms

Classical tracking algorithms detect object trajectories by a two-step approach: 1) feature extraction (where are objects in this timeframe?), 2) feature linking (what is the relation between objects in consecutive frames?).

Discriminating objects of interest from background purely on intensity is the simplest approach to feature extraction, but also the most error prone, as bright noise easily results in false positive detection, and discriminating objects in a crowded environment is nearly impossible. Other algorithms have been described, that differ in their performance depending on the object tracked (Cheezum et al., 2001; Sbalzarini and Koumoutsakos, 2005). Detecting objects can be challenging, especially if the SNR is low or if objects need to be tracked in a crowded environment (Sage et al., 2005).

Linking objects in consecutive frames can be based on different criteria. For example, intensity, position, directionality or speed of movement (this requires linking objects in more than 2 frames) and shape (especially when tracking larger particles and cells) can all be used to link objects. This is relatively straightforward if no objects appear or disappear and all objects remain separated during the image sequence. Reality for biological tracking problems is non-ideal, with objects appearing, getting dimmer or disappearing due to photobleaching, particles merging, and crossing particle paths. This makes intracellular object tracking challenging (Kalaidzidis, 2007).

2.4.3.2. Tracking based on probabilities

Commonly used tracking approaches extract information from single frames and often only link two consecutive frames. These approaches thus ignore the majority of available data. If the SNR is low, the human eye is not able to discern particles in a single frame, but can follow moving objects in a timeseries. A comparable approach is taken by probability-based tracking algorithms. Traditional tracking algorithms are quite error prone, because they attempt to determine with 100% probability if a given bright spot is a particle, where precisely this particle is located, and how it is moving. Probability-based algorithms use all available information from previous frames to calculate the probability of a given spot to be a particle and its most probable trajectory. Probability-based approaches have long been used in other areas like people tracking, but tracking in biological samples is more challenging

and only just being developed (Smal et al., 2007), because particle behavior is less predictable and often suffers from a worse SNR.

2.4.4. Track analysis

Tracks in time-lapse imaging contain much implicit information. Initial examination of these tracks by eye may reveal some qualitative information about the process studied, but in order to quantify differences between experimental conditions or accurately describe particle behavior, explicit numeric values need to be extracted from the tracks. Extracted data can be roughly divided in three groups – geometry, diffusion and velocity.

Geometry measurements encompass not only the shape of measured trajectories (Is the particle moving in a confined environment? Are membranes divided in distinct patches?), but also the shape of the tracked object itself (How easily does a cell change its shape during migration?).

Measuring diffusivity tells something about the nature of particle movement. The mean square displacement (MSD) of a freely diffusing particle increases linearly with time. A smaller increase of the MSD over time than expected can be caused by anomalous diffusion or confined movement (MSD reaches a plateau in this case). A larger increase of the MSD over time on the other hand is caused by directed transport.

Velocity of a tracked cell reveals its migration speed, and the comparison between trajectory length and migration distance gives insight into the directionality of cell migration. Not only the velocity of a particle or cell is important, but also trajectory length, for example the number of frames a growing microtubule can be tracked, depends directly on the persistence of microtubule growth.

2.5. Measuring protein-interactions with fluorescence

Traditionally, protein-protein interactions are probed with yeast-two-hybrid screens, pull-down assays and immunofluorescence experiments. Binding is therefore investigated under non-physiological conditions – either in a different cell system or in fixed cells or in vitro. With the advent of GFP and other fluorescent proteins, the visualization of protein-protein interactions in vivo became feasible (reviewed in Hink et al., 2002).

2.5.1. Colocalization

Colocalization is the most basic measurement that is used for the description of possible protein interactions in vivo. Measurement of colocalization does not depend on complicated set-ups or the fit of a complicated formula and is therefore often used to confirm protein-interactions that were found in in vitro experiments. It needs to be stressed though, that colocalization of two proteins does not prove their binding, but merely that they can be at the same position at the same time.

Sound interpretation of colocalization experiments depends on precise overlap of the image for different fluorophores and the separation of signal generated from different fluorophores. In real colocalization experiments, emission spectra of the fluorophores often overlap and the beam path contains chromatic aberrations

resulting in image shift. Correction for these non-ideal situations are described in a comprehensive review by Bolte and Cordelieres (2006).

2.5.2. Fluorescence Cross-Correlation Spectroscopy (FCCS)

Molecular interactions have been studied with FCS based on changes of the diffusion coefficient D upon binding. D is inversely proportional to the hydrodynamic radius r_h of the diffusing molecule, see (Eq. 2.3), which in turn is proportional to the cubic root of the mass of the molecule $r_h \sim \sqrt[3]{M}$. Meseth et al. (1999) have examined the ability of FCS to separate two species with identical brightness based on their diffusion time, and concluded that the diffusion times need to differ at least 1.6-fold, which corresponds to a fourfold mass difference. Therefore, FCS can not distinguish between monomers and dimers, or between unbound or bound molecules if the unlabelled binding partner is less than three times bigger than the fluorescent one.

Better suited to detect interactions is fluorescence cross-correlation spectroscopy, a technique that makes use of two differently labelled fluorescent species (Schwille et al., 1997). In analogy to FCS (Eq. 2.9), the cross-correlation function for two species A and B is described as

$$G_{AB}(\tau) = \frac{\langle \delta F_A(t) \cdot \delta F_B(t + \tau) \rangle}{\langle \delta F_A(t) \rangle \langle \delta F_B(t) \rangle} \quad (\text{Eq. 2.25})$$

In parallel to the solution for FCS, the cross-correlation curve for freely diffusing complexes can be described with

$$G_{AB}(\tau) = 1 + \frac{\langle C_{AB} \rangle}{V_{\text{eff}} (\langle C_A \rangle + \langle C_{AB} \rangle) (\langle C_B \rangle + \langle C_{AB} \rangle)} \cdot \frac{1}{\left(1 + \frac{\tau}{\tau_{\text{diff}, AB}} \right) \sqrt{1 + \left(\frac{\omega_{xy}}{\omega_z} \right)^2} \frac{\tau}{\tau_{\text{diff}, AB}}} \quad (\text{Eq. 2.26})$$

The detection volumes of the different dyes overlap completely in the ideal FCCS set-up, but small differences in the detection volumes almost always remain in real FCCS experiments, which need to be taken into account. Commonly used dye pairs have partly overlapping excitation and/or emission spectra, resulting in “leaking” of the shorter-wavelength dye into the detection channel of the longer-wavelength dye. Solutions to the cross-correlation function that correct for these shortcomings of real experiments have been published (Weidemann et al., 2002).

FCCS was first realized experimentally in 1997 (Schwille et al., 1997). Since then, FCCS has been used to study a variety of processes. These include protein cleavage, DNA-protein interactions and nucleotide hybridization in vitro, and enzymatic cleavage, signaling pathways and intracellular trafficking in vivo (reviewed in Bacia et al., 2006).

The advantage of FCCS over colocalization studies is its high sensitivity and the probing of interaction rather than purely colocalization. The spatial constraints of FRET (discussed in chapter 2.5.3) do not apply for FCCS, making it also suitable to study non-adjacent members of a large complex. This comes at a tradeoff though,

because FCCS only detects moving objects, and is “blind” to slow molecules that are bound to the same scaffold for a longer period of time.

2.5.3. Fluorescence Resonance Energy Transfer (FRET)

Fluorescence resonance energy transfer (FRET) detects the close proximity of two fluorophores of which the excitation spectrum of one overlaps with the emission spectrum of the other. For a single fluorophore, most excitation energy gets converted into fluorescence emission, and non-fluorescent relaxation processes like triplet decay play a subordinate role. In the presence of a second fluorophore (the acceptor), which can be excited with the energy normally contained in the emitted photons of the donor, a non-fluorescent relaxation process can occur, which has been termed FRET. This radiation-less energy transfer is due to dipole-dipole-interactions, which depends on the orientation of donor and acceptor, and their distance. FRET efficiency E decays with the 6th power of the inter-fluorophore distance R .

$$E = \frac{1}{1 + \left(\frac{R}{R_0} \right)^6} \quad (\text{Eq. 2.27})$$

The Förster distance R_0 , at which the FRET efficiency drops to 50%, is constant for a given experiment. It only depends on the fluorescent molecules involved, and their orientation towards one another (Hink et al., 2002). The most extensively used fluorophore couple for intracellular applications is CFP and YFP, with $R_0 \approx 50 \text{ \AA}$ (Hink et al., 2002). The short distance over which efficient FRET occurs, ensures that two fluorophores exhibiting FRET are indeed very close to one another, and thus most probably bound to one another. The inverse, i.e. that binding partners exhibit FRET, does not hold true in all cases, as the two fluorophores could be unfavorably aligned or be positioned far from the binding domains.

FRET can not only probe intermolecular binding reactions, but also intramolecular interactions (or rearrangements). Many methods have been developed to visualize FRET. They are all based on measuring deviation of either donor or acceptor fluorescence properties from the non-FRET state (Lippincott-Schwartz et al., 2001).

2.5.4. Fluorescence cumulant analysis and Photon counting histogram

FCS investigates the motile behavior of a given protein (the time domain), but does not look at the brightness of individual fluorescent particles (the amplitude domain). This allows discrimination of complexes that differ at least four times in weight (Meseth et al., 1999). If the mass difference is less than four times, heteromeric complexes can still be studied by FCCS experiments – but when looking at homodimerization reactions, both approaches fail.

While homodimerization results in little change in the time domain, it doubles the signal in the amplitude domain. The first statistical approach to discern fluorescent particles based on the amplitude of fluorescence fluctuations was made nearly 20 years ago (Qian and Elson, 1990). This approach has been further elaborated into fluorescence cumulant analysis (FCA Muller, 2004), which uses higher order

factorial cumulants to determine the brightness of a fluorescent species and separate mixtures of fluorescent species based on their brightness.

A different approach to extract information about the molecular brightness of fluorescent species has been taken in photon counting histogram (PCH) analysis (Chen et al., 1999). Due to the quantummechanical nature of photons, the probability to collect N photons per sampling time from constant light source is given by a Poisson distribution

$$p(N) = \frac{\bar{N}^N e^{-\bar{N}}}{N!} \quad (\text{Eq. 2.28})$$

Due to fluctuations in fluorescence intensity, experimentally obtained PCH curves of fluorescent proteins show a broadening of the curve into a super-poissonian distribution. Fluctuations in fluorescence intensity are caused by fluctuations in particle number, and inhomogenous excitation and detection efficiency over the sample volume. Information about the number of fluorescent molecules in the detection volume and their molecular brightness can be extracted from the deviation of the experimentally obtained PCH curve from a Poissonian distribution.

PCH has been used to show that the molecular brightness of EGFP does not differ between the nucleus and the cytoplasm (Chen et al., 2002), but other applications of PCH or FCA have remained very limited.

Chapter 3

Role of CLASP2 in Microtubule Stabilization and the Regulation of Persistent Motility

Ksenija Drabek*
Marco van Ham*
Tatiana Stepanova
Katharina Draegestein
Remco van Horssen
Carmen Laura Sayas
Anna Akhmanova
Timo ten Hagen
Ron Smits
Riccardo Fodde
Frank Grosveld
Niels Galjart

* contributed equally

adapted from:
Current Biology 2006; 16, 2259-64

3.1. Summary

In motile fibroblasts stable microtubules (MTs) are oriented towards the leading edge of cells (Bulinski and Gundersen, 1991). How these polarized MT arrays are established and maintained, and the cellular processes they control, have been the subject of many investigations. Several MT “plus end tracking proteins”, or +TIPs (Schuyler and Pellman, 2001), have been proposed to regulate selective MT stabilization, including the CLASPs (Akhmanova et al., 2001), a complex of CLIP-170, IQGAP1 and activated Cdc42 or Rac1 (Fukata et al., 2002), a complex of APC, EB1 and mDia1 (Wen et al., 2004), and the actin-MT crosslinking factor ACF7 (Kodama et al., 2003). Using mouse embryonic fibroblasts (MEFs) in a wound healing assay, we show here that CLASP2 is required for the formation of a stable, polarized MT array, but that CLIP-170 and an APC-EB1 interaction are not essential. Persistent motility is also hampered in CLASP2-deficient MEFs. We find that ACF7 regulates cortical CLASP localization in HeLa cells, indicating it acts upstream of CLASP2. Fluorescence-based approaches show that GFP-CLASP2 is immobilized in a bimodal manner in regions near cell edges. Our results suggest that the regional immobilization of CLASP2 allows MT stabilization and promotes directionally persistent motility in fibroblasts.

3.2. Results and Discussion

3.2.1. CLASP2 regulates MT stability and directionally persistent motility in MEFs

We generated a CLASP2 knock out allele using homologous recombination in embryonic stem (ES) cells (Fig. 3-1A). Mouse embryonic fibroblasts (MEFs) were derived from E13.5 day CLASP2 knock out embryos and wild type littermates. RT-PCR analysis showed that *CLASP2* mRNA expression downstream of the targeting site is abolished in knock out MEFs (Figure 3-S1A). Western blot analysis confirmed that no functional CLASP2 is produced in the knock out fibroblasts (Fig. 3-1B). The levels of tubulin (Fig. 3-1B), CLASP1, CLIP-115 and -170, EB1, p150(gGlued), and actin (Fig. 3-S1B), were similar in CLASP2 knock out and wild type MEFs.

In spite of the intrinsic dynamic nature of MTs (Desai and Mitchison, 1997), a subset of these fibers is stable and does not appear to undergo net growth or shrinkage (Schulze et al., 1987). In migrating cells polarized, stable MTs are post-translationally modified, and can be specifically stained by antibodies (Bulinski and Gundersen, 1991). We examined whether CLASP2 knock out cells could form stable MTs efficiently in a wound healing assay (Liao et al., 1995). In wild type and CLASP2 knock out fibroblasts MT arrays were present after serum induction (Figure 3-S2A-D). Furthermore, CLASP1, EB1, EB3, CLIP-115 and CLIP-170 (Fig. 3-S2I-X and data not shown) were detected at MT ends in both cell types. However, the formation of stable MTs, as measured with antisera against acetylated tubulin (Fig. 3-1C, D) and detyrosinated (glu-tub) alpha-tubulin (Fig. 3-S2E-H), was hampered in knock out cells. Quantification of fluorescent signals revealed that the ratio of total MTs in knock out versus wild type MEFs was 89% ($P < 0.05$), whereas that of stable MTs was 52% ($P < 0.0001$; Fig. 3-1D).

Cold- and nocodazole-resistant MTs represent distinct subsets of stable MTs (Baas et al., 1994; Guillaud et al., 1998). Their levels are reduced in CLASP2 knock out MEFs (Fig. 3-1E, F), confirming that a CLASP2 deficiency affects stable MTs. Western blot analysis indicated that in CLASP2 knock out cells the formation of stable MTs is hampered in the first hours of wound healing (Fig. 3-S3F). Since stable MTs are not absent in CLASP2 knock out cells, CLASP2-independent pathways of MT stabilization must also exist. For example CLASP1, which is expressed in MEFs, could partially substitute for CLASP2.

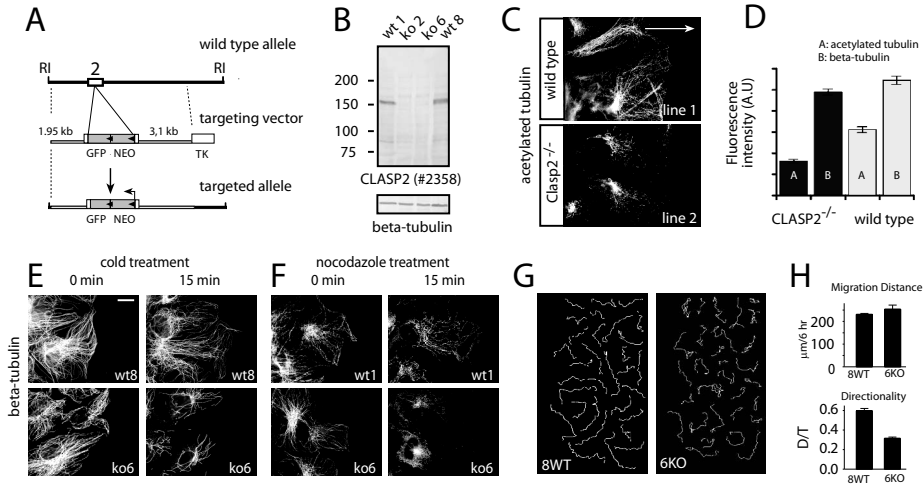


Figure 3-1. CLASP2 regulates MT stabilisation and persistent motility in fibroblasts.

- A) Targeting of the murine *Clasp2* gene. A GFP-lox-neo-lox cassette was inserted into a common exon used by all known *CLASP2* mRNA splice variants (common exon 2). The neo gene is transcribed antisense with respect to the *Clasp2* gene. Length of 5'-end and 3'-end homologous arms is indicated. RI: Eco RI restriction enzyme site, TK: thymidine kinase negative selection marker. LoxP sites are indicated by triangles.
- B) Western blot analysis. Protein extracts of two wild type (lines 1 and 8) and two CLASP2-deficient (lines 2 and 6) MEF lines were incubated on western blots with antibodies against CLASP2 (#2358) and beta-tubulin.
- C) Levels of acetylated MTs. Wild type and CLASP2 knockout MEFs were fixed 4 hours after migration into a wound. Cells were incubated with antibodies against acetylated tubulin, a marker for stable MTs. Arrow (20 μm) indicates direction of cell migration.
- D) Comparison of acetylated and total MTs. Fluorescent intensities of acetylated tubulin and beta-tubulin stainings were quantified for wild type and CLASP2 knock out MEFs, 4 hours after migration into a wound. More than 50 cells were measured from each genotype and for each staining. Standard error of the mean is indicated.
- E) Cold-resistant MTs in motile MEFs. After cold-treatment wild type and CLASP2 knock out MEFs were fixed and stained with antibodies against beta-tubulin.
- F) Nocodazole-resistant MTs in motile MEFs. After treatment with 10 μM nocodazole wild type and CLASP2 knock out MEFs were fixed and stained with antibodies against beta-tubulin. Scale bar, 10 μm.
- G, H) Cell motility assay. Total and directionally persistent migration distance were measured in wild type (line 8) and CLASP2 knock out (line 6) MEFs. The directionally persistent migration (D/T) is the ratio of direct distance from start to end point (D), divided by the total track distance (T). Of each genotype 30 cells were measured (SEM indicated), each individual track is shown in (G).

CLASP2 is not essential for centrosome repositioning (Supplemental Data and Fig. 3-S3A). However, immunofluorescent stainings revealed polarity defects in CLASP2 knock out MEFs, which could be related to cell migration (Supplemental Data and Fig. 3-S3B-E). To test the effect of a CLASP2 deletion on intrinsic cell motility (Pankov et al., 2005), we measured both total and directionally persistent migration velocities of MEFs, after attachment of cells on fibronectin-coated cover-slips and stimulation with basic fibroblast growth factor (Fig. 3-1G, H). The results suggest that a CLASP2 deficiency has no effect on the total migration distance of MEFs, but reduces their effective migration by a factor of two. We conclude that MTs stabilized by CLASP2 serve a role in directionally persistent migration. Our results link the asymmetric distribution of stable MTs to a highly polarized cell behavior.

3.2.2. Roles of CLIP-170 and an APC-EB1 interaction in the formation of stable MTs

An interaction between CLIP-170 and CLASPs (Akhmanova et al., 2001), as well as complexes of CLIP-170, IQGAP1 and activated Rac1 or Cdc42 (Fukata et al., 2002), and of APC, EB1 and mDia1 (Wen et al., 2004), have all been proposed to play a role in the stabilization of MTs at the leading edge of cells. We recently described CLIP-170 knock out mice and MEFs and showed that, apart from a mislocalization of dynactin, cultured fibroblasts lacking CLIP-170 have no obvious phenotype (Akhmanova et al., 2005). Using the wound healing paradigm, we could not detect an effect of a CLIP-170 deletion on stable MTs (data not shown).

To examine the function of an APC-EB1 interaction, we performed wound healing experiments with MEFs from mice with a truncated APC allele (Smits et al., 1999). In these cells APC translation is interrupted at amino acid residue 1638 (APC1638T) and mutant APC can not interact with EB1 or EB3. Using two wild type and two APC1638T cell lines, we detected similar levels of stable MTs after 4 hours in the wound healing assay (Fig. 3-2A-D, G). Both EB1 (data not shown) and EB3 (Fig. 3-2E, F) localized at the ends of MTs in 1638T and wild type fibroblasts. These data argue against essential roles for CLIP-170 and an APC-EB1 interaction in the formation of stable MTs in motile fibroblasts.

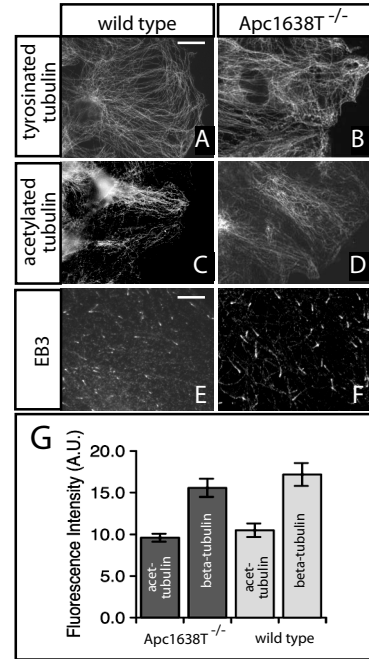
3.2.3. ACF7 regulates cortical localization of CLASP2 in HeLa cells

Another factor implicated in selective MT stabilization and directed cell migration is the spectraplakine ACF7 (Kodama et al., 2003). We explored a putative link between ACF7 and CLASPs in HeLa cells, since – in contrast to MEFs – these cells can be efficiently transfected with siRNAs. Moreover, CLASPs have been shown to localize at the cell cortex of HeLa cells and to regulate MT dynamics at this position (Mimori-Kiyosue et al., 2005). These data indicate that the cell edges of HeLa cells and of migrating fibroblasts share functional characteristics. We recently found that the protein LL5 β interacts with the C-terminus of CLASPs and may form cortical platforms, to which CLASPs attach distal microtubule ends (Lansbergen et al., 2006). Like CLASP2, LL5 β is localized at the cortex of HeLa cells and the leading edge of migrating fibroblasts.

Figure 3-2. MT network in APC1638T MEFs.

A-F) Immunofluorescence analysis. Wild type (A, C, E) and APC1638T (B, D, F) MEFs were examined 4 hours after migration (towards the right) into a wound. Antibodies against tyrosinated tubulin (A, B), acetylated tubulin (C, D) and EB3 (E, F) were used. Scale bar in A, 7.5 μ m, in E, 2.5 μ m.

G) Comparison of stable and total MTs. Fluorescence intensities of acetylated tubulin and beta-tubulin were quantified for two wild type and two APC1638T MEF lines, 4 hours after migration into a wound. More than 50 cells were measured from each genotype and for each staining. SEM indicated.



The localization of ACF7 and CLASP2 in HeLa cells overlapped, especially at the cell cortex and in areas of cells that did not make contact with other cells (Fig. 3-3A-C). Cortical ACF7 distribution actually resembles that of the CLASP-interaction partners LL5 β and ELKS (Lansbergen et al., 2006). Using an siRNA approach, we achieved a partial depletion of ACF7 with two different oligos (Fig. 3-3E, H), whereas a scramble oligo did not cause a knock down (Fig. 3-3B). Strikingly, ACF7 depletion resulted in the partial disappearance of CLASP2 signal at the cell cortex of HeLa cells (Fig. 3-3D, F, G, I). We obtained similar results with GFP-CLASP2 in live cells; in untreated cells GFP-CLASP2 accumulated at the cell cortex (Fig. 3-4A), whereas in ACF7-depleted cells, this was not the case (data not shown).

A combined knock down of CLASP1 and -2 did not have an obvious effect on ACF7 localization (Fig. 3-3J-L). These results are similar to our LL5 β knock down data (Lansbergen et al., 2006) and indicate that in HeLa cells ACF7 acts upstream of CLASPs. ACF7 might interact directly with CLASP2, as we identified ACF7 peptides by mass spectrometry in a recent pull down of potential CLASP2-associated proteins (data not shown). We noted previously that LL5 β -independent mechanisms of CLASP attachment to the cell cortex exist (Lansbergen et al., 2006). Whether ACF7 acts independently of, or in conjunction with, LL5 β (and ELKS) remains to be determined.

3.2.4. Dynamic behavior of GFP-CLASP2 in HeLa cells

In HeLa cells, GFP-CLASP2 acts as a +TIP and accumulates at the Golgi and cell cortex (Fig. 3-4A); the distribution of GFP-CLASP2 resembles that of endogenous CLASP2 (Mimori-Kiyosue et al., 2005). Time-lapse analysis revealed dynamic “comet-like” dashes of GFP-CLASP2, which represent “plus end tracking protein” at the ends of

polymerizing MTs (Supplemental Data, Movie 3-1). We refer to other intracellular increases in GFP-CLASP2 signal, which do not have a “comet-like” shape and hardly move compared to “plus end tracking” CLASP2, as “accumulations”, or “CLASP2-positive domains”.

To examine dynamic GFP-CLASP2 behavior in relation to stable MTs, we analyzed diffusion characteristics and conformation of soluble GFP-CLASP2, using fluorescence correlation spectroscopy (FCS) and Photon Counting Histogram (PCH) approaches (Supplemental Data and Fig. 3-S4). Our data suggest that soluble GFP-CLASP2 is monomeric, consistent with a report using mitotic *Xenopus laevis* extracts (Emanuele et al., 2005).

We next investigated GFP-CLASP2 in HeLa cells using fluorescence recovery after photobleaching (FRAP). We bleached regions in the interior and at the edge of cells (Fig. 3-4A). In the interior recovery was very rapid (Fig. 3-4B). By contrast, GFP-CLASP2 recovery at the cell cortex was slower and appeared to be bimodal, with a relatively immobile fraction that did not recover within the time frame of the experiment, and a more mobile fraction with a half-time of recovery of ~1 second (Fig. 3-4B). These data suggest that GFP-CLASP2 is retained by at least two different mechanisms at the cortex of HeLa cells.

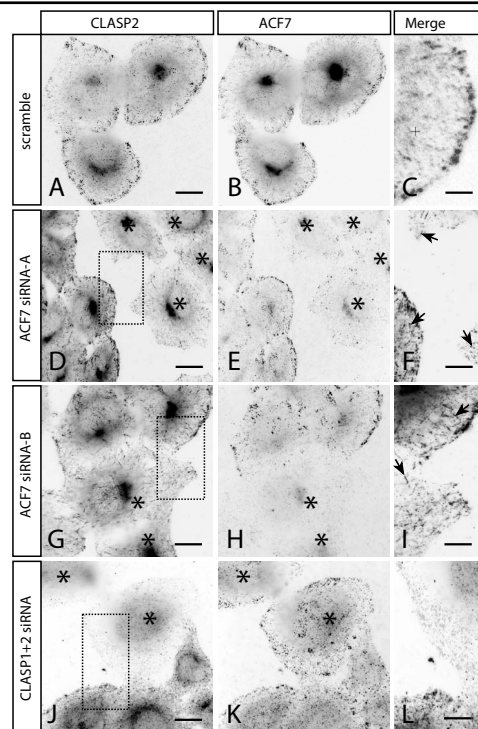
Phosphatidylinositol-3 (PI-3) kinase is an important regulator of CLASP2 localization at the leading edge of motile cells (Akhmanova et al., 2001). The effect of PI-3 kinase seems to be mediated in part by LL5 β , which can bind phosphatidylinositol-3,4,5-triphosphate (PIP3) (Lansbergen et al., 2006). Since ACF7 can crosslink MTs

Figure 3-3. ACF7 regulates CLASP2 localisation in HeLa cells.

A-C) HeLa cells, transfected with a scramble siRNA oligo, were fixed 3 days after transfection and stained for CLASP2 (green in merge) and ACF7 (red in merge). CLASP2 and ACF7 accumulate at the cell cortex. Note that there is not a complete colocalisation.

D-I) HeLa cells were fixed 3 days after transfection with different siRNAs against ACF7, and stained for CLASP2 (green in merge) and ACF7 (red in merge). Cells depleted of ACF7 (indicated by asterisks), show reduced CLASP2 signal at the cell cortex. MT-end staining of CLASP2 (indicated by arrows in merges) is not affected.

J-L) HeLa cells, transfected with siRNAs against CLASP1 and -2, were fixed 3 days after transfection and stained for CLASP1 and -2 (green in merge) and ACF7 (red in merge). Cells depleted of CLASPs (indicated by asterisks), still show ACF7 staining at the cell cortex. Bars in A, D: 10 μ m, in G, J: 7.5 μ m, and in C, E, I, L: 3 μ m.



and actin, the actin cytoskeleton may also regulate cortical localization of CLASP2. We tested whether inhibition of PI-3 kinase activity by wortmannin, or disassembly of the actin network with cytochalasin D, affected the dynamic behavior of GFP-CLASP2. When added to serum-grown cells, these compounds had a clear effect on cell morphology and the cortical localization pattern of CLASP2 (data not shown). However, the dynamic behavior of GFP-CLASP2 was not significantly altered (Fig. 3-4C and data not shown).

3.2.5. GFP-CLASP2 behavior in non-motile 3T3 cells

To analyze CLASP2 dynamics during cell migration, we generated 3T3 cells expressing GFP-CLASP2 under control of the reverse tetracyclin transcriptional activator (rtTA, see Supplemental Data). Control experiments suggested that GFP-CLASP2 recapitulates the behavior of endogenous CLASP2 in these cells (Supplemental Data, Fig. 3-S5). In 3T3 cells GFP-CLASP2 is present in at least three fractions: a diffuse cytoplasmic pool, a MT end-bound fraction, and in accumulations near the leading edge, near the Golgi complex, and near focal adhesions.

FRAP analysis of GFP-CLASP2 in non-motile 3T3 cells demonstrated that GFP-CLASP2 recovered much faster in the cytoplasm than in accumulations (data not shown). In the latter GFP-CLASP2 partitioned again into relatively mobile and immobile fractions (Fig. 3-4E, F). Nocodazole treatment did not affect behavior of GFP-CLASP2 in accumulations (Fig. 3-4F, see also Supplemental Data, Movie 3-3), indicating that the protein is maintained independently of dynamic MTs. These data are consistent with the observation that the interaction of CLASP2 with the cell cortex is mediated by its C-terminus, which does not bind MTs (Mimori-Kiyosue et al., 2005), but does bind LL5 β (Lansbergen et al., 2006). The recovery of the mobile GFP-CLASP2 fraction could be fitted as described (Bulinski et al., 2001),

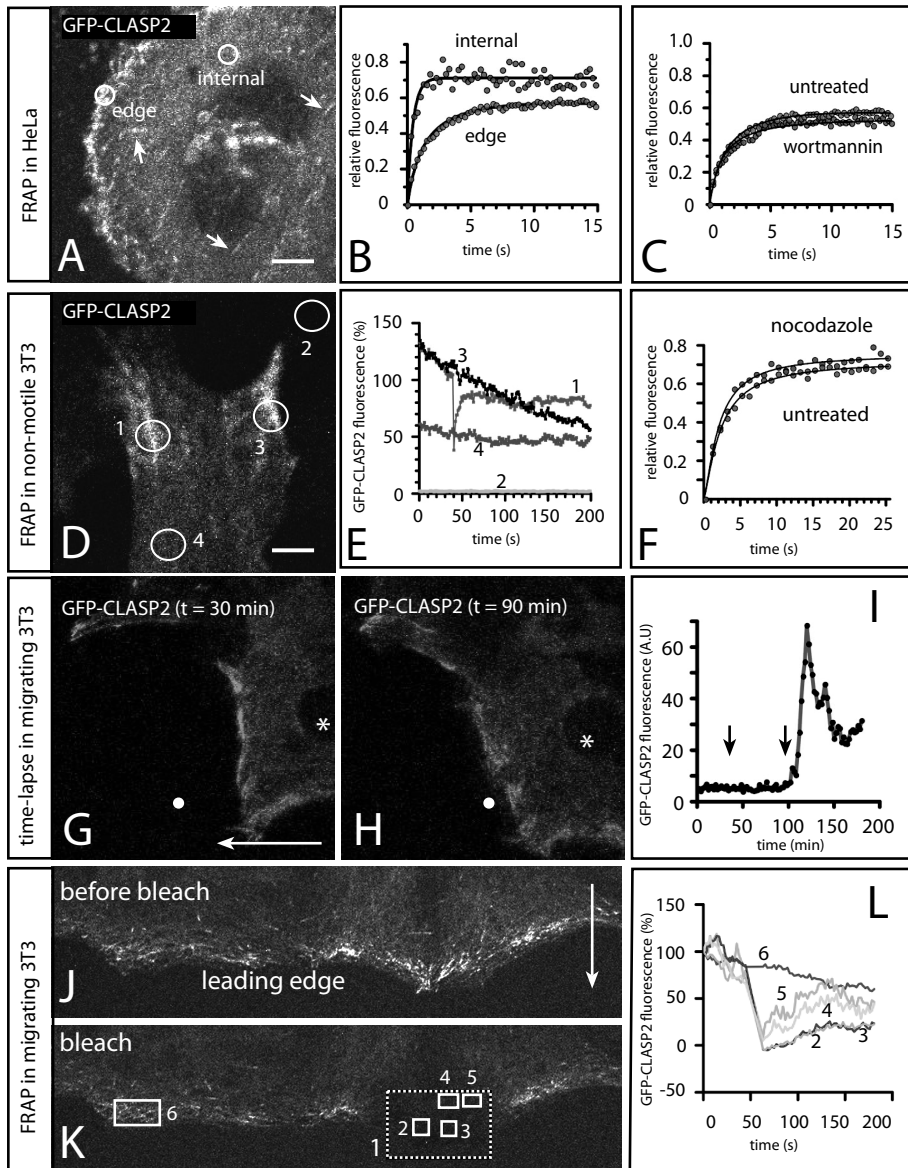
Figure 3-4. GFP-CLASP2 behaviour in 3T3 cells.

- A-C) FRAP analysis in transfected HeLa cells. GFP-CLASP2 localises at the ends of growing MTs (arrows) and accumulates at the cell cortex. In (A) a still image of a high resolution time-lapse experiment (Movie 3-1) is shown. Transfected cells were bleached in the cell body (internal, n=9) and at the cell cortex (edge, n=11). Average fluorescence recoveries are shown in (B). In (C) fluorescence recovery at the edge in untreated cells is compared to cells treated with 100 nM wortmannin (n=8). Bar in (A), 2.5 μ m.
- D-F) FRAP analysis in non-motile 3T3 cells. GFP-CLASP2-positive accumulations were bleached (region of interest, or ROI, 1). Fluorescence intensities were measured in ROIs 1-4. In (F) the average fluorescence recovery is shown from accumulations measured in different cells (n=16, untreated cells, n=10, nocodazole treated cells). In E, relative fluorescence expressed as percentage of prebleach intensity in ROI1 is drawn on the vertical axis. Bar in (D), 1.5 μ m.
- G-I) GFP-CLASP2 behaviour in migrating 3T3 cells. Panels (G) and (H) show migrating cells 30 and 90 minutes after serum induction, respectively. The arrow in G (30 μ m) indicates direction of migration. The complete time lapse analysis is shown in Movies 3-4 and 3-5. The asterisk indicates the nucleus of a migrating cell. White round dots represent a stationary circle, within which fluorescence intensity of GFP-CLASP2 was measured during the time lapse analysis. This intensity is depicted in (I), where the arrows indicate the 30 and 90 minute time points. A.U., arbitrary units.
- J-L) FRAP analysis in migrating fibroblasts. Cells were bleached (ROI 1, stippled rectangle in (K)) and fluorescence intensities were measured in the indicated ROIs. In panels J, K selected still images are shown. The arrow in J (5 μ m) indicates direction of cell migration. The complete time lapse analysis is shown in Movie 7. In (L) fluorescence intensities are plotted with time (s) on the horizontal axis and relative fluorescence (percentage) on the vertical axis.

which yielded a k_{off} of 0.31 sec^{-1} with a corresponding half-time of recovery of 2.2 s. This recovery of GFP-CLASP2 is somewhat slower than in HeLa cells.

3.2.6. GFP-CLASP2 behavior in migrating 3T3 cells

Wound healing experiments were performed to investigate GFP-CLASP2 during cell motility. GFP-CLASP2 redistributed towards the leading edge within 3-5 minutes after serum addition (data not shown) and was subsequently continuously targeted towards this area (Fig. 3-4G, H, see also Supplemental Data, Movies 3-4



and 3-5). High resolution imaging of GFP-CLASP2 in motile cells showed that “plus end tracking” protein was present, in addition to GFP-CLASP2 accumulations at the leading edge (Supplemental Data, Movie 3-6). Because cells move, GFP-CLASP2 accumulations at the leading edge also change position (Figure 4I). With respect to a stationary point the accumulations remained at one position for 49 ± 19 minutes (22 accumulations counted, SD indicated). Thus, these domains generally turn over in less than one hour.

To analyze the intracellular mobility of GFP-CLASP2, we bleached a relatively large area of a motile cell (Fig. 3-4J-L, see also Supplemental Data, Movie 3-7), that included a leading edge accumulation. We then selected small regions of interest (ROIs) inside and outside of the bleached areas to compare fluorescence in ROIs that contained an accumulation of GFP-CLASP2, to fluorescence recovery in cytoplasmic areas adjacent to accumulations. As shown in Fig. 3-4J-L fluorescence recovery in ROIs within a GFP-CLASP2 accumulation is incomplete and slower compared to recovery in ROIs adjacent to the area of local GFP-CLASP2 accumulation. We subsequently performed circular spot bleachings in motile cells with similar results (data not shown). Together these data indicate that, comparable to non-motile cells, GFP-CLASP2 is immobile in accumulations at the leading edge of motile cells when compared to GFP-CLASP2 in adjacent areas.

In the epithelial Ptk1 cell line, CLASP2 is a +TIP in the cell body, but is associated with the MT lattice of “pioneering” MTs in the lamellipodium of migrating cells (Wittmann and Waterman-Storer, 2005). GFP-CLASP2 exchange on lamellipodial MTs is fast, with a half-time of recovery of ~ 600 ms. Behavior of GFP-CLASP2 in 3T3 and HeLa cells differs significantly from that in Ptk1 cells. As “pioneering” MTs are not stabilized, we propose that migrating Ptk1 cells lack components in their lamellipodium that can render CLASP2 more immobile and cause MT stabilization.

While the data in MEFs show that CLASP2 is involved in MT stabilization and is required for efficient persistent motility, results in HeLa cells and with GFP-CLASP2 start to indicate the order of events in CLASP2-mediated MT stabilization. CLASP2 accumulates in domains at the edge of cells, through interaction with LL5 β and ELKS (Lansbergen et al., 2006), and possibly ACF7 and other factors. Since wortmannin, cytochalasin and nocodazole do not significantly modulate CLASP2 behavior in accumulations, we hypothesize that regulation by PI-3 kinase and actin is at the level of upstream factors, for example LL5 β – a protein immobilized at the plasma membrane (Lansbergen et al., 2006). The amount of upstream factors determines the number of monomeric CLASP2 molecules in a particular domain at the cell edge. MT stabilization in CLASP2-positive domains might be related to its +TIP properties. MT-lattice binding of CLASP2 is allowed by the local inactivation of glycogen synthase kinase-3 β (GSK-3 β), downstream of PI-3 kinase (Akhmanova et al., 2001) and/or the small GTPase Rac1 (Wittmann and Waterman-Storer, 2005). While a MT is bound in a CLASP2-positive accumulation monomeric CLASP2 molecules continuously exchange (in a bimodal fashion). The residence time of GFP-CLASP2-positive domains in migrating cells might provide an estimate of the turnover time of stable MTs. However, MT stabilization by CLASP2 is temporary, to allow efficient persistent motility.

3.3. Experimental Procedures

3.3.1. Antibodies and standard procedures

We used rabbit polyclonal antibodies against CLIP-115 (Hoogenraad et al., 2000), CLIP-170 (Coquelle et al., 2002), CLASP1 (Mimori-Kiyosue et al., 2005), CLASP2 (Akhmanova et al., 2001), EB1 and -3 (Komarova et al., 2005), and detyrosinated alpha-tubulin (a kind gift of Dr. C. Bulinski). Mouse polyclonal anti-ACF7 antiserum was purchased from Abnova. Monoclonal antisera were against GFP (Clontech), actin, beta-tubulin, gamma-tubulin, acetylated alpha-tubulin, vinculin, paxillin (Sigma), mDia1, p150Glued and GM130 (BD Biosciences). Secondary goat anti-rabbit and anti-mouse antibodies were coupled to alkaline phosphatase (Sigma, 1:7000) for western blotting, or to Alexa-350, -488 or -594 (Molecular Probes, 1:300 or 1:500) for immunofluorescent studies.

Protein extract preparation and western blotting procedures have been described (Hoogenraad et al., 2000). RT-PCR was performed as described (Akhmanova et al., 2005). The forward CLASP2 primer was located immediately downstream of the targeting site (5'AGCTTTTACAGATGTTCTT3'), whereas the reverse primer was located on a downstream exon (5'GCAACAGTGATGCAAGCTTCCCTGAC3'). We followed published procedures for siRNA-mediated depletion (Mimori-Kiyosue et al., 2005). HeLa cells were examined 3 days after transfection. The siRNAs for CLASP1 and -2 have been reported (Mimori-Kiyosue et al., 2005). For ACF7 we designed two sequences (siRNA-A: 5'-UUGCAGCAGGUGAAUGGAC-3'; siRNA-B: 5'-CCAAAGUGACUUGAAGGAU -3'). siRNAs were purchased from Ambion.

3.3.2. Cell culture, migration and centrosome repositioning

The CLIP-170 (Akhmanova et al., 2005) and APC1638T (Smits et al., 1999) mutant mice have been described. To generate the CLASP2 knock out construct a mouse PAC genomic library RPCI21 (UK HGMP Resource Centre, Hinxton, Cambridge), prepared from female 129S6/SvevTac mouse spleen genomic DNA (Osoegawa et al., 2000), was screened for the *Clasp2* gene, using human *CLASP2* cDNA as a probe. One positive clone (P635-K11), containing a 7.3 kb Eco RI-fragment which included the second common exon, was chosen to generate the targeting construct. A GFP-lox-neo-lox cassette (where "neo" is the *neomycin resistance* gene) was inserted into a common exon used by all known *CLASP2* mRNA splice variants (common exon 2, see Figure 3-1A). In this allele translation is stopped after GFP and the *neo* gene is transcribed antisense to the mouse *Clasp2* gene. Targeting techniques and the procedures for selection of ES cells and generation of knock out mice have been described (Akhmanova et al., 2005; Hoogenraad et al., 2002).

Isolation and culture of mouse embryonic fibroblasts (MEFs) was performed as published (Akhmanova et al., 2005). Swiss 3T3 fibroblasts were cultured as described (Akhmanova et al., 2001). We used a wound healing model (Akhmanova et al., 2001), based on the method of Gundersen and coworkers (Liao et al., 1995). Briefly, cells were grown to confluence, after which serum was removed for 24-48 hours. A stripe of cells was then scratched off, creating a "wound" in the monolayer. Subsequently serum was added to the culture medium. Fibroblasts were fixed 4-6 hours after serum induction.

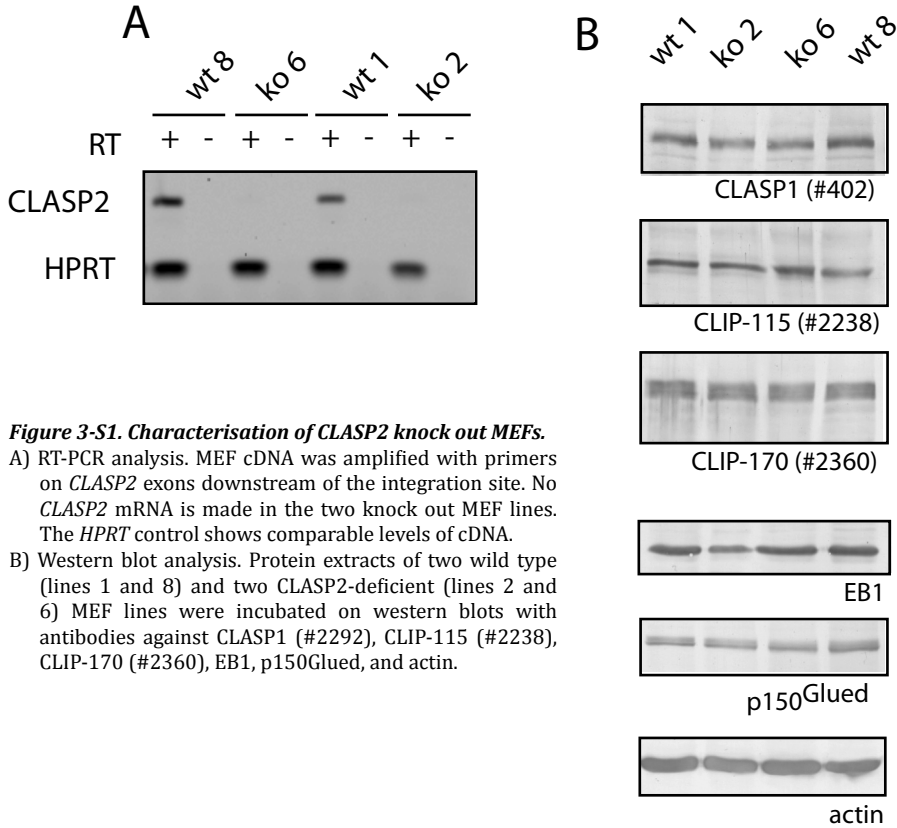


Figure 3-S1. Characterisation of CLASP2 knock out MEFs.

- A) RT-PCR analysis. MEF cDNA was amplified with primers on *CLASP2* exons downstream of the integration site. No *CLASP2* mRNA is made in the two knock out MEF lines. The *HPRT* control shows comparable levels of cDNA.
- B) Western blot analysis. Protein extracts of two wild type (lines 1 and 8) and two CLASP2-deficient (lines 2 and 6) MEF lines were incubated on western blots with antibodies against CLASP1 (#2292), CLIP-115 (#2238), CLIP-170 (#2360), EB1, p150Glued, and actin.

The centrosome repositioning assay was performed as published (Etienne-Manneville and Hall, 2003), using antibodies against gamma-tubulin as marker for centrosomes. To test the levels of cold- and nocodazole resistant MTs, cells were allowed to migrate for 4 hours after serum-induction, and subsequently incubated on ice, or treated with 10 μ M nocodazole (Kodama et al., 2003). Both treatments lasted for 15 minutes. Cells were subsequently fixed and analyzed with anti-tubulin antibodies.

Intrinsic cell motility assays were carried out as described (Pankov et al., 2005), using freshly plated cells 90 minutes after adhesion. Cells were plated on coverslips with 10 μ g/ml fibronectin (Roche). Serum-free medium contained 400 ng/ml basic fibroblast growth factor (PeproTech). Single cell motility was monitored for 6 hours. Images were collected every 2 minutes using an AxioCam MRC (Carl Zeiss) digital camera. AxioVision software (Carl Zeiss) was used to analyze cell movements.

HeLa cells were cultured and transfected with GFP-CLASP2 as described (Mimori-Kiyosue et al., 2005). Serum-grown cells were incubated for 1 hour with wortmannin (100 nM) or cytochalasin D (2 μ M), prior to image analysis. To test the efficacy of these compounds we also fixed cells and investigated their morphology and the intracellular distribution of selected proteins by immunofluorescence.

3.3.3. Immunofluorescence analysis

Cells were fixed and immunofluorescence was performed as described (Akhmanova et al., 2001; Akhmanova et al., 2005; Stepanova et al., 2003). Cells were stained with the polyclonal antisera (1:100 or 1:300) or monoclonal antisera (1:100) described above.

Fluorescence intensities of acetylated tubulin and beta-tubulin in whole cells, or in part of the cell that was directed towards the wound, were measured using ImageJ software (Rasband, W.S., ImageJ, U. S. National Institutes of Health, Bethesda, Maryland, USA, <http://rsb.info.nih.gov/ij/>, 1997-2006). In each experiment and for each cell line 15-20 cells were measured. Mean fluorescence intensities were calculated and multiplied with cell area to obtain total intensity. We performed at least 2 independent experiments for each cell line and obtained values for at least two independent cell lines from one genotype.

3.3.4. Live imaging

Live fluorescence analysis was performed at 37°C on a Zeiss LSM510 confocal laser scanning microscope. The time-lapse imaging procedure to record the growth speed of MTs (Stepanova et al., 2003) and FRAP protocols (Akhmanova et al., 2005; Bulinski et al., 2001) have been published. Different parameters (velocities of MT growth, cell migration, fluorescent intensities in the FRAP assay) were initially calculated using LSM 510 software. Data were exported to Excel (Microsoft) and Aabel (Gigawiz) for statistical analysis and graphical representation.

3.3.5. Fluorescence correlation spectroscopy (FCS) and photon counting histogram (PCH)

COS-7 cells were transfected using Polyfect (Qiagen) with GFP, GFP-EB3, EB3-GFP and GFP-CLASP2. Cells were lysed by collecting them on ice in lysis buffer (20 mM Tris-HCl pH 8, 100mM NaCl, 0.5% Triton-X100, supplemented with a cocktail of protease inhibitors (Roche)) 20 hours after transfection. Samples were centrifuged for 10 minutes at 13,000 rpm and 4°C to remove cell debris, and the supernatant was used for further experiments.

FCS measurements were conducted at room temperature with the LSM 510-Confocor II (Zeiss) and the 488nm Ar-laser (beampath: HFT488-Mirror-BP505-550). Laser power was attenuated to approximately 15 µW during measurements. A total of 20 measurements per lysate were conducted, each measurement lasting 30 s. The system was calibrated with rhodamine 6G (diffusion coefficient: $28 \times 10^{-10} \text{ m}^2/\text{s}$ at 20°C). The experimentally obtained autocorrelation function was analyzed with the Confocor II software package. The autocorrelation function was fit with

$$G(\tau) = 1 + \frac{1}{\langle N \rangle} \cdot \frac{1 - T + T e^{-\tau/\tau_T}}{(1 - T)} \cdot \sum_i^M \frac{1}{\left(1 + \frac{\tau}{\tau_i}\right) \sqrt{1 + \frac{\tau}{S^2 \cdot \tau_i}}} \quad (\text{Eq. 3.1})$$

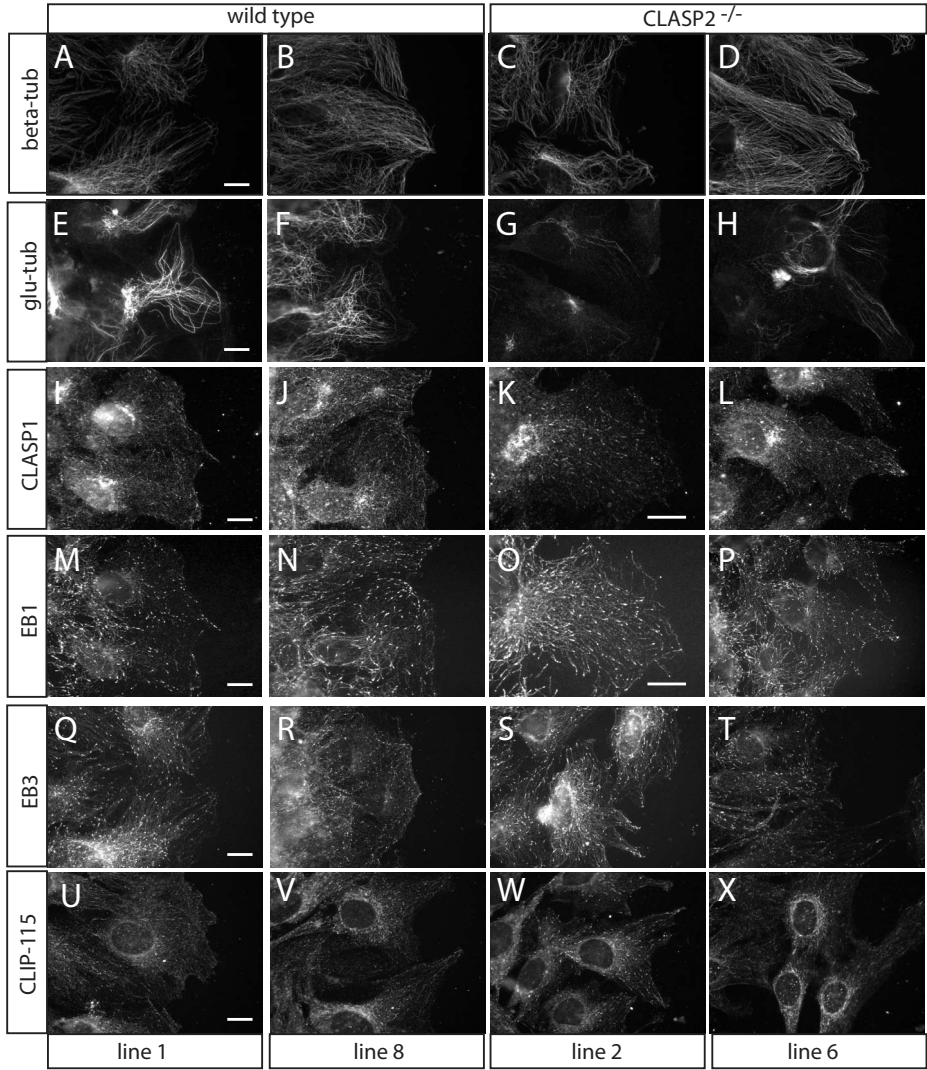


Figure 3-S2. Immunofluorescent analysis of motile wild type and CLASP2 knock out MEFs.

A-X) Immunofluorescent analysis of wild type (lines 1 and 8) and CLASP2 knock out (lines 2 and 6) MEFs. Fibroblasts were examined in the wound healing assay, 4-6 hours after serum induction. In all panels cells migrate towards the right. We used antibodies against beta-tubulin (A-D) detryosinated (glu-) tubulin (E-H), CLASP1 (I-L), EB1 (M-P), EB3 (Q-T) and CLIP-115 (U-X). Both CLASP2 knock out cell lines contain fewer stable MTs after serum induction. Scale bars, 10 μ m

where τ_T is the triplet time (set to 9 μ s for GFP), S the structural parameter (set to 6, as obtained from calibration measurements with rhodamine 6G), N is the number of particles, M the number of components (in these experiments M was set to 1), F_i the fraction of component i , τ_i the diffusion time of fraction i , and T the fraction of triplet decay.

The molecular brightness of the lysates was analyzed by photon counting histogram (PCH) analysis (Chen et al., 1999). The raw data of FCS measurements was converted into PCH curves using our own custom-written program and a binning time of 50 μ s. Data thus obtained was analyzed using the Globals software package developed at the Laboratory for Fluorescence Dynamics at the University of Illinois at Urbana-Champaign.

3.3.6. Generation and characterization of a 3T3 cell line stably expressing GFP-CLASP2.

We generated 3T3 cell lines expressing GFP-CLASP2 under control of the reverse tetracyclin transcriptional activator (rtTA; Tet-on system). Using the same approach, we generated 3T3 cell lines expressing GFP-CLIP170 (data not shown), as control for GFP-CLASP2 behavior. The rtTA2-M2 (pUHRt 62-1) regulator plasmid DNA (Baron and Bujard, 2000) was a kind gift of Dr. H. Bujard. The neomycin resistance plasmid (pHA178neo, vector pSP72), is a derivative of pMC1-NeopolyA. In the puromycin resistance plasmid (which is also pSP72 based), the selection gene is under control of the PGK promoter. pTRE-GFP-CLASP2 was generated using the gamma isoform of CLASP2 (accession number AJ276961, Akhmanova et al., 2001). We added a beta-globin intron just after GFP-CLASP2 in the pTRE vector.

Stable, doxycyclin inducible cell lines were generated according to the instructions of the supplier (Clontech). Briefly, 3T3 cells were grown to 80% confluence and subsequently transfected with two linearized DNA plasmids (rtTA2-M2 and pHA178neo), using lipofectamine 2000 (Invitrogen). Cotransfection yielded 33 rtTA-positive clones from 100 resistant ones. These neomycin-positive clones were subsequently transfected with linearized pTRE-GFP-CLASP2 DNA, together with a PGK-puromycin DNA, again using lipofectamine 2000. Clone selection for GFP fusion proteins was done by fluorescence microscopy, i.e. clones that contained fluorescent cells after doxycyclin induction were considered as positive. Positive clones after neomycin and puromycin selection represent stable cell lines containing GFP-CLASP2 fusions under control of rtTA. This procedure yielded 9 GFP-CLASP2-positive clones out of 100 puromycin resistant clones. Different amounts of doxycyclin were initially added to measure expression levels of GFP-fusion proteins. In the experiments described here, doxycyclin was added at 500 ng/ml. For western blotting 3T3 cell cultures were harvested 24 hours after doxycyclin induction.

3.4. Supplemental Results

3.4.1. Cell polarity features in wild type and CLASP2 knock out MEFs

Centrosome reorientation in fibroblasts is dependent on Cdc42 and the dynein-dynactin motor complex, but not on stable MTs (Palazzo et al., 2001). In line with this hypothesis CLASP2-deficient cells are able to reorient their centrosomes after serum induction in the wound healing paradigm (Fig. 3-S3A). These results indi-

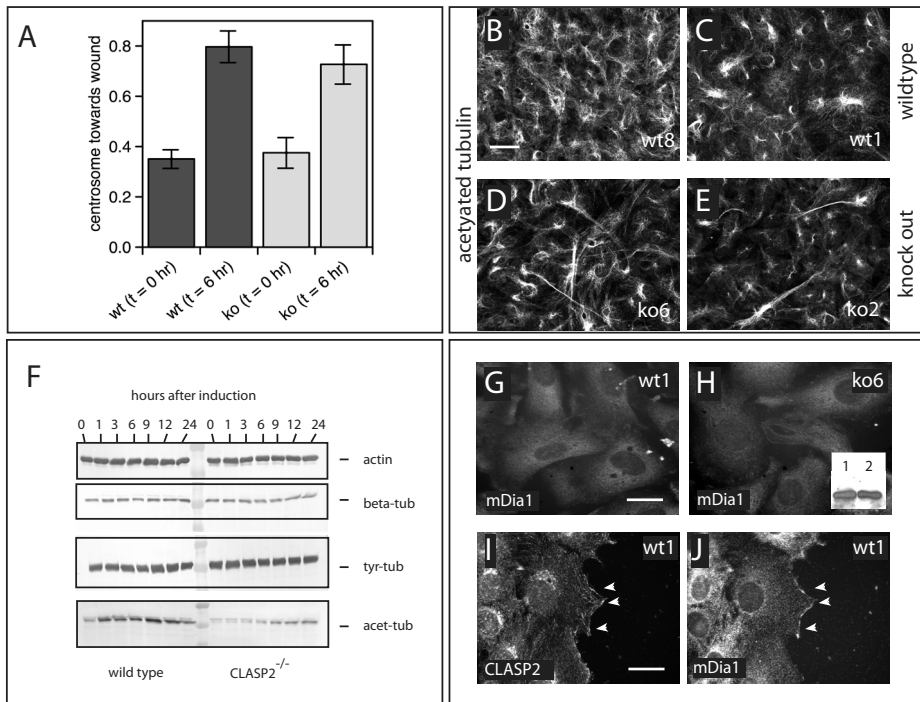


Figure S3. Effects on cell polarity after CLASP2 knock out.

- A) Centrosome repositioning in wild type (lines 1 and 8) and CLASP2 knock out (lines 2 and 6) MEFs. Cells were fixed and stained with antibodies against gamma-tubulin, a centrosomal marker. In 6 independent experiments 100 cells at the leading edge were scored for centrosome orientation towards the leading edge. The fraction of cells with such an orientation is plotted (standard deviation indicated). Both types of cells reorient centrosomes after serum induction.
- B-E) Acetylated tubulin staining in wild type (B, D) and CLASP2 knock out (C, E) MEFs. Confluent cells were stained. Notice the increased amount of cytoplasmic extensions, or "tails", in CLASP2 knock out cells, indicative of a cell polarity defect. Scale bar 25 μ m.
- F) Western blot analysis of proteins after serum starvation and induction. Antibodies against actin, beta-tubulin, tyrosinated tubulin (tyr-tub) and acetylated tubulin (acet-tub) were used. CLASP2-deficient cells do not form stable MTs efficiently after serum induction.
- G, H) mDia1 distribution. Normal proliferating wild type (line 1, G) and CLASP2 knock out (line 6, H) MEFs were stained for mDia1. A diffuse localization pattern is visible. The inset in panel (H) shows a Western blot of wild type (1) and CLASP2 knock out (2) MEFs. mDia1 levels are similar in the two cell types. Scale bar, 15 μ m.
- I, J) Comparison of CLASP2 and mDia1 in migrating cells. Wild type MEFs (line 1) were fixed after migration into a cell-free area and stained with anti-CLASP2 (I) and anti-mDia1 (J) antisera. Three cells at the wound are shown. While CLASP2 localizes at the leading edge in all three cells, mDia1 only does this in the middle cell (arrowheads). Scale bar, 15 μ m.

cate that CLASP2-mediated stabilisation of MTs is not required for centrosome reorientation.

In cultures of CLASP2-deficient fibroblasts we noted the formation of thin and long cell protrusions, that were stained by antisera against acetylated tubulin (Fig. 3-S3B-E), detyrosinated tubulin and phalloidin (data not shown). In addition, CLASP2 knock out fibroblasts that migrated into a wound often appeared more randomly oriented in comparison to wild type cells (data not shown). These results indicate that deletion of CLASP2 causes specific cell polarity and/or migration defects.

A complex of APC, mDia and EB1 has been implicated downstream of Rho in the control of stable, leading edge-oriented MTs (Wen et al., 2004). In Fig. 3-2 we provide evidence that an APC-EB1 interaction is not essential for MT stabilization in MEFs. We also investigated a possible link between mDia1 and CLASP2. Levels of mDia1 were similar in cultures of wild type and CLASP2 knock out MEFs (Fig. 3-S3G, H). In motile wild type fibroblasts mDia1 and CLASP2 signals only colocalized occasionally (Fig. 3-S3I, J). Thus, in contrast to CLASP2, the distribution of mDia1 in MEFs does not appear to correlate with the formation of polarized, stable MTs.

3.4.2. Soluble GFP-CLASP2 is monomeric

We examined diffusion characteristics and conformation of soluble GFP-CLASP2, compared to GFP, EB3-GFP and GFP-EB3 extracts. The FCS analysis indicates that in cell extracts GFP-CLASP2 diffuses approximately 4 times more slowly than GFP (Fig. 3-S4A). The diffusion time of GFP-CLASP2 is marginally less than that of EB3-GFP and GFP-EB3, in spite of the fact that the M_r of GFP-CLASP2 (approximately 170 kDa), is three times that of monomeric EB3-GFP. In addition, the counts per molecule (cpm) value is lower for GFP-CLASP2 than for EB3-GFP or GFP-EB3 (Fig. 3-S4). We therefore performed a PCH analysis to examine molecular brightness of

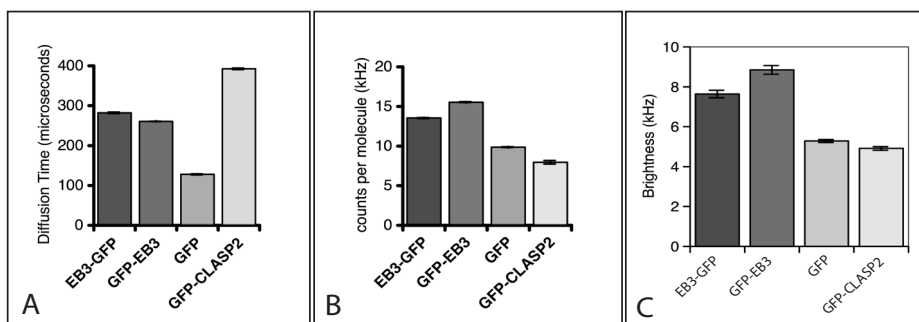


Figure S4. FCS and PCH analysis of GFP-CLASP2.

A, B) FCS analysis of GFP-CLASP2, EB3-GFP, GFP-EB3 and GFP in extracts of transfected COS-7 cells. In panel A diffusion times are indicated, in panel B the counts per molecule.

C) PCH analysis of GFP-CLASP2, EB3-GFP, GFP-EB3 and GFP in extracts of transfected COS-7 cells. Molecular brightness is indicated.

these molecules. The results show that GFP-CLASP2 has a molecular brightness that is comparable to that of monomeric GFP and lower than that of dimeric EB3-GFP, or GFP-EB3 (Fig. 3-S4C). Thus, soluble GFP-CLASP2 is a monomeric protein.

3.4.3. Generation and characterization of a 3T3 cell line stably expressing GFP-CLASP2.

Although the rtTA system is leaky in our hands (Fig. 3-5A), the expression of GFP-CLASP2 can be regulated, which is important because abundant overexpression of this protein may have consequences for the MT network. In one cell line (clone 86) GFP-CLASP2 expression was induced after treatment with doxycyclin, hence this clone was chosen for further analysis. Western blot analysis demonstrated a correct size of GFP-CLASP2 (Fig. 3-S5A).

Immunofluorescence analysis showed that in nonmigratory clone 86 cells GFP-CLASP2 is localised near the Golgi apparatus and on MT ends (Fig. 3-S5D-F). The application of lithium chloride, an inhibitor of GSK3 β , caused a significant increase of GFP-CLASP2 signal at distal ends of MTs (data not shown). In wound healing experiments we detected GFP-CLASP2 at the distal ends of stable MTs, which were mostly directed towards the leading edge of clone 86 cells (Fig. 3-S5G-I). Staining of migrating clone 86 cells with anti-CLASP2 antibodies revealed virtually identical patterns of GFP and antibody fluorescence (Fig. 3-S5I-L), indicating that GFP-CLASP2 and endogenous CLASP2 localize in a similar manner.

Time-lapse analysis (Movies 3-2 and 3-6, and data not shown) demonstrated the presence of comet-like GFP-CLASP2 dashes, which moved with an average velocity of $0.48 \pm 0.09 \mu\text{m/s}$ (63 dashes analyzed in 11 cells, \pm SD). These values are consistent with the speed of movement of other GFP-tagged +TIPs (Stepanova et al., 2003) and are similar to the movement of GFP-CLASP2 in transiently transfected COS-1 cells (Akhmanova et al., 2001). Combined, these data strongly suggest that GFP-CLASP2 recapitulates the behavior of endogenous CLASP2 in 3T3 cells, including the regulation of its MT binding capacity by GSK3. Thus, GFP-CLASP2 expressing 3T3 cells are suitable to investigate dynamic aspects of CLASP2 behavior.

In fixed 3T3 cells, some of the GFP-CLASP2-positive accumulations colocalized with anti-paxillin and anti-vinculin antibodies (Fig. 3-S5B, C). Thus, GFP-CLASP2 distributes near (but does not overlap with) focal adhesions. Similar results were recently obtained with LL5 β (Lansbergen et al., 2006). Addition of the MT depolymerizing drug nocodazole abolished GFP-CLASP2 dashes on dynamic MT ends but did not cause an immediate depletion of GFP-CLASP2-positive accumulations (Movie 3-3). These data suggest that dynamic MTs are not required to maintain GFP-CLASP2 within these domains.

3.5. Acknowledgements

We thank Dr. H. Bujard (Heidelberg, Germany) for the rtTA2-M2 regulator plasmid. This research was supported by grants from the Netherlands Organisation for Scientific Research (NWO-ALW and NWO-MW), the Netherlands Ministry of Economic Affairs (BSIK), the Dutch Cancer Society (KWF) and an EC integrated project on Molecular Imaging (LSHG-CT-2003-503259).

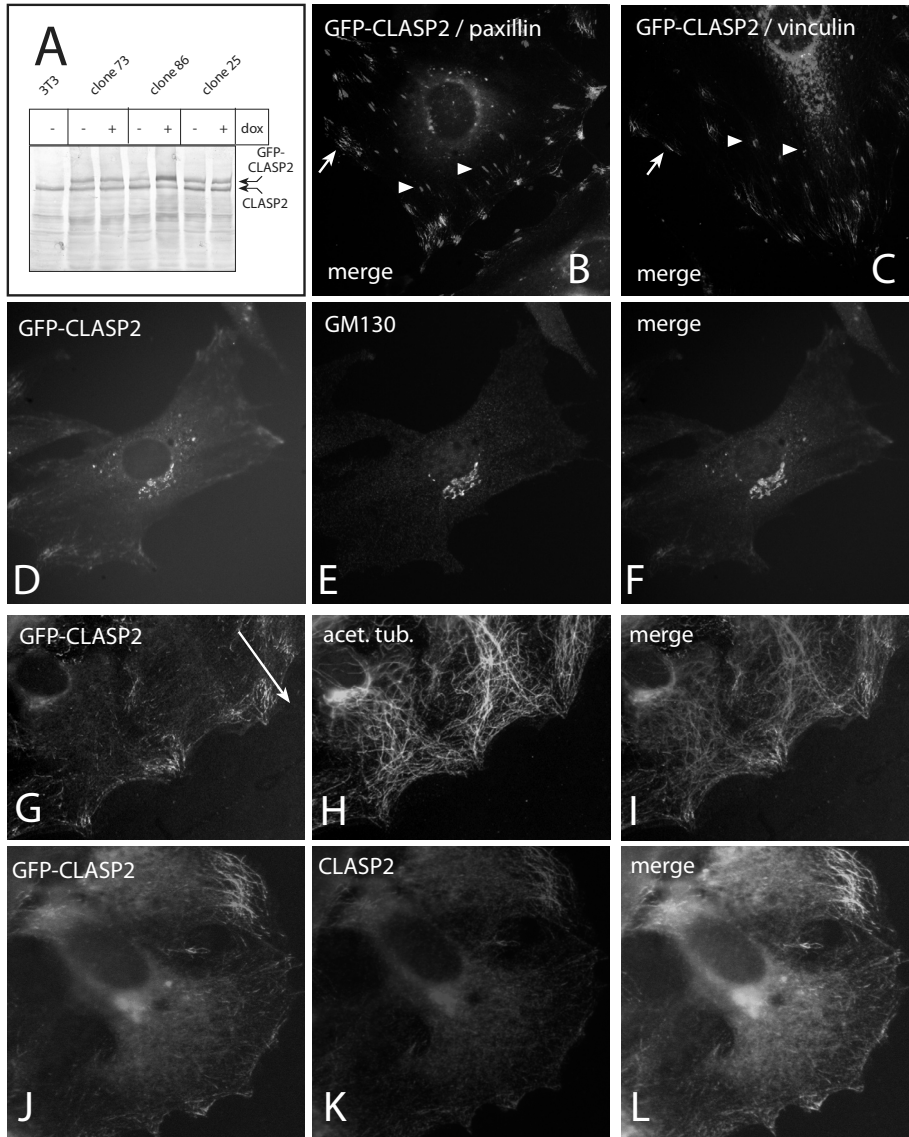


Figure S5. Generation of GFP-CLASP2 expressing 3T3 cell lines.

- A) 3T3 cells, stably expressing GFP-CLASP2, were either treated with doxycycline (dox) or not treated. Protein extracts of three different, GFP-CLASP2 expressing cell lines, were analyzed by western blot with anti-CLASP2 antiserum (#2358). Only clone 86 shows inducible GFP-CLASP2 expression. The level of fusion protein is comparable to endogenous CLASP2.
- B) 3T3 fibroblasts, expressing GFP-CLASP2 (green), were fixed and stained with anti-paxillin (red).
- C) 3T3 fibroblasts (clone 86), expressing GFP-CLASP2 (green), were fixed and stained with anti-vinculin (red).
- D-L) Localization GFP-CLASP2 in stably transfected 3T3 cells. 3T3 cells were fixed and stained with anti-GM130 (D-F), anti-acetylated tubulin (G-I), and anti-CLASP2 (J-L). For the latter experiments cells were first allowed to migrate into a wound so that stable, polarized MTs would be generated (the arrow in (F) indicates the direction of cell migration). Notice that GFP-CLASP2 recapitulates the behavior of the non-tagged protein (Akhmanova et al., 2001).

3.6. Movies

These supplemental movies are available at <http://www.current-biology.com/cgi/content/full/16/22/2259/DC1/>.

Movie 3-1

Time lapse analysis of GFP-CLASP2, transiently expressed in HeLa cells. We acquired one image every second. As documented previously using transient transfections in COS-1 cells (Akhmanova et al., 2001), GFP-CLASP2 is a +TIP. Notice also accumulation of fusion protein at sites near the cell edge and at the Golgi.

Movie 3-2

Time lapse analysis of GFP-CLASP2, expressed in doxycyclin-induced clone 86 cells. We acquired one image every 2.4 seconds. Again, GFP-CLASP2 is a +TIP. Notice also the accumulation of fusion protein at sites near the cell edge. GFP-CLASP2 enters and exits these areas of “static” GFP-CLASP2 accumulation, which have their own dynamic behavior.

Movie 3-3

Time lapse analysis of GFP-CLASP2, expressed in doxycyclin-induced clone 86 cells. One image was acquired every 3 seconds. After 3 minutes nocodazole was added to the medium (10 μ M final concentration). This causes an immediate dissociation of GFP-CLASP2 from the ends of MTs. Addition of nocodazole does not cause the immediate depletion of GFP-CLASP2 from “static” accumulations.

Movies 3-4 and 3-5

Time lapse analysis of GFP-CLASP2, expressed in doxycyclin-induced clone 86 cells, after serum addition. One image was acquired every 2 minutes. Cells were followed for 3 hours. Notice the persistent accumulation of GFP-CLASP2 at the leading edge of cells. In Movie 3-4 only fluorescent signal is shown, in Movie 3-5 both phase-contrast and fluorescent signals are shown. Notice how GFP-CLASP2 is constantly recruited at the leading edge, but the protein does not penetrate the most distal lamellae.

Movie 3-6

GFP-CLASP2 behavior in migrating cells. One image was acquired every 2 seconds. The speed of GFP-CLASP2 displacements (representing polymerization rate of MTs) in the cytoplasm is the same in motile and non-motile cells. Notice the accumulation of fusion protein at sites near the cell edge.

Movie 3-7

FRAP analysis of GFP-CLASP2 in migrating 3T3 cells. One image was acquired every 2 seconds. GFP-CLASP2 displacements in the cytoplasm and near the cell edge are seen, as are accumulations near the cell edge. One of these accumulations was bleached. For detailed explanation, see results and Fig. 3-4.

Chapter 4

Dynamic Behavior of GFP-CLIP-170 Reveals Fast Protein Turnover on Microtubule Plus-Ends

Katharina A. Dragestein

Wiggert A. van Cappellen

Jeffrey van Haren

George D. Tsibidis

Anna Akhmanova

Tobias A. Knoch

Frank Grosveld

Niels Galjart

adapted from:

Journal of Cell Biology, in press

4.1. Summary

Microtubule plus-end tracking proteins (+TIPs) specifically recognize the ends of growing microtubules. +TIPs are involved in diverse cellular processes, such as cell division, cell migration, and the establishment and maintenance of cell polarity. While tip-tracking is important for these processes, the mechanisms underlying plus-end specificity of mammalian +TIPs are not completely understood. CLIP-170, the prototype +TIP, was proposed to bind to microtubule ends with high affinity, possibly by co-polymerization with tubulin, and to dissociate seconds later. However, using fluorescence-based approaches, we show that CLIP-170 and another +TIP, EB3, rapidly turn over on microtubule ends. Diffusion of CLIP-170 and EB3 appear to be rate-limiting for the binding on microtubule plus-ends. We also find that the end of a growing microtubule contains a surplus of sites to which CLIP-170 binds with relatively low affinity. We propose that the observed loss of fluorescent +TIPs at plus-ends does not reflect the behavior of single molecules, but is a reflection of overall structural changes of the microtubule end.

4.2. Introduction

Microtubules (MTs) exhibit dynamic instability (Mitchison and Kirschner, 1984), repeatedly switching between growth and shrinkage phases, thereby constantly moving through the cytoplasm. This facilitates contacts between MT-ends and relatively immobile cellular structures, such as chromosomes and focal adhesions, and allows the cell to react to external cues. Plus-end-tracking proteins, or +TIPs (Schuyler and Pellman, 2001), specifically bind to MT plus-ends and are ideally positioned to influence MT dynamics and MT-target interactions.

Time-lapse imaging of fluorescently tagged +TIPs reveals typical “comet-like” dashes, which represent fluorescent +TIP molecules bound to the ends of growing MTs. This unique behavior has been explained by different mechanisms (for reviews, see Akhmanova and Hoogenraad, 2005; Carvalho et al., 2003; Howard and Hyman, 2003). For example, CLIP-170, the prototype +TIP (Perez et al., 1999), was suggested to bind MT-ends by “treadmilling” (Fig. 4-S1A), binding with high affinity to newly synthesized MT-ends and detaching with a half-life of 1-3 seconds (Folker et al., 2005; Komarova et al., 2005; Perez et al., 1999). The same mechanism was apparently used by GFP-tagged EB1 (Tirnauer et al., 2002). Others proposed that CLIP-170 co-polymerizes with tubulin (Arnal et al., 2004; Diamantopoulos et al., 1999; Folker et al., 2005) (Fig. 4-S1B). In both models, dissociation of +TIPs from MT-ends is correlated to the loss of fluorescence in the “comet-like” dash.

One CLIP-170 monomer has two MT binding domains (Pierre et al., 1992), each of which contains a CAP-Gly motif (Riehemann and Sorg, 1993). This motif is also present in two other +TIPs, CLIP-115 (De Zeeuw et al., 1997) and p150glued (Gill et al., 1991). Recently, CAP-Gly domains were shown to interact with the C-terminal tails of α -tubulin and EB1 (Honnappa et al., 2006; Mishima et al., 2007). In cultured cells CLIP-170 (but not EB1) fails to recognize the ends of detyrosinated MTs (Peris et al., 2006), showing that the C-terminal tyrosine of α -tubulin is essential for the accumulation of CLIP-170 on MT-ends. On the other hand, evidence has been presented for a role of EB1 in the MT-end localization of CLIP-170 (Komarova et al., 2005; Watson and Stephens, 2006). To reconcile these results we examined the

dynamics of GFP-CLIP-170 on MT plus-ends, using fluorescence recovery after photobleaching (FRAP) and fluorescence correlation spectroscopy (FCS) approaches.

Here, we show that MT plus-ends contain a surplus of binding sites for CLIP-170, to which CLIP-170 molecules bind with low affinity, resulting in their rapid exchange on MT plus-ends. Our data imply that MT polymerization generates a large number of binding sites that decay exponentially. This turnover of binding sites explains the fluorescent “comet-like” dashes of GFP-CLIP-170 and other +TIPs observed in cells. Thus, CLIP-170 accumulates on MT-ends due to the number of binding sites rather than the strength of binding. Our findings may lead to a re-evaluation of other protein-accumulations at MT plus-ends.

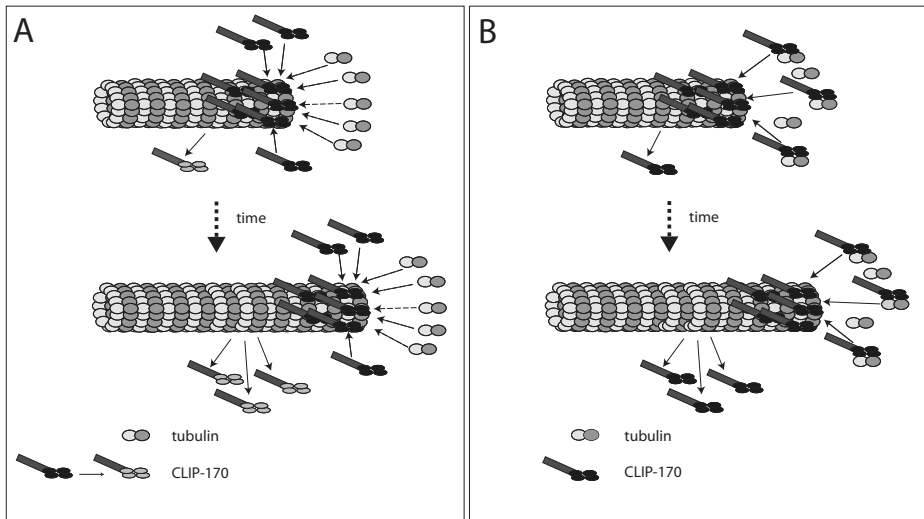


Figure 4-S1. Treadmilling of CLIP-170 at MT-ends and co-polymerization with tubulin.

- A) In the “treadmilling” model (Perez et al., 1999) dimeric CLIP-170 (blue ellipses indicate MT-binding motifs) binds with high affinity to the very end of a growing MT (upper MT). As the MT grows further (lower MT), new CLIP170 molecules associate, while the “old” molecules dissociate, an event that may be triggered by posttranslational modifications (indicated by the conversion of the MT-binding motif from dark to light grey). In the “treadmilling” model, the half-life of CLIP-170 on MT-ends is 1-2 seconds.
- B) In the “co-polymerization” model a complex of CLIP-170 and tubulin is incorporated at the MT-end (Arnal et al., 2004; Diamantopoulos et al., 1999; Folker et al., 2005). As the MT grows further (lower MT), new CLIP170-tubulin complexes associate, while “older” CLIP-170 molecules dissociate. In the “co-polymerization” model (like in the “treadmilling” model), half-life of CLIP-170 on MT-ends is 1-2 seconds. Importantly, in both models, once dissociated, CLIP-170 does not associate with the same region of a MT again.

4.3. Results and discussion

4.3.1. Transient binding of GFP-CLIP-170 to MT-ends

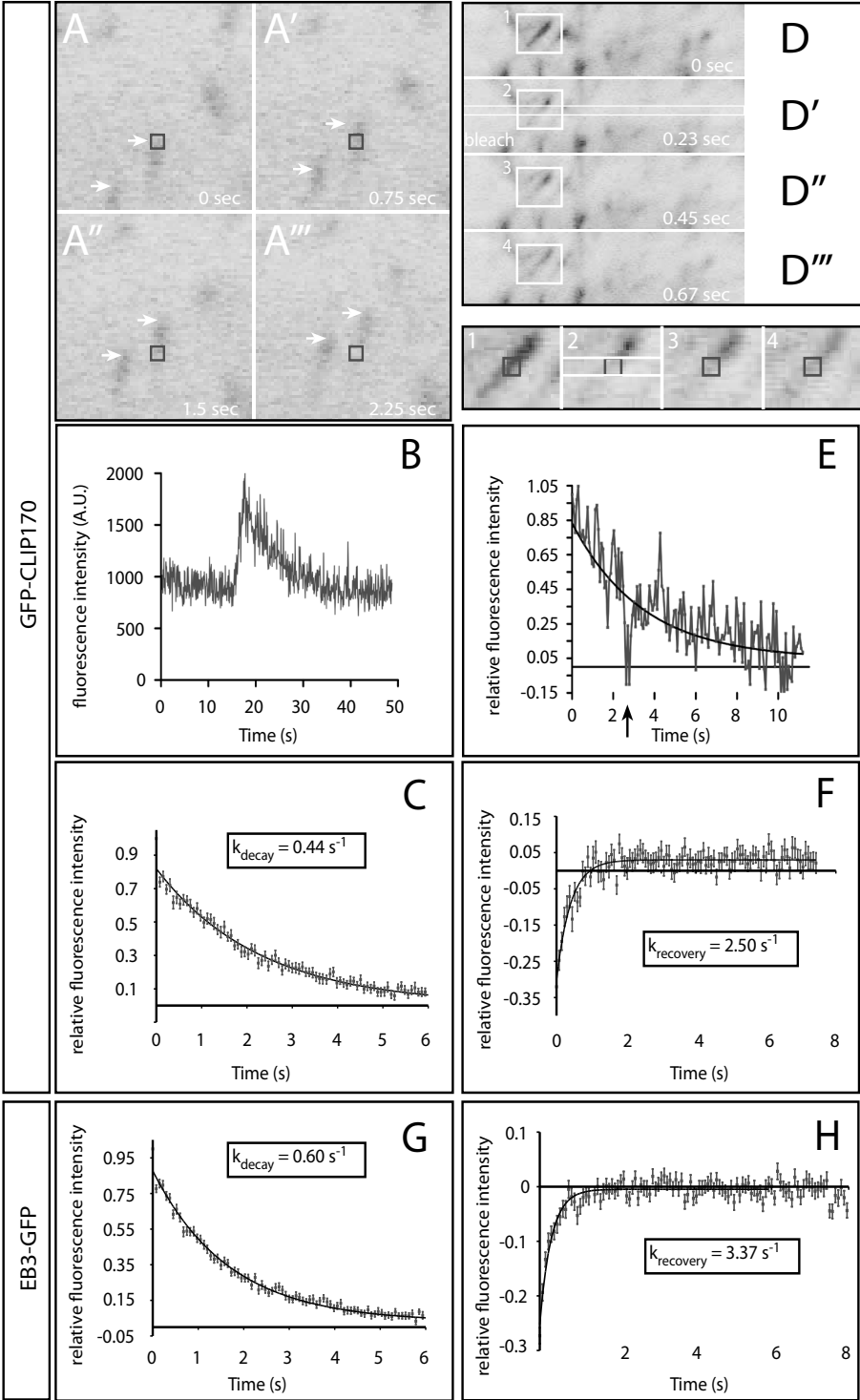
GFP-CLIP-170 behaves indistinguishable from endogenous CLIP-170 (Akhmanova et al., 2005; Perez et al., 1999), making it a useful tool to study the dynamic behavior of CLIP-170 *in vivo*. In cells expressing GFP-CLIP-170, MT plus-ends were visible as fluorescent “comets”. In order to study these “comets” with high temporal resolution, we acquired confocal images at 13.3 frames per second (Fig. 4-1A and movie 4-S1). MT plus-ends traversing regions of interest (ROIs) of 200 x 200 nm appeared as fluorescent peaks in the corresponding fluorescence intensity track (Fig. 4-1A, B). Average peak decays could be fitted with an exponential curve, yielding a k_{decay} of 0.44 s^{-1} for COS-7 cells at 37°C (Fig. 4-1C and Table I). This translates to a half-life of approximately 1.6 s for GFP-CLIP-170-derived fluorescence on MT plus-ends, which correlates well with reported half-lives of CLIP-170 on MT-ends (Folker et al., 2005; Komarova et al., 2005).

The macroscopic loss of fluorescence of GFP-CLIP-170 on MT plus-ends over time (i.e. the fluorescent decay) does not reveal the dynamic behavior of single CLIP-170 molecules. In order to get more insight in the dynamics of GFP-CLIP-170 on MT plus-ends, we performed FRAP experiments. Repeatedly bleaching a strip of $0.2 \times 18.5 \mu\text{m}$ in an imaged area of $4.5 \times 18.5 \mu\text{m}$ resulted mainly in bleaching of freely diffusing cytoplasmic GFP-CLIP-170 molecules, but also in bleaching of MT-bound GFP-CLIP-170 (Fig. 4-1D). We measured fluorescence intensity over time in areas of 200 x 200 nm on the bleached strip and observed recovery of fluorescence, not only in the cytoplasm, but also on MT plus-ends (Fig. 4-1E). These data indicate that on MT-ends non-fluorescent GFP-CLIP-170 molecules exchange with fluorescent ones. Various control experiments (see Supplemental Material and Fig. 4-S2) supported this interpretation. These results are not compatible with the original “treadmilling” model.

4.3.2. Exchange of CLIP-170 on MT plus-ends under non-steady state conditions

The FRAP analysis of GFP-CLIP-170 bound to MT plus-ends occurs under non-steady state conditions, that is, recovery of fluorescence on MT plus-ends takes place while their total fluorescence decreases. It was therefore not possible to analyze FRAP recovery with common models (e.g. Sprague et al., 2004). Instead, under these conditions, fluorescence recovery is governed by k_{off} , and by another constant that describes overall remodeling of the MT plus-end (Lele et al., 2006).

In order to calculate fluorescence recoveries on MT-ends, we corrected the recovery on bleached GFP-CLIP-170-positive MT plus-ends for the underlying overall loss of GFP-CLIP-170 fluorescence over time (shown in Fig. 4-1C). The resulting recoveries could be described with a simple exponential curve. We calculated an apparent k_{recovery} of 2.50 s^{-1} for the exchange of GFP-CLIP-170 on MT-ends in COS-7 cells at 37°C (Fig. 4-1F and Table 4-I). This corresponds to a half-life of association of 0.28 s, which is about six times shorter than the half-life of GFP-CLIP-170-derived fluorescence on MT plus-ends as described by k_{decay} .



Our data suggest that the disappearance of GFP-CLIP-170 from MT-ends as described by k_{decay} (Fig. 4-1C) actually reflects the loss of binding sites for CLIP-170 at MT-ends rather than the dissociation of individual CLIP-170 molecules. As we observed exchange of GFP-CLIP-170 all along MT plus-ends, even more than 1 μm distal from the tip, co-polymerization of CLIP-170 with tubulin does not appear to be the dominant mechanism underlying the accumulation of CLIP-170 on MT plus-ends.

4.3.3. EB3 also shows rapid turnover on MT plus-ends

EB1 and -3 are two highly related +TIPs (Su and Qi, 2001), which interact with many other +TIPs and are thought to play a central role in the association of +TIPs to MT ends (reviewed by Lansbergen and Akhmanova, 2006). In COS-7 cells expressing EB3-GFP we observed fluorescent peaks whose k_{decay} was 0.60 s^{-1} (Fig. 4-1G and Table 4-I). This value is slightly higher than the one obtained for GFP-CLIP-170 under similar conditions. Previous studies using mono-specific antibodies against EB1 and CLIP-170 in fixed cells have shown that EB1 and CLIP-170 have overlapping fluorescence staining patterns at MT ends (Komarova et al., 2005), supporting our results in live cells.

Using the fast FRAP approach in cells expressing EB3-GFP we observed recovery of fluorescence in the cytoplasm and on MT plus-ends (Fig. 4-1H). Thus, like GFP-CLIP-170, EB3-GFP exchanges rapidly on MT-ends. After correction for cytoplasmic recovery and fluorescence decay we found an apparent k_{recovery} of 3.37 s^{-1} for the exchange of EB3-GFP on MT-ends (Fig. 4-1H and Table 4-I). This corresponds to a half-life of association of 0.20 s, which is faster than the half-life of CLIP-170. Thus, there is a continuous exchange of GFP-CLIP-170 and EB3-GFP on MT plus-ends.

Figure 4-1. Fast FRAP analysis of GFP-CLIP-170.

- A-A'') COS-7 cells expressing GFP-CLIP-170 were imaged at 13.3 frames per second. Still images of a part of every 10th frame of a time-lapse series are shown. The distal ends of two MTs are indicated by arrows. At 0 s (panel A) a GFP-CLIP-170-labeled MT-end is about to traverse a 200 x 200 nm ROI (red rectangle). After 2.25 s (panel A'') this MT-end has traversed the ROI.
- B) Fluorescence intensity in a ROI of 200 x 200 nm as a GFP-CLIP-170-labeled MT-end traverses.
- C) Average fluorescence decay of non-bleached, GFP-CLIP-170-labeled MT-ends (k_{decay} is indicated).
- D-D'') COS-7 cells expressing GFP-CLIP-170 were imaged as in (A). An area of 256 x 3 pixels (indicated in D') was bleached every 6 seconds, which occasionally resulted in bleaching of MT-end-bound GFP-CLIP-170. Rectangles 1-4 are shown enlarged underneath panels D-D''). Fluorescence intensity was measured in ROIs of 200 x 200 nm (red rectangles).
- E) Fluorescence intensity measurement of bleached GFP-CLIP-170-labeled MT-end (black arrow indicates bleach moment; black line represents fluorescence decay). Notice the recovery of fluorescence.
- F) Average fluorescence recovery of GFP-CLIP-170 on MT-ends (k_{recovery} indicated).
- G) Average fluorescence decay of non-bleached, EB3-GFP-labeled MT-ends (k_{decay} indicated), imaged as in (A).
- H) Average fluorescence recovery of EB3-GFP on MT-ends (k_{recovery} indicated).

4.3.4. Observed exchange of CLIP-170 and EB3 on MT-ends appears limited by diffusion

Analysis of k_{recovery} of GFP-CLIP-170 in COS-7 cells at 37°C in the cytoplasm yielded a value of 2.80 s^{-1} (Table 4-I), which is not much different from the apparent k_{recovery} of 2.50 s^{-1} on MT-ends. The values for k_{recovery} of EB3-GFP on MT ends and in the cytoplasm are also similar (3.37 s^{-1} and 3.42 s^{-1} , respectively, see Table 4-I). These results indicate that the time a CLIP-170 or EB3 molecule is actually bound to the MT-end is shorter than the time it takes these molecules to diffuse through the bleached strip. The fact that k_{recovery} for EB3-GFP in the cytoplasm as well as on MT-ends is higher than the corresponding values of GFP-CLIP-170 is consistent with EB3-GFP being smaller and diffusing more rapidly.

Biochemical reaction rates are temperature dependent, with an approximate doubling of reaction constant every 10°C. We reasoned that the behavior of GFP-CLIP-170 at MT ends might be influenced by temperature changes and analyzed cells at different temperatures. We examined both 3T3 cells that stably express GFP-CLIP-170 (Drabek et al., 2006) as well as transiently transfected COS-7 cells to evaluate the behavior of CLIP-170 in different cell types. In 3T3 cells the rates of GFP-CLIP-170 displacements, which reflect MT growth rates, diminished from about $0.4 \mu\text{m/s}$ at 37°C, to $0.19 \mu\text{m/s}$ at 27°C (Fig. 4-2A), emphasizing the temperature dependence of MT assembly. Previous results in transiently transfected COS-7 cells are consistent with this observation (Stepanova et al., 2003). Interestingly, reducing the temperature by 10°C increased the half-life of the fluorescence decay of GFP-CLIP-170 on MT plus-ends, from 1.4 s to 2.7 s in 3T3 cells (Fig. 4-2B), and from 1.6 s to 2.8 s in transiently transfected COS-7 cells (Fig. 4-2C and Table 4-I).

+TIP	Cell type	Method	Temp. (°C)	$k_{\text{decay}} (\text{s}^{-1})$ MT end	$k_{\text{recovery}} (\text{s}^{-1})$ MT end	$k_{\text{recovery}} (\text{s}^{-1})$ Cytoplasm
EB3	COS-7	FRAP	37	0.60 0.58 - 0.62 (n = 175)	3.37 2.89 - 3.85 (n = 298)	3.43 2.75 - 4.12 (n = 1756)
Full length CLIP-170	COS-7	FCS	37	0.48 0.39-0.59 (n = 17)	n.d.	n.d.
Full length CLIP-170	COS-7	FRAP	37	0.44 0.42 - 0.46 (n = 77)	2.50 2.06 - 2.94 (n = 94)	2.80 2.29 - 3.31 (n = 534)
Full length CLIP-170	COS-7	FRAP	27	0.25 0.23 - 0.27 (n = 87)	n.d.	n.d.
Full length CLIP-170	MEF (WT)	FRAP	27	0.25 0.23 - 0.26 (n = 71)	1.66 1.36 - 1.97 (n = 83)	2.34 1.90 - 2.78 (n = 553)
Full length CLIP-170	MEF (DKO)	FRAP	27	0.25 0.244 - 0.256 (n = 171)	2.04 1.86 - 2.21 (n = 214)	2.43 2.14 - 2.51 (n = 1550)
CLIP-170 Xmnl	MEF (DKO)	FRAP	27	0.31 0.30 - 0.33 (n = 86)	3.56 2.62 - 4.55 (n = 93)	4.87 4.09 - 5.65 (n = 666)

Table 4-I. Behavior of transiently transfected GFP-tagged +TIPs on MT plus-ends.

Average k_{decay} and k_{recovery} values are given with (underneath) the 95% confidence interval and the number (n) of fluorescent decays and recoveries, respectively, used to calculate average values. WT: wild type, DKO: double knockout, n.d.: not determined.

These results indicate that temperature has a significant influence on GFP-CLIP-170 behavior, which might be caused by changes in MT behavior.

Because it takes longer for GFP-CLIP-170 fluorescent comets to disappear at 27°C than at 37°C fast FRAP experiments are easier to perform at lower temperature. Furthermore, in two mouse embryonic fibroblast (MEF) cell lines with different genetic backgrounds (see below) the half-life of the fluorescence decay of GFP-CLIP-170 on MT plus-ends at 27°C was identical to that observed in 3T3 and COS-7 cells (i.e. 2.8 s, Table 4-I), indicating that GFP-CLIP-170 behaves similar in different cell types. We therefore performed most of our other fast FRAP experiments in transiently transfected MEFs at 27°C. In wild type MEFs the half-lives of

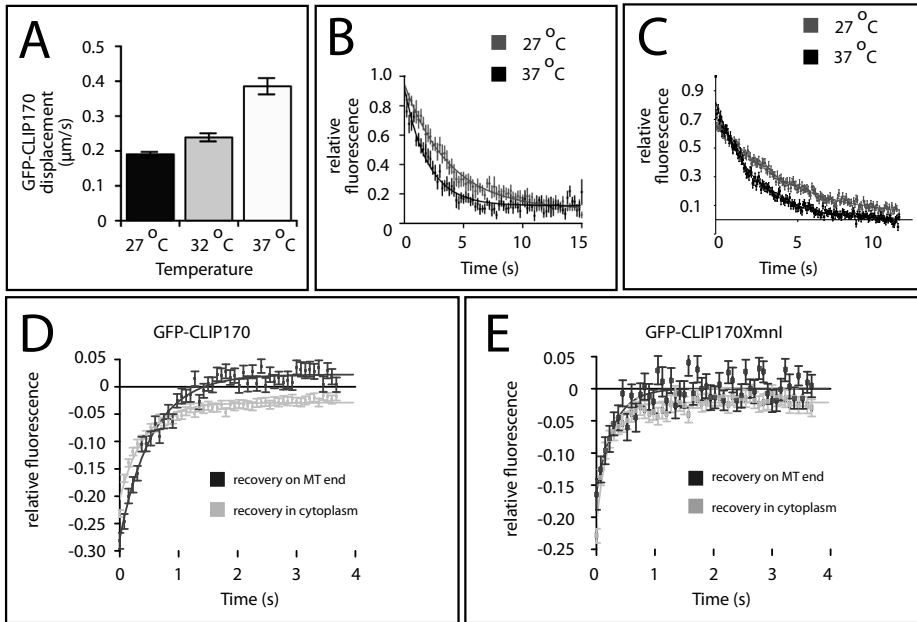


Figure 4-2. Influence of temperature on GFP-CLIP-170 behavior.

- A) Speed of GFP-CLIP-170 displacement at different temperatures. 3T3 cells stably expressing GFP-CLIP-170 were analyzed (13 MT-ends analyzed at 37°C, 19 at 32°C, and 14 at 27°C, SEM indicated, see also Movies 4-S2 and 4-S3).
- B) 3T3 cells stably expressing GFP-CLIP-170 were analyzed at 37°C (black) or 27°C (grey). Fluorescence loss of GFP-CLIP-170 at MT-ends was examined (13 MT-ends analyzed at 37°C, and 12 at 27°C, SEM indicated). A fit was obtained with $A+B \cdot \exp(-C \cdot X)$. This yielded a half-life of GFP-CLIP-170 fluorescence of 1.35 s at 37°C and of 2.67 s at 27°C.
- C) COS-7 cells expressing GFP-CLIP-170 were analyzed at 37°C (black) and 27°C (grey). Fluorescence loss of GFP-CLIP-170 at MT-ends was examined at 37°C and 27°C (SEM indicated, see Table 4-I for values).
- D) MEFs were transiently transfected with GFP-CLIP-170. FRAP analysis was carried out at 27°C. Fluorescent recovery of GFP-CLIP-170 was analyzed in the cytoplasm of cells (light grey) as well as on MT-ends (dark grey). SEM indicated. For k_{recovery} values see Table 4-I.
- E) MEFs were transiently transfected with GFP-CLIP-170Xmnl, a mutant protein that only contains the MT binding domains of CLIP-170. FRAP analysis was carried out at 27°C. Fluorescent recovery of GFP-CLIP-170Xmnl was analyzed in the cytoplasm of cells (light grey) as well as on MT-ends (dark grey). SEM is indicated. For k_{recovery} values see Table 4-I.

recoveries were 0.30 s for cytoplasmic GFP-CLIP-170 (k_{recovery} of 2.34 s^{-1}), and 0.42 s for MT-end-bound GFP-CLIP-170 (k_{recovery} of 1.66 s^{-1} , see also Fig. 4-2D and Table 4-I). These values did not differ significantly from each other. Thus, despite the fact that MT growth rates decrease and binding sites for CLIP-170 disappear more slowly at 27°C , the average time a CLIP-170 molecule is bound to a MT plus-end remains short. We propose that diffusion of CLIP-170 and EB3 is rate-limiting for the observation of binding/unbinding reactions on MT plus-ends.

4.3.5. Fast exchange of CLIP-170 on MT-ends is independent of self-interaction

CLIP-170 is a rod-like molecule that can interact with itself in a head-to-tail fashion (Lansbergen et al., 2004; Scheel et al., 1999). Both intra- and intermolecular interactions of CLIP-170 are possible. One could therefore envision a “first layer” of CLIP-170 molecules, tightly bound to the MT surface and turning over by the classic “treadmilling” mechanism, to which a “second layer” of CLIP-170 molecules bind through intermolecular head-to-tail interactions, which enables the “second layer” to turn over rapidly on the “first layer”. To investigate this, we tested the dynamic behavior of a fragment of GFP-CLIP-170 (GFP-CLIP-170XmnI) that contains only the MT binding domain, lacking the central coiled-coil domain and the C-terminal domain mediating interactions between CLIP-170 molecules (Komarova et al., 2002a). FRAP analysis in GFP-CLIP-170XmnI transfected COS-7 cells showed that this truncated form of CLIP-170 also exchanges on MT-ends (data not shown).

To eliminate the possibility of interaction of fluorescent GFP-CLIP-170XmnI with endogenous non-fluorescent CLIP-170, we next tested recovery of the truncated protein in MEFs derived from CLIP-115/CLIP-170 double knock out mice, which contain neither CLIP-115 nor CLIP-170 (M. Miedema and N. Galjart, manuscript in preparation). FRAP analysis at 27°C showed fast recovery of GFP-CLIP-170XmnI (Fig. 4-2E and Table 4-I), both in the cytoplasm (k_{recovery} of 4.87 s^{-1}) and on MT-ends (k_{recovery} of 3.56 s^{-1}). These results indicate that the transient binding of CLIP-170 molecules on MT-ends does not occur via a layer of MT-bound CLIP-170.

GFP-CLIP-170 has a dimer-weight of about 400 kDa, whereas GFP-CLIP-170XmnI weights only 65 kDa. That GFP-CLIP-170XmnI is diffusing faster through the cytoplasm is reflected by a bigger cytoplasmic k_{recovery} . The apparent k_{recovery} on MT plus-ends is bigger as well, and it is not significantly different from the cytoplasmic one. These results suggest that the observed binding/unbinding of GFP-CLIP-170XmnI on MT plus-ends is also diffusion-limited.

4.3.6. CLIP-170 binds MT plus-ends with low affinity

Fluorescence correlation spectroscopy (FCS) is a sensitive single-molecule technique that allows the determination of diffusive behavior and concentration of proteins *in vivo* and in real time (Elson, 2004). Using FCS, we analyzed GFP-CLIP-170 in COS-7 cells expressing low amounts of GFP-CLIP-170 (Fig. 4-3A). Strikingly, many fluorescence intensity tracks of FCS measurements showed peaks, which generally had a steep and relatively linear upward slope and a curved downward slope (Fig. 4-3B), similar to the k_{decay} curves obtained by confocal imaging. Combined with

other experiments (Supplemental Material and Fig. 4-S3D), this suggests that peaks in FCS intensity tracks represent GFP-CLIP-170-labeled ends of growing MTs.

In order to correlate the cytoplasmic GFP-CLIP-170 concentration to the number of peak-bound GFP-CLIP-170 molecules, we calculated the number of particles present in the cytoplasm and on peaks observed in fluorescence intensity

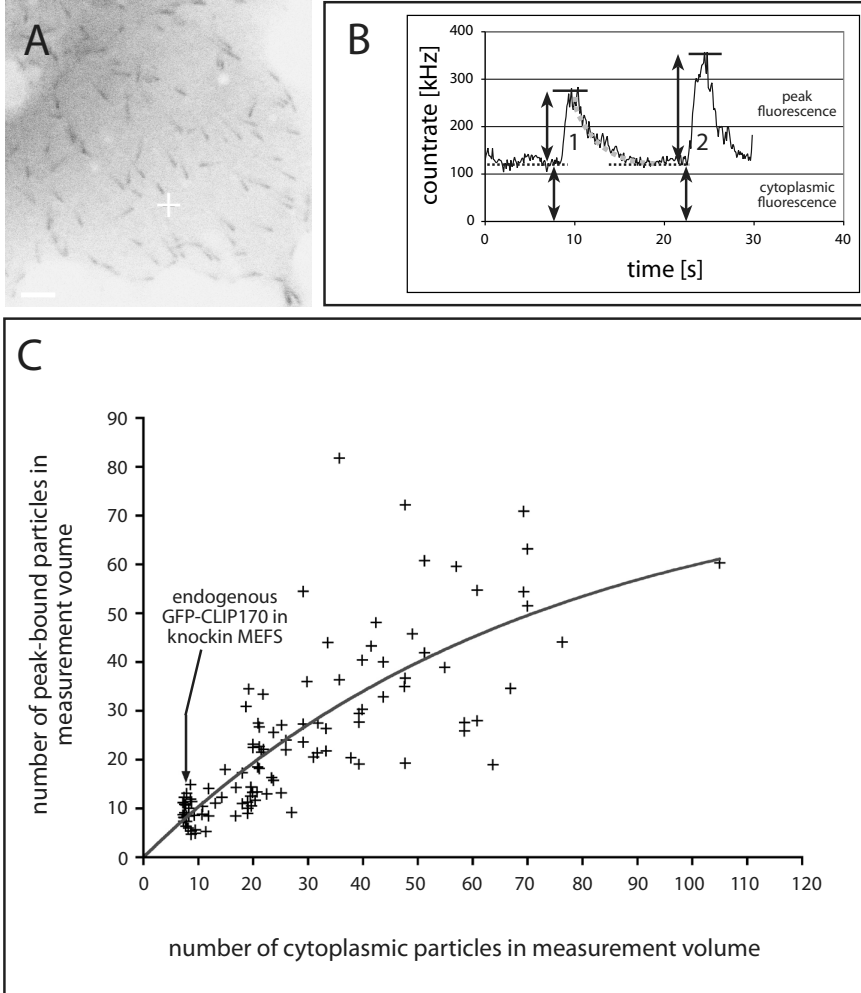


Figure 4-3. Analyzing GFP-CLIP-170 on MT-ends with FCS.

- A) Confocal image of a COS-7 cell transfected with GFP-CLIP-170. White crosshair indicates location of FCS measurement.
- B) Intensity-trace of FCS measurement in a transfected COS-7 cell. Peaks of fluorescence are occasionally detected. Dashed red line: exponential fluorescence decay, lower double-headed arrows: cytoplasmic fluorescence, upper double-headed arrows: peak fluorescence.
- C) Comparison of the number of cytoplasmic and peak-bound GFP-CLIP-170 particles. Values as depicted in (B) were measured and number of particles were determined for 110 peaks. A scatter plot of these values is best approximated by an exponential curve, $Y=Y_{\max} \cdot (1-\exp(-K \cdot X))$.

tracks of FCS measurements (see Fig. 4-3B). We assumed that fluorescence emitted from a cytoplasmic and a MT-bound GFP-CLIP-170 molecule is the same, and that non-GFP derived signal intensity is negligible. A positive correlation between cytoplasmic and MT-associated GFP-CLIP-170 was found (Fig. 4-3C). Peak fluorescence values still increased at the highest concentrations of GFP-CLIP-170. These results indicate that the binding of GFP-CLIP-170 to MT-ends was not yet saturated. Thus, CLIP-170 binds MT-ends with low affinity.

We recently generated GFP-CLIP-170 knock-in MEFs, in which GFP-CLIP-170 is expressed at wild-type level, associates with the ends of growing MTs (Supplemental Movie 4-S4), and can functionally replace the normal protein (Akhmanova et al., 2005). Using FCS, we calculated an intracellular GFP-CLIP-170 dimer concentration of 44 ± 11 nM ($n = 26$; 13 cells, 4 independent experiments, \pm SD). We estimated that ~ 10 GFP-CLIP-170 molecules are bound per MT-end in knock-in MEFs. The about 200-500 growing MTs in MEFs (our unpublished observations, see also Schulze and Kirschner, 1987) therefore bind 2,000-5,000 CLIP-170-dimers. If the volume of an average fibroblast is $2,000 \mu\text{m}^3$ (Bussolati et al., 1996; Imaizumi et al., 1996), $\sim 60,000$ CLIP-170-dimers are present in a cell. Thus, less than 10% of CLIP-170 is MT-bound. Assuming a maximum number of ~ 100 binding sites for CLIP-170 per MT end, that 10 % of these sites is occupied by CLIP-170, and that CLIP-170 does not bind other proteins (Fig. 4-3C), results in a dissociation constant (K_d) of $0.44 \mu\text{M}$.

The concentration of CLIP-170 in MEFs is approximately 0.5% of the concentration of soluble tubulin (Hiller and Weber, 1978). The MT-binding domain of CLIP-170 has been reported to interact with tubulin *in vitro* with a K_d of $0.03 \mu\text{M}$ (Folker et al., 2005). More recently, a K_d of $0.5 \mu\text{M}$ was reported for the association of the monomeric head domain of CLIP-170 with a C-terminal peptide of α -tubulin (Mishima et al., 2007). If we assume a similar affinity of full length CLIP-170, then virtually all cytoplasmic CLIP-170 in knock-in MEFs should be bound to tubulin and not be available for rapid exchange on MT ends. Based on observations that binding of CLIP-190 from *D. melanogaster* to MT plus-ends is strong in interphase and greatly reduced during mitosis (Dzhindzhev et al., 2005; Tanenbaum et al., 2006), we speculate that the affinity of CLIP-170 for tubulin *in vivo* is regulated by posttranslational modifications, and that CLIP-170 switches between tubulin- and MT-end-binding forms during the cell cycle.

4.3.7. Fast exchange model for CLIP-170 interaction with MT-ends

We propose a “fast exchange” model for the binding of CLIP-170 to MT-ends (Fig. 4-4). In our view MT polymerization generates a vast number of binding sites that decay exponentially (described by k_{decay}) and that can bind and release CLIP-170 molecules several times before disappearing. CLIP-170 binds sites on MT-ends with (sub)micromolar affinity. Like CLIP-170, EB3 also turns over rapidly on MT plus-ends and our data indicate that diffusion plays a major role in the binding of CLIP-170 and EB3. Although this may obscure true binding and unbinding rates, these results suggest that CLIP-170 and EB3 “reach” MT plus-ends independently of each other.

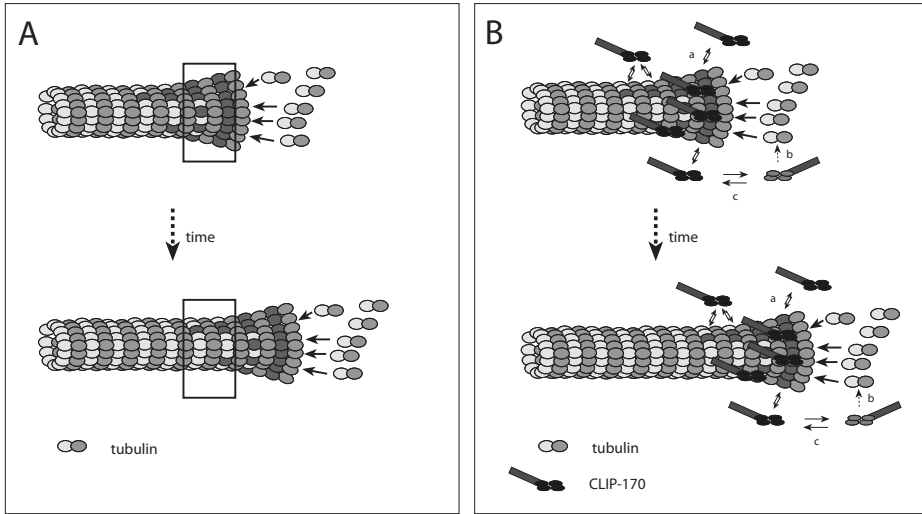


Figure 4-4. Fast-exchange model.

- A) MT polymerization generates a large number of binding sites (orange ellipses). Fifteen of these sites are present within the rectangle in the upper MT. Binding sites disappear with single-order reaction kinetics. Thus, as time progresses less binding sites are present within the rectangle.
- B) Dimeric CLIP-170 exchanges rapidly on binding sites, irrespective of their position on the MT-end. During the lifetime of a binding site a number of interactions with CLIP-170 molecules can occur. Because there are more binding sites at the very distal end, more CLIP-170 molecules bind there. The equilibrium between cytoplasmic and MT-end bound CLIP-170 (reaction a) might be determined by posttranslational modifications, conformational changes and/or protein-protein-interactions. As we find CLIP-170 exchange on MT-ends at positions distal to sites of MT polymerization, co-polymerization of CLIP-170 with tubulin (reaction b) does not explain the comet-like distribution of +TIPs. However, it is not excluded (hence the stippled arrow), and modified forms of CLIP-170 (indicated by the purple ellipses) might bind tubulin with higher affinity.

A critical determinant for MT plus-end recognition *in vivo* is the C-terminal tyrosine residue of α -tubulin (Peris et al., 2006). Here we show that CLIP-170 binding to MT plus-ends is reduced after application of 10 nM taxol (Supplemental Material and Fig. 4-S4). Taxol stabilizes MTs by binding to α -tubulin and changing MT conformation (Arnal and Wade, 1995). These data indicate that CLIP-170 recognizes a structural feature of the MT plus-end besides the C-terminal tyrosine of α -tubulin. It has been shown that MTs in *Xenopus* egg extracts grow by the extension of a two-dimensional sheet of protofilaments, which later closes into a tube (Arnal et al., 2000). As suggested by others (Nogales and Wang, 2006), binding sites for CLIP-170 (and other +TIPs) might be localized on the lumen-side of the MT sheet. However, given the size of fluorescent comets, this would imply a sheet-length of at least 2 μ m. Using cryo-electron microscopy we have not found evidence for the existence of such long sheets in interphase fibroblasts (Koning et al., 2007).

The “fast exchange” model implies that the fluorescence decay at MT-ends, which is measured in kymographs (Folker et al., 2005; Komarova et al., 2005; Tirnauer et al., 2002), does not correlate with dissociation rates of +TIPs, but rather with the disappearance of binding sites for these proteins (hence the name k_{decay}). A combined knock down of the +TIPs EB1 and EB3 resulted in faster fluorescence

decay of YFP-CLIP-170 (Komarova et al., 2005). We hypothesize that EB1-like proteins directly influence the turnover of binding sites at MT-ends and that their depletion causes altered remodeling of MT-ends, and thereby a faster disappearance of CLIP-170.

In migrating Ptk1 cells, GFP-CLASP2 is associated with the MT lattice of MTs “pioneering” into the lamellipodium while it is a +TIP in the cell body (Wittmann and Waterman-Storer, 2005). FRAP analysis of GFP-CLASP2 in the cell body indicated a recovery along the whole MT-end (Wittmann and Waterman-Storer, 2005). If CLASP2 was “treadmilling” on MT-ends, one would expect fluorescence to reappear only in MT segments of new plus-end growth. However, the observed uniform recovery of CLASP2 on MT-ends is well explained by the “fast exchange” model. We therefore propose that the “fast exchange” model is not limited to CLIP-170 and EB3 but is a more general mechanism for +TIP behavior at MT-ends.

4.4. Experimental procedures

4.4.1. Fusion proteins

The GFP-CLIP-170 knock-in fusion protein is functional *in vivo* because GFP-CLIP-170 knock-in mice are completely normal, whereas CLIP-170 knock out mice have severe defects in spermatogenesis (Akhmanova et al., 2005). The GFP-CLIP-170 cDNA, used for transient transfections of COS-7 cells as well as for the generation of the stable 3T3 cell line, has been described (Hoogenraad et al., 2000). It is based on a brain-specific CLIP-170 isoform (Akhmanova et al., 2005) isolated from a rat brain cDNA library (De Zeeuw et al., 1997). Normal cellular morphology and localization of the dynactin complex at MT plus-ends are restored (M. Miedema and N. Galjart, manuscript in preparation) when the GFP-CLIP-170 fusion protein is introduced into CLIP-115/-170 deficient MEFs, proving its functionality. The rat brain CLIP-170 cDNA was also used to generate the truncated CLIP-170 XmnI-protein (amino acids 4-309), which is called CLIP-170 “Head” in the original study (Komarova et al., 2002a). The “Head” domain of CLIP-170 is able to restore MT dynamics in cells in which CLIP-170 does not localize to MT-ends (Komarova et al., 2002a). EB3-GFP has been described previously (Stepanova et al., 2003), and localizes to MT plus-ends. Positioning of GFP at the C-terminus prevents interaction with CAP-Gly motif containing proteins (Komarova et al., 2005), but other protein-protein interactions are not perturbed.

4.4.2. Cell lines, cell culture and transfection

GFP-CLIP-170 knock-in mice and MEFs have been published (Akhmanova et al., 2005). The CLIP-115/-170 double knock out MEFs will be described elsewhere (M. Miedema and N. Galjart, manuscript in preparation). They were derived from double knock out mice, which were generated by crossing the *Clip1* (CLIP-170 encoding gene) and *Clip2* (CLIP-115 encoding gene) single knock out lines (Akhmanova et al., 2005; Hoogenraad et al., 2002).

The 3T3 cell line expressing GFP-CLIP-170 under control of the reverse tetracyclin transcriptional activator (rtTA; Tet-on system) was described previously (Drabek et al., 2006). We also generated a stable HeLa cell line expressing

rat brain CLIP-170, N-terminally tagged with GFP, and a short (22 amino acids) biotinylation sequence at the N-terminus of GFP (Lansbergen et al., 2006). HeLa cells (80 % confluent) were transfected using lipofectamine 2000 and split one day later. Neomycin was added to the culture medium to select for cells expressing GFP-CLIP-170. One stable HeLa cell line was further characterized. As shown in Supplemental Fig. S4A, these cells express ~2-fold more GFP-CLIP-170 compared to endogenous CLIP-170.

For transient transfections, we used Polyfect (Quiagen), Fugene 6 (Roche) or DEAE-Dextran, and analyzed cells 24 hours after transfection. For protein extracts, cells were incubated in lysis buffer (20 mM Tris-HCl pH 8, 100 mM NaCl, 0.5 % Triton-X100, supplemented with protease inhibitors (Roche)) for 10 minutes on ice. Cell lysates were centrifuged for 10 minutes at 13,000 rpm and 4°C. The supernatants were used for further experiments.

4.4.3. Live imaging

Fluorescence time-lapse analysis in transiently transfected COS-7 cells, 3T3 cells and MEFs was performed on a Zeiss LSM510 confocal laser scanning microscope as described (Akhmanova et al., 2001; Akhmanova et al., 2005; Stepanova et al., 2003). We either used a 40x water immersion lens (numerical aperture 1.2), or a 63x oil immersion lens (numerical aperture 1.4). Cells were normally imaged at 37°C. For temperature-dependence experiments in 3T3 cells, the temperature was first set at 27°C, and subsequently increased to 32°C, and 37°C, while cells were kept in the microscope set-up. This allowed examination of the same cells at different temperatures. For temperature-dependence experiments in COS-7 cells, different cells were measured at 27°C and 37°C.

FRAP analysis was performed on images of 256 x 64 pixels (lateral pixel size: 70 nm). The same area of 256 x 3 pixels was bleached every 6 seconds. This set-up allowed for image acquisition every 75 ms, and resulted in bleaching of GFP-CLIP-170-positive MT-ends. Fluorescence recovery in a region of 3 x 3 pixels was measured. This area encompassed part of the fluorescent MT-end. We measured bleached and non-bleached MT-ends, and cytoplasmic regions. For better visualization of MT-ends in Figure 4-1, the walking average plug-in of Image J (Rasband, W.S., NIH, <http://rsb.info.nih.gov/ij/>) was used (5 consecutive frames in panels A-A'', and 3 consecutive frames in panels D-D''). However, time-frames were not averaged before analyzing fluorescence intensity.

Fluorescence time-lapse analysis in stably transfected HeLa cells was performed using an epifluorescent Zeiss 200M inverted microscope equipped with a Hamamatsu ORCA-ER camera. Images were acquired every second, and the movement of GFP-CLIP-170 comets in time, reflecting MT growth, was measured in these cells as described (Stepanova et al., 2003). Taxol was added to the stable HeLa cell line in concentrations ranging from 2-100 nM. We visualized GFP-CLIP-170 behavior prior to and one hour after addition of taxol.

4.4.4. FCS

FCS measurements were conducted on an LSM 510-Confocor II system (Carl Zeiss, Jena) equipped with a CW (continuous wave) Ar-laser, a 40x water immersion

objective (C-Apochromat, NA 1.2), and two avalanche photodiodes. EGFP was excited with the 488nm-line (beam path: HFT488-Mirror-BP505-550). Cell lysates were measured for 30 s at room temperature with 17.5 μ W laser power. Experiments were repeated 10 times. Cultured cells were measured 5 times for 30 s at one position, with laser power ranging between 8.5 and 55 μ W. Laser power was set to 17.5 μ W for measuring GFP-VLP2/6 particles (see below and Supplemental Material).

Experimentally obtained autocorrelation functions were analyzed with the Confocor II software package (Zeiss) and fitted with

$$G(t) = \frac{1 + \frac{T}{1-T} e^{-t/\tau_T}}{N} \left(\sum_{i=1}^M \frac{F_i}{(1 + t/\tau_i) \sqrt{1 + t/(S^2 \tau_i)}} \right) + 1 \quad (\text{Eq. 4.1})$$

where t is time (in microseconds); τ_T is the triplet time, set to 9 μ s for GFP; T the fraction of triplet decay; S the structural parameter, obtained from calibration measurements with rhodamine 6G (diffusion coefficient: 28×10^{-10} m²/s at 20°C) and set to 6; N the number of particles; M the number of fluorescent species (1 or 2); F_i the fraction of species i ; and τ_i the diffusion time of species i .

Rotavirus-like particles with 120 molecules of GFPVLP2/6 per virus-like particle (Charpilienne et al., 2001) (a kind gift of Dr. Jean Cohen, CNRS-INRA, Gif-sur-Yvette, France) were stored as a highly purified stock of approximately 1 mg/ml at 4°C. Prior to FCS measurements, particles were filtered through a Sephadex G25 column.

4.4.5. FCA

FCA (Muller, 2004) was performed on raw data of FCS measurements, which we analyzed with the FCS data processor (Scientific Software Technologies Center, Minsk, Belarus, <http://www.SSTCenter.com>). The first 8 cumulants were determined; data was fitted with 2 components (background and GFP), and global analysis of 10 measurements of the same lysate was done. Results were averaged over 2-4 different lysates.

The molecular brightness of the lysates was also examined using photon counting histogram (PCH) analysis (Chen et al., 1999). Raw data of FCS measurements was converted into PCH-curves using our own custom-written program and a binning time of 50 μ s. Data thus obtained was analyzed using the Globals software package developed at the Laboratory for Fluorescence Dynamics at the University of Illinois at Urbana-Champaign.

4.4.6. Analysis of fluorescence intensity tracks

Data was analyzed with Prism (GraphPad Software Inc., San Diego, USA). To derive a corrected fluorescence decay curve for GFP-CLIP-170-labeled MT-ends from confocal images, we first subtracted the average cytoplasmic background value. The resulting curves were normalized to 1 as initial value and averaged. The average

decay of fluorescent peaks was fitted as a first-order exponential decay with a non-linear least-square fitting routine.

$$dc / dt = -k_{decay} * c \quad (\text{Eq. 4.2})$$

$$c(t) = A + B * e^{-k_{decay} * t} \quad (\text{Eq. 4.3})$$

where t is time, c is the concentration, k_{decay} the reaction constant, A the plateau value and B the span of the reaction. The half time of fluorescence decay was calculated as $\ln(2)/k_{decay}$.

4.4.7. Analysis of FRAP data

Data was analyzed with Prism (GraphPad Software Inc., San Diego, USA). To calculate the diffusion constant (D) and the dimensionality of diffusion of cytoplasmic GFP-CLIP-170 we used a recently published method (Seiffert and Oppermann, 2005). We divided the image of 256 x 64 pixels (with a lateral pixel size of 70 nm) in 20 strips. Thus, each strip was approximately 0.2 μm wide and 18.5 μm long. For each strip the fluorescence over time after the bleach was measured for 20 frames after bleaching. Values were divided by the fluorescence value 75 ms before the bleach (pre-bleach value). The bleach profile in the imaged area is described by a Gaussian curve. At least six bleaches at the same position were performed to obtain an average curve. The standard deviation (SD) derived from the Gaussian is related to the full-width-half-maximum (ω) by $\omega = 2.355 \text{ SD}$. Furthermore, $\omega^2 = D/2 * t$ (Seiffert and Oppermann, 2005), where D is the diffusion coefficient and t is time. Thus, by plotting ω^2 versus time (see Supplemental Material) we obtained a value for the diffusion constant of GFP-CLIP-170.

In order to be able to calculate the recovery of GFP-CLIP-170 fluorescence on MT-ends we subtracted background values and normalized curves to 1. We subsequently subtracted the fit of the fluorescent decay, and combined them for an average recovery curve. This curve could be fitted with a simple exponential curve.

$$\text{Bleach}(t) = \text{Bleach}(\infty) - \text{Bleach}(0) * e^{-k_{recovery} * t} \quad (\text{Eq. 4.4})$$

where t is time, and $k_{recovery}$ is a rate constant that is related to k_{off} (Lele et al., 2006). The half-life of GFP-CLIP-170 recovery was calculated as $\ln 2/k_{recovery}$.

4.5. Acknowledgements

We thank Shehu Ibrahim for help with setting up the Zeiss Confocor II system, Dr. Jean Cohen (CNRS-INRA, Gif-sur-Yvette, France) for GFPVLP2/6, Martin van Royen for the GFP-GFP-construct and W.A. van Beusekom for software development. This work was supported by the Dutch Ministry of Economic Affairs (BSIK), the divisions of Earth and Life Sciences (ALW) and Medical Sciences (ZonMw) of the Netherlands Organization for Scientific Research (NWO) and by an EC integrated project on Molecular Imaging (LSHG-CT-2003-503259).

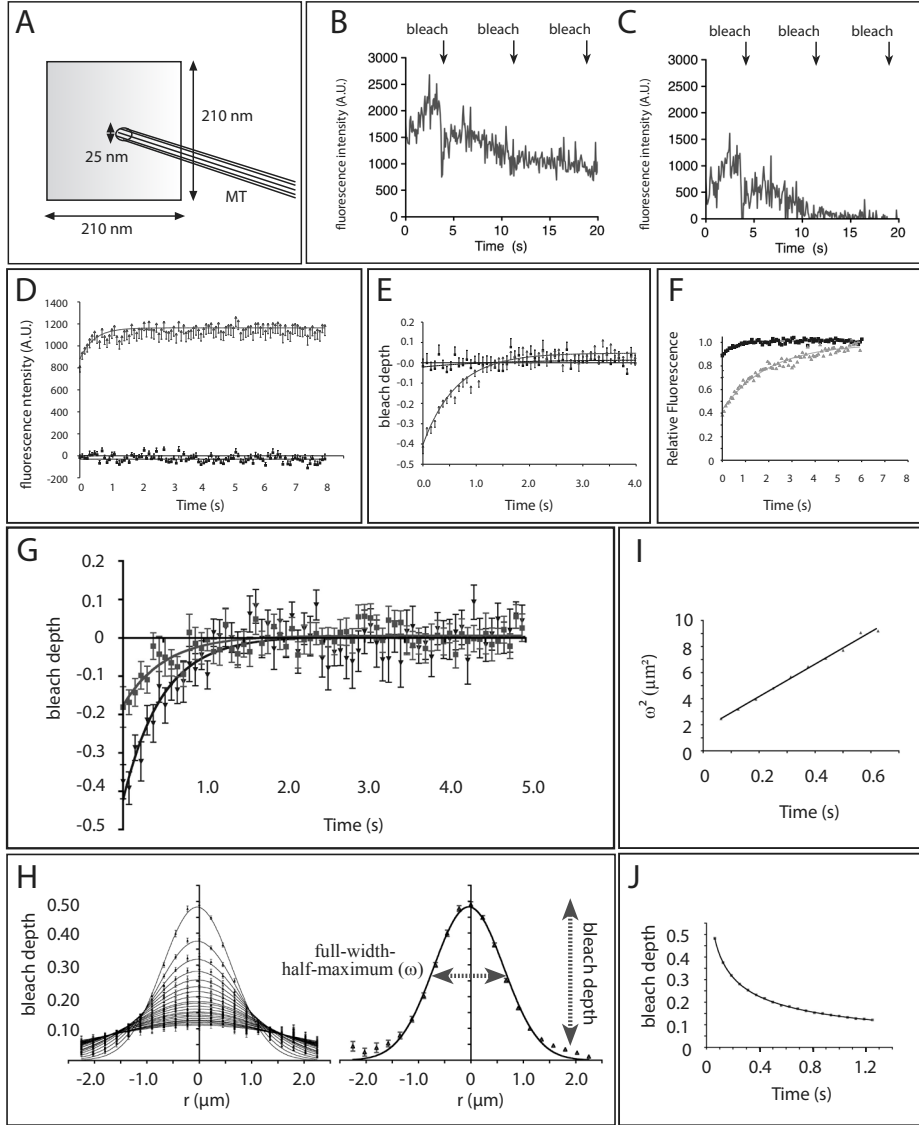
4.6. Supplemental results

4.6.1. FRAP analysis of GFP-CLIP-170 and GFP-CLIP-170XmnI

We considered a number of possible drawbacks to our fastFRAP experiments. First, as MTs have a diameter of only 25 nm, ROIs of 200 x 200 nm will always contain cytoplasmic GFP-CLIP-170 molecules even in the presence of a MT plus-end (Fig. 4-S2A). Thus, one limitation of our experiments could be that the fluorescence recovery observed after bleaching GFP-CLIP-170 on MT plus-ends was due to recovery in the cytoplasm. We therefore subtracted the average fluorescence

Figure 4-S2. FRAP-related schemes and control experiments.

- A) Representation of the different dimensions in a fast FRAP analysis. A MT (diameter: 25 nm) traverses a ROI of 200 x 200 nm (3 x 3 pixels).
- B, C) Fluorescence intensity of a repeatedly bleached GFP-CLIP-170-labeled MT-end measured in a ROI of 200 x 200 nm. The raw data (B) was corrected (C) for the average bleach occurring in the cytoplasm surrounding the MT-end.
- D) Comparison of corrected (blue) and non-corrected (red) cytoplasmic bleaches. If we correct cytoplasmic recoveries for cytoplasmic recovery clearly no recovery is left. This result is in stark contrast to the results in panels (B) and (C), where correction of MT plus-end bleaches for the cytoplasmic recovery still yields a nice and detectable recovery curve.
- E) Comparison of non-bleached (blue) and bleached (red) peaks. Non-bleached peaks were chosen outside of the bleached strip at the moment that a bleach was performed. The same calculations were performed on these peaks as on truly bleached peaks. No recovery is observed on peaks that are away from the bleached strip, while peaks within the bleached strip do show a clear recovery. Thus, recovery is due to bleaching of plus-end bound GFP-CLIP-170 molecules.
- F) Fast FRAP analysis in transiently transfected COS-7 cells abundantly overexpressing GFP-CLIP-170. In these cells GFP-CLIP-170 labels MTs along their entire length. The movie belonging to this FRAP experiment is shown as Supplemental Movie S5. Recovery of GFP-CLIP-170 is shown in the cytoplasm (blue data points, $k = 1.9 \text{ s}^{-1}$), and on MTs (green data points, $k = 0.50 \text{ s}^{-1}$). Clearly, GFP-CLIP-170 recovers faster in the cytoplasm than on the MT (note: in the same experiment we also performed fast FRAP analysis in cells expressing much lower amounts of CLIP-170; in these cells we observed "normal" MT-end recovery).
- G) Average fluorescence recovery of GFP-CLIP-170 on MT-ends. Recoveries were grouped according to the position of the bleach on the fluorescent peak. Fluorescent recoveries shown are near the peak (red, 0.5-1 s after the maximum, $k_{\text{recovery}} = 2.06 \pm 0.27 \text{ s}^{-1}$, $n = 25$, SEM indicated), or further away (blue, 3.7-4.6 s after the maximum, $k_{\text{recovery}} = 1.96 \pm 0.45 \text{ s}^{-1}$, $n = 25$, SEM indicated). K_{recovery} did not differ significantly between these two datasets.
- H) Example of a bleach profile in FRAP experiments with GFP-CLIP-170. Maximum bleach depth decreases over time ("fluorescence recovers"), while the area containing bleached molecules increases.
- I) Example of $\omega^2 (\mu\text{m}^2)$ plotted versus time (s) for FRAP experiment of GFP-CLIP-170.
- J) Plot of maximum bleach depth versus time shows recovery of fluorescence in a representative FRAP experiment of GFP-CLIP-170.



recovery occurring in the cytoplasm from the fluorescence recovery on MT plus-ends. Fluorescence still recovered on “corrected” bleached MT-ends (Fig. 4-S2B, C). However, when we took cytoplasmic bleaches and corrected for cytoplasmic recovery, no recovery remained after correction (Fig. 4-S2D). This indicates that the corrected recovery we see on plus-ends can not be due to cytoplasmic bleaches in that area. Thus, although a MT plus-end traversing a ROI of 200 x 200 nm is small in terms of volume, MT plus-end-bound GFP-CLIP-170 can clearly be distinguished.

In a second control experiment, we analyzed non-bleached +ends (outside of the bleached strip) that were present during a bleach. We performed the same calculations on these peaks as on the truly bleached peaks. No recovery was observed

on peaks away from the bleached strip, while peaks within the bleached strip did show a clear recovery (Fig. 4-S2E). Thus, even though the fast FRAP approach forces us to analyze images with relatively low signal-to-noise ratio, the recovery due to bleaching can be clearly distinguished from random fluctuations.

As a third control experiment, we performed fast FRAP in transiently transfected COS-7 cells that abundantly overexpress GFP-CLIP-170 (Fig. 4-S2F). In such cells GFP-CLIP-170 labels MTs along their length and appears immobile (the movie belonging to this FRAP experiment is shown as Movie 4-S5). Under these conditions we observed a four times faster recovery of GFP-CLIP-170 in the cytoplasm (blue data points, $k = 1.9 \text{ s}^{-1}$, 95 % confidence interval 1.4 to 2.4 s^{-1}) than on MTs (green data points, $k = 0.50 \text{ s}^{-1}$, 95 % confidence interval 0.43 to 0.57 s^{-1}). These data show that the FRAP set-up can distinguish between cytoplasmic and MT-bound CLIP-170, when GFP-CLIP-170 dwells on MTs for longer periods of time.

Our data suggest that individual CLIP-170 molecules can exchange rapidly on MT plus-ends and that fluorescence decay at a given position on the MT-end reflects the loss in time of binding sites for CLIP-170. This loss could be due to a quantitative loss in number of binding sites and/or the “weakening” of interactions between CLIP-170 and binding sites on MT-ends (i.e a qualitative change). In the first case, no relationship between k_{recovery} of GFP-CLIP-170 and the position on the MT plus-end is expected. We tested this by comparing recovery-curves over the length of MT plus-ends. Although the bleach depth depended on the time interval between maximal fluorescence intensity and the bleach, we found no differences for k_{recovery} (Fig. 4-S2G). We propose that the disappearance of CLIP-170 fluorescence from MT plus-ends is due to a declining number of binding sites for CLIP-170. Our results do not allow us to conclude whether the properties of these binding sites are similar over the length of the MT plus-end, since binding and unbinding of CLIP-170 may be faster than diffusion.

As we bleach a very thin strip, diffusion of GFP-CLIP170 during bleaching can not be neglected in our FRAP set-up. Furthermore, the bleaching beam has a finite width, and although we outlined a bleach strip of $0.2 \times 18.5 \text{ }\mu\text{m}$, the actual bleached area was larger. Recently, a mathematical model was described that allows calculation of the diffusion constant under these conditions (Seiffert and Oppermann, 2005). We adapted this method to estimate the diffusion coefficient D of GFP-CLIP-170 from our FRAP experiments. The bleach profile was fitted with a Gaussian curve (Fig. 4-S2H), which yielded ω (full width at half maximum). Plotting ω^2 versus time (Fig. 4-S2I, J), we obtained the diffusion coefficient $D = 10.34 \pm 6.1 \text{ }\mu\text{m}^2/\text{s}$ ($n = 48$, SD indicated) for GFP-CLIP-170 and $D = 24.7 \pm 15.2 \text{ }\mu\text{m}^2/\text{s}$ ($n = 25$, SD indicated) for GFP-CLIP-170XmnI. These values are comparable to the values measured by FCS (see below), strongly suggesting that the FRAP set up measures diffusion correctly.

4.6.2. FCS analysis of GFP-CLIP-170

We first verified our FCS set-up by analyzing the diffusion of GFP. The diffusion coefficient D of GFP was about $50 \text{ }\mu\text{m}^2/\text{s}$ in the cytoplasm and $70 \text{ }\mu\text{m}^2/\text{s}$ in cell lysates (Fig. 4-S3A, B), which is comparable to published data (about $30 \text{ }\mu\text{m}^2/\text{s}$ in

cells, $90 \mu\text{m}^2/\text{s}$ in lysates Kim and Schwille, 2003). The diffusion coefficient of GFP in cells as determined by FRAP-experiments is slightly lower (Arrio-Dupont et al., 2000; Coscoy et al., 2002; Swaminathan et al., 1997). We conclude that our FCS set-up can be used to interpret the behavior of GFP-CLIP-170 and other fluorescently tagged +TIPs.

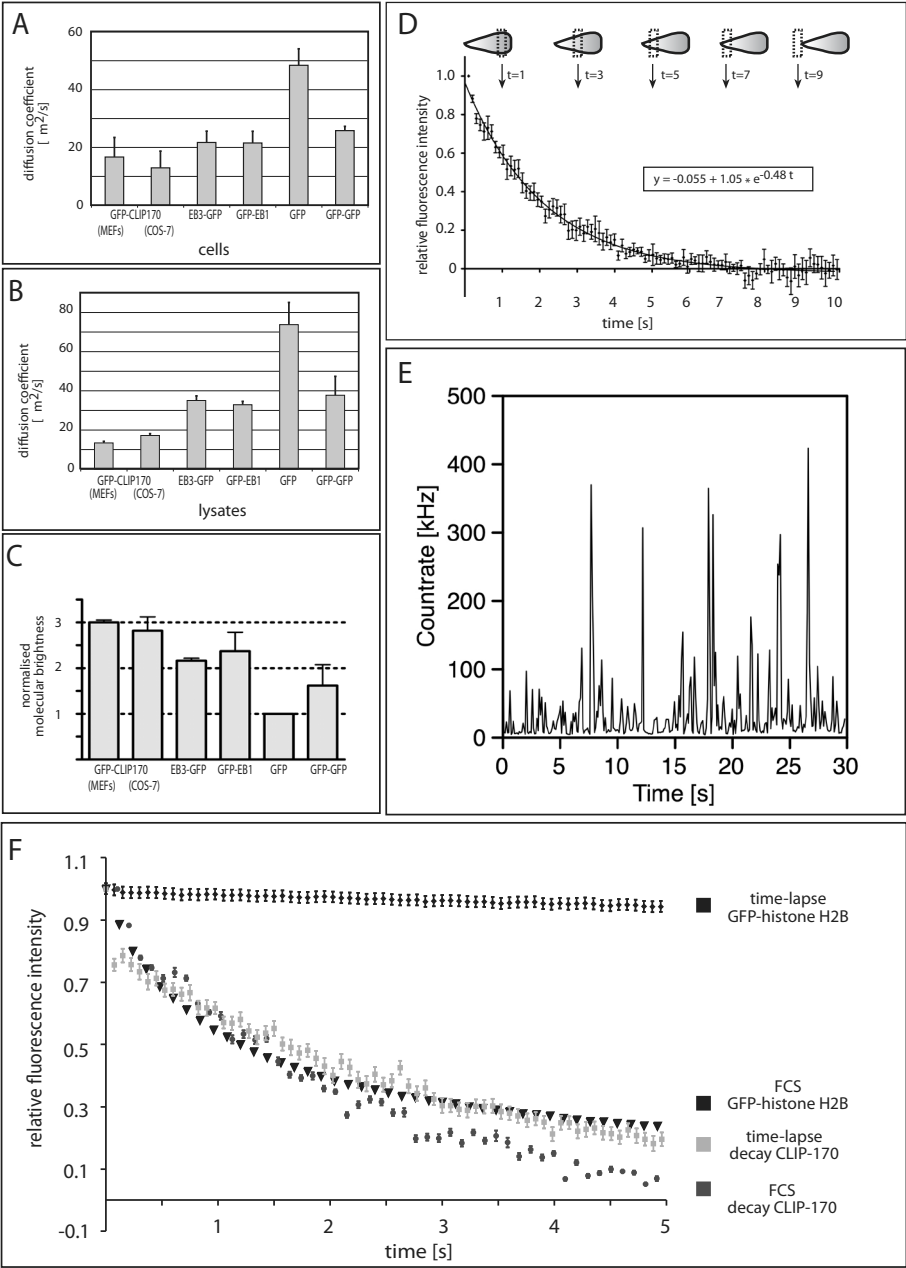
Using FCS, we studied the dynamics of GFP-CLIP-170 in knock-in MEFs (Akhmanova et al., 2005). Fluorescence autocorrelation curves could be fitted with a two-component model, implying a fast-moving (i.e. freely diffusing) and a slow-moving fraction of GFP-CLIP-170 in MEFs. The fast-moving GFP-CLIP-170 species in MEFs has a diffusion coefficient that is 3-4 times lower than that of monomeric GFP and about two times lower than that of a GFP-GFP fusion protein (Fig. 4-S3A). Diffusion coefficients of EB3-GFP and GFP-EB1 are somewhat smaller than that of GFP-GFP. Similar results were obtained in cell lysates (Fig. 4-S3B). Data are consistent with the relative molecular mass of dimeric GFP-CLIP-170 (approximately 400 kDa) being higher than that of the other proteins (GFP, 27 kDa; GFP-GFP, 54 kDa; dimeric EB3-GFP and GFP-EB1 approximately 120 kDa). Note that the diffusion coefficient is linear to the radius of a molecule. Thus doubling the radius of a globular protein also doubles the diffusion coefficient, but this correlates with an 8-fold increase in the relative molecular mass of a protein. Our results indicate that if the fast GFP-CLIP-170 species is dimeric, it is either not a globular protein, or it must be part of a bigger complex.

Fluorescence cumulant analysis (FCA) revealed that GFP-CLIP-170, EB3-GFP and GFP-EB1 have a molecular brightness that is 2-3 times that of GFP (Fig. 4-S3C). Values are higher than for a GFP-GFP fusion protein, which might be due to fluorescence quenching in the latter. FCA results were supported by photon-counting histogram (PCH) analysis (data not shown). All data are consistent with previous results (Lansbergen et al., 2004; Pierre et al., 1992; Scheel et al., 1999) that indicate a dimeric, non-globular conformation of CLIP-170.

4.6.3. Fluorescent peaks in FCS intensity tracks

Peaks were visible in the fluorescence intensity tracks of FCS measurements of COS-7 cells expressing GFP-CLIP-170. Most of these peaks had a relatively linear and steep upward slope and a curved downward slope (see Fig. 4-2B). Several experiments suggest that these peaks represent the ends of growing MTs, labeled by GFP-CLIP-170. Peaks were absent in cells expressing fluorescently tagged proteins that did not associate with MT-ends. Also, they disappeared when cells expressing GFP-CLIP-170 were treated with nocodazole or high doses of taxol (data not shown), reagents that perturb MT dynamics and have been shown to cause dissociation of GFP-CLIP-170 from MT-ends (Perez et al., 1999). Furthermore, peaks reached their maximum intensity after 1-2 s, corresponding to the time it takes a microtubule to traverse the FCS measurement-volume (growth speed of a MT: $\sim 0.3 \mu\text{m}/\text{s}$, measurement-volume diameter: $0.4 \mu\text{m}$). To rule out that the peaks represent aggregates of GFP-CLIP-170, we analyzed a suspension of highly purified VLP2/6 rotavirus-like particles containing 120 GFP molecules each (Charpilienne et al., 2001). Intensity tracks of FCS measurements of these particles showed very sharp peaks (Fig. 4-S3E).

The downward slope of peaks could be approximated with an exponential decay curve corresponding to first-order reaction-kinetics (Fig. 4-S3D). Deviations from the fit were small and did not show any trend. The calculated k_{decay} of 0.48 s^{-1} for disappearance of GFP-CLIP-170 (see Table 4-1) translates to a fluorescence half-life of approximately 1.5 s, which correlates well with reported half-lives of CLIP-170 on MT-ends (Folker et al., 2005; Komarova et al., 2005).



4.6.4. Comparison between FCS and FRAP

While a given position is imaged intermittently in FRAP experiments, the same position is imaged continuously in FCS experiments. Consistently, we observed significant bleaching of the immobile nuclear protein GFP-histone H2B (Wachsmuth et al., 2003) with FCS, whereas this was not the case in time-lapse imaging (Fig. 4-S3F). In fact, the curve showing the bleach-dependent decay of GFP-histone H2B was similar to the one showing fluorescence decay of GFP-CLIP-170 (Fig. 4-S3F). If CLIP-170 were transiently immobile on MT-ends, one would expect the FCS curve, reflecting a combination of dissociation and bleaching of CLIP-170, to be steeper than the FRAP decay curve, only reflecting dissociation of CLIP-170. The fact that FRAP and FCS curves are so similar indicates short binding times of GFP-CLIP-170 on MT-ends.

4.6.5. Effect of low doses of taxol on CLIP-170 behavior

Taxol is a MT stabilizing agent that binds to the β -tubulin subunit of the tubulin dimer thereby changing MT conformation (Arnal and Wade, 1995). When added at micromolar concentrations it causes displacement of GFP-CLIP-170 from the MT end (Perez et al., 1999). However, the effect of a nanomolar application of taxol on CLIP-170 behavior has, to our knowledge, not yet been investigated. Taxol does affect MT dynamics in HeLa cells even at these low concentrations, possibly because it is able to accumulate inside cells (Jordan et al., 1996).

We generated a stable HeLa cell line expressing ~ 2.5 times more GFP-CLIP-170 than CLIP-170 (Fig. 4-S4A). The rate of GFP-CLIP-170 displacement (Fig. 4-S4B), which reflects MT growth, was comparable to that observed in other cell types (Akhmanova et al., 2001; Stepanova et al., 2003). Maximum intensity projections (Fig. 4-S4F) and kymograph analysis (Fig. 4-S4H) showed relatively constant “comet-like” GFP-CLIP-170 fluorescence within individual tracks. One hour after

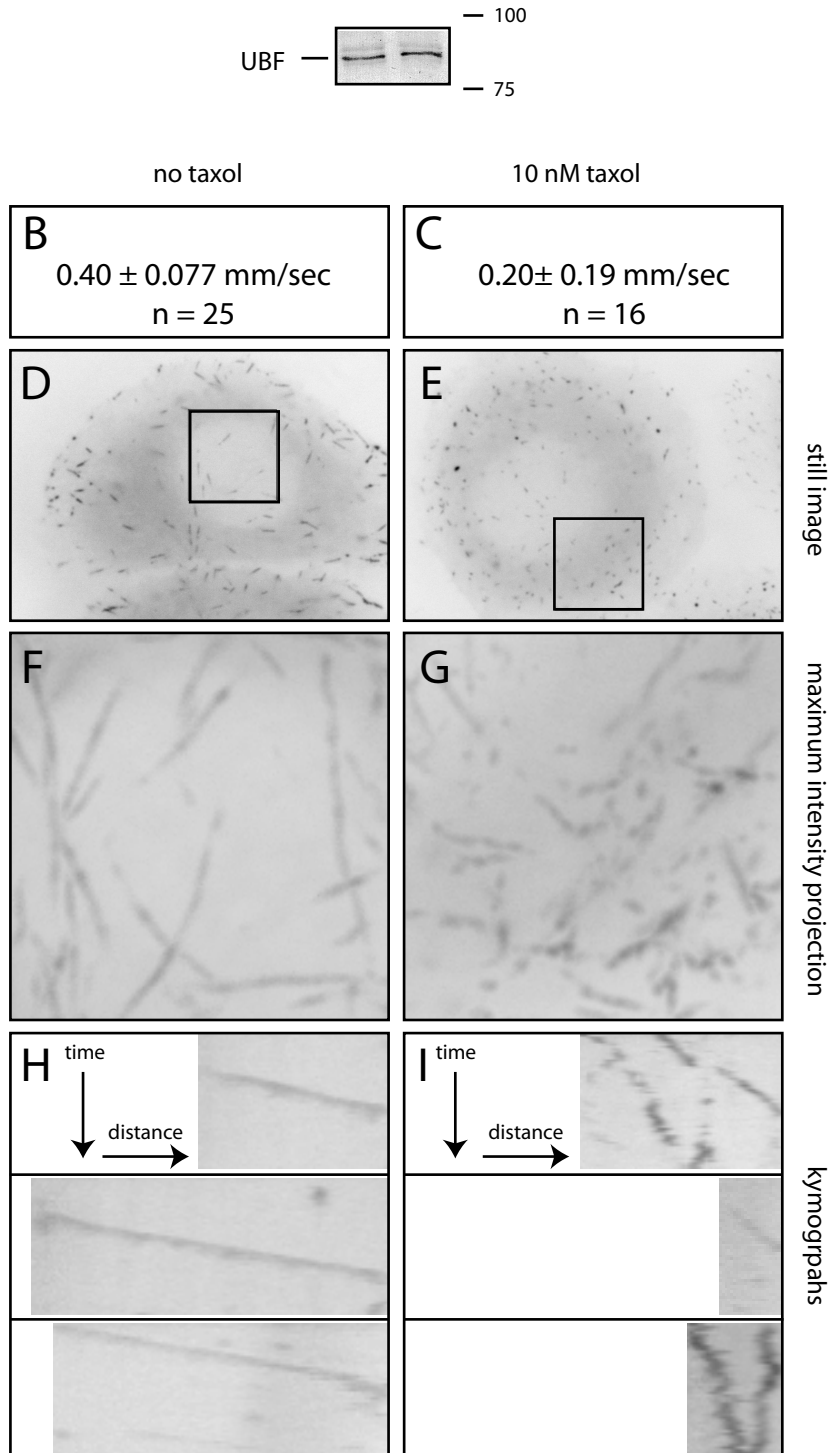
Figure 4-S3. FCS-related control experiments.

- A, B) Diffusion coefficients in cells (A) expressing different fluorescently labeled proteins and in lysates (B) thereof. Both MEFs (expressing GFP-CLIP-170 at endogenous levels) and transfected COS-7 cells (expressing the indicated fluorescent proteins) were measured. Only fast components of the two-component analysis in cells are shown.
- C) FCS data from cell lysates was used to calculate the molecular brightness of fluorescent proteins by fluorescence cumulant analysis (FCA). Values were normalized to GFP. Error bars indicate standard deviation in all panels.
- D) Fluorescence decay of GFP-CLIP-170 peaks in FCS measurements. Decay was measured at 17.5 μ W laser power, normalized, averaged and fitted (SEM indicated). The k_{decay} is 0.48 s^{-1} (see also Table I). A GFP-CLIP-170-positive MT-end (visualized as a green “comet”) is drawn above the graph. As it enters and exits the FCS-volume (dashed rectangle) fluorescence intensity is measured (examples indicate measurements at 1, 3, 5, 7 and 9 seconds). Fluorescence from consecutively older parts of the MT-end shows an apparent decay.
- E) Rotavirus-like particles, containing 120 molecules of GFP-VLP2/6 each, were analyzed with the FCS set-up. Sharp peaks characterize movement of particles through the measurement volume.
- F) Comparison of the behaviour of GFP-CLIP-170 and GFP-histone H2B in time in FRAP and FCS experiments. With FCS significant bleaching of the immobile nuclear protein GFP-histone H2B is observed (black triangles), whereas with FRAP (black squares) this is not the case. The FCS curve showing the bleach-dependent decay of GFP-histone H2B is similar to the FCS and FRAP curves showing fluorescence decay of GFP-CLIP-170 (red and blue squares, respectively). Error bars indicate SEM.

application of 10 nM taxol the rate of GFP-CLIP-170 displacements were reduced, but movements were highly erratic, leading to a high SEM (Fig. 4-S4C, G, I). The qualitative changes in CLIP-170 displacement can also be seen in Movies 4-S6 and 4-S7, showing GFP-CLIP-170 behaviour in untreated and treated cells respectively. Thus, consistent with previous results (Yvon et al., 1999), the nanomolar application of taxol interferes with MT dynamics. Interestingly, GFP-CLIP-170 remained bound to MT ends under these conditions, even when MT ends appeared to be shrinking (Fig. 4-S4I), and its binding pattern changed from “comet-like” to a more “dotted” pattern. These results are consistent with CLIP-170 recognizing a structural feature on MT plus-ends, a feature that is changed by taxol.

Figure S4. Characterization of a HeLa cell line stably expressing GFP-CLIP-170.

- A) Western blot analysis of parent HeLa cell line and of the GFP-CLIP-170-expressing clone. Expression of GFP-CLIP-170 was analyzed with antibodies against CLIP-170. Intensities of the signals were measured in 3 experiments; the expression of CLIP-170 is ~ 2.5 fold lower ($42 \pm 3\%$) than that of GFP-CLIP-170. Control staining with antibodies against UBF (a nucleolar protein) show that equal amounts of protein lysates were loaded on gel.
- B, C) Displacement of GFP-CLIP-170 in time (equivalent to MT growth rates) in untreated HeLa cells (B) and in cells treated with 10 nM taxol (C). Notice that not only MT growth rates are reduced in the treated cells but that also the variation in growth rates has significantly increased. N = number of dashes analyzed.
- D) Still image of a time-lapse analysis of GFP-CLIP-170 in stably expressing HeLa cells. Notice the fluorescent “comet-like” dashes, typical of GFP-CLIP-170 behavior.
- E) Still image of a time-lapse analysis of GFP-CLIP-170 in stably expressing HeLa cells after treatment with 10 nM taxol. Notice the fluorescent “dots” that appeared after taxol application.
- F) Maximum intensity projections of the rectangle depicted in (D). Tracks represent movement of GFP-CLIP-170 in time in non-treated HeLa cells. Track length is not only determined by catastrophes (which cause GFP-CLIP-170 displacement from the MT-end), but also by GFP-CLIP-170 moving in and out of focus.
- G) Maximum intensity projections of the rectangle depicted in (E). Tracks represent movement of GFP-CLIP-170 in time in cells treated with taxol.
- H) Kymograph analysis of GFP-CLIP-170 in non-treated HeLa cells. Three representative kymographs are shown, with time plotted in the vertical axis and distance horizontally. GFP-CLIP-170 moves with a relatively constant average speed and decorates MT plus-ends in an even manner.
- I) Kymograph analysis of GFP-CLIP-170 in HeLa cells treated with 10 nM taxol. Three kymographs are shown, with time plotted in the vertical axis and distance horizontally. GFP-CLIP-170 moves erratically, and even seems to remain bound on pausing and shrinking MTs. Moreover, it decorates MT plus-ends in an uneven manner.



4.7. Movies

These supplemental movies will be available at <http://www.jcb.org>.

Movie 4-S1

GFP-CLIP-170 expression in transfected COS-7 cells. COS-7 cells were transfected with GFP-CLIP-170 and analyzed by confocal microscopy. Cells were maintained in normal culture medium at 37°C. Images were acquired every 75 ms. The walking average of 3 consecutive frames was calculated using Image J to show the GFP-CLIP-170 signal more clearly.

Movie 4-S2

GFP-CLIP-170 behavior at 37°C in stably transfected 3T3 cells. 3T3 cells expressing GFP-CLIP-170 were analyzed by confocal microscopy. Cells were maintained in normal culture medium at 37°C. Images were acquired every 200 ms. Notice GFP-CLIP-170 moving in bright, comet-like dashes.

Movie 4-S3

GFP-CLIP170 behavior at 27°C in stably transfected 3T3 cells. T3 cells expressing GFP-CLIP-170 were analyzed by confocal microscopy. Cells were maintained in normal culture medium at 27°C. Images were acquired every 200 ms. GFP-CLIP-170 is moving in bright, comet-like dashes despite the reduction in temperature.

Movie 4-S4

GFP-CLIP-170 expression in knock-in MEFs. Cultured MEFs, isolated from GFP-CLIP-170 knock-in mice, were analyzed by confocal microscopy. Cells were maintained in normal culture medium at 37°C. 88 images were acquired (1 image per 2 seconds). Notice GFP-CLIP-170 moving in dashes and dots.

Movie 4-S5

GFP-CLIP-170 overexpression in transiently transfected COS-7 cells. COS-7 cells were transfected with GFP-CLIP-170 and analyzed by confocal microscopy. Cells were maintained in normal culture medium at 37°C. Images were acquired every 75 ms. The walking average of 3 consecutive frames was calculated using Image J to show the GFP-CLIP-170 signal more clearly.

Movie 4-S6

GFP-CLIP-170 expression in non-treated HeLa cells. HeLa cells stably expressing GFP-CLIP-170 were analyzed using fluorescence microscopy. Cells were main-

tained in normal culture medium at 37°C. Images were acquired every second. Notice GFP-CLIP-170 moving in bright, comet-like dashes.

Movie 4-S7

GFP-CLIP-170 expression in HeLa cells treated with 10 nM taxol. HeLa cells stably expressing GFP-CLIP-170 were analyzed using fluorescence microscopy. Cells were maintained in normal culture medium at 37°C. Taxol was applied at 10 nM and images were acquired one hour after application of the drug (1 image per second). Notice the erratic movement of GFP-CLIP-170. Instead of bright, comet-like dashes a dotted pattern is observed.

Chapter 5

General Discussion

The three components of the cytoskeleton, microtubules, actin filaments, and intermediate filaments, all form distinct networks. Cytoskeletal networks do not form independent entities, but are highly integrated. This is illustrated by polymerization of microtubules along existing actin filaments (Kodama et al., 2003), and the existence of a group of proteins that can bind different components of the cytoskeleton simultaneously (Sonnenberg and Liem, 2007). Disturbing the structure of a cytoskeletal network, its interaction with the other networks, or with other subcellular components, can have detrimental effects in mitosis, cell migration and signaling. Our research focuses on microtubules and their binding partners. Microtubules form a dynamic network that is essential for cell migration, for chromosome segregation during mitosis, influences cell shape and plays a role in signaling. Studying microtubule dynamics therefore generates more insight in these fundamental processes.

Initially, microtubule dynamics were studied *in vitro*, but results were obtained that did not reflect *in vivo* behavior (Cassimeris, 1993). This is due to the lack of proteins that regulate microtubule dynamics, different conditions, and also a different microtubule protofilament number. Studying microtubule dynamics *in vivo* provides a more realistic picture than trying to mimic the *in vivo* situation *in vitro*. On the other hand, *in vitro* studies provide information on the properties of isolated components, which can not be revealed in *in vivo* studies. Many *in vivo* studies have been performed with cells either expressing a GFP-tagged tubulin isoform, or microinjected with rhodamine-tubulin. The drawback of both approaches is that a single tubulin isoform is introduced in larger than normal quantities, which can lead to an imbalance between α - and β -tubulin that is toxic for cells. Furthermore, adding GFP to tubulin introduces a tag of nearly 30 kDa that not only interferes with protein function itself, but also with the properties of the lattice as a whole, even if the fluorescently tagged protein only forms the minority of total protein inside the lattice. Rhodamine is a much smaller tag and gets linked to different residues of the tubulin molecule, making interference with protein function less likely. However, microinjection is the only way in which rhodamine-labeled tubulin can be introduced into cells. This is laborious and restricted to few cells, while many cells can be investigated in a cell line stably expressing GFP-tagged tubulin.

Tagged tubulin visualizes the complete pattern of microtubule dynamics, but it gets increasingly difficult to discern single microtubules when they bundle or are located together, like in neuronal extensions. Fluorescently tagged +TIPs are better suited to study microtubule dynamics in these cases, visualizing growing microtubule ends even in neuronal extensions (Stepanova et al., 2003). The obvious drawback of +TIPS is their inability to track depolymerizing or pausing microtubules.

Expression of a fluorescently tagged +TIP in cells lacking another +TIP of interest is often used to investigate the influence of the lacking +TIP on MT-dynamics. As many +TIPs influence microtubule dynamics (especially if they are overexpressed), expression levels of the read-out construct can have influence on MT-dynamics. Knock-in mice that express a GFP-tagged +TIP from the endogenous locus might be a good alternative to transfected cells, but knock down of a protein under investigation is difficult in primary cells. The suitability of a given fluorescently tagged

+TIP as read-out construct is another consideration that needs to be taken into account. As mentioned above (for tubulin) tags can have a profound influence on protein function. The functionality of EB-proteins is, for example, hampered by a GFP-tag – adding the tag at the C-terminus interferes with Cap-Gly protein binding, while adding it at the N-terminus interferes with microtubule plus-end binding. However, the addition of a GFP-tag to the N-terminus of CLIP-170 has been shown to be non-detrimental as GFP-CLIP-170 can fully rescue defects in spermatogenesis that arise from CLIP-170 deficiency (Akhmanova et al., 2005). All of the data actually suggest that fluorescently tagged CLIP-170 and non-tagged CLIP-170 behave identical.

Different theories have been proposed on how CLIP-170 and its yeast homologues accumulate on MT +ends (see chapter 1.3.1). Many of the underlying experiments have been performed *in vitro*, in fixed cells, or with truncated protein constructs (for example Diamantopoulos et al., 1999), making the transferability of the results to the *in vivo* situation difficult. We therefore set out to investigate the processes leading to accumulation of full length CLIP-170 on MT +ends *in vivo*.

Live cell behavior of +TIPs has often been studied by kymograph analysis and fluorescent speckle microscopy. Both techniques focus on macroscopic protein behavior, not looking at the dynamics of individual molecules but at the dynamics of whole +end accumulations (a.o. Komarova et al., 2005; Perez et al., 1999). Molecules that are stably bound to few binding sites on a given scaffold give the same macroscopic image as molecules that interact only transiently with a surplus of binding sites (see chapter 4.3.7), although they have very different implications for protein function. Thus, investigating single molecule behavior on +ends or analyzing +TIP dynamics on +ends with FRAP reveals information not accessible by macroscopic techniques. We adapted a FRAP protocol to gain enough temporal resolution to be able to study protein dynamics of GFP-CLIP-170 and EB3-GFP on dynamic MT +ends. These experiments revealed, that – underlying the overall dynamics of +TIP accumulation following a growing MT +end – individual molecules are even more dynamic and can repeatedly bind to the same stretch of microtubule. The fission yeast homologue of EB1, Mal3, has very recently been shown to exhibit the same behavior *in vitro* (Bieling et al., 2007) – with short dwell times of individual molecules.

Short dwell times for individual +TIP molecules (less than 300 ms for Mal3 *in vitro* (Bieling et al., 2007), maximum of 200 ms for EB3-GFP *in vivo* (chapter 4 of this thesis)) is incompatible with +end accumulation of EB3 or CLIP-170 purely due to co-polymerization with tubulin. Treadmilling as the sole underlying reaction leading to +end accumulation can also be excluded, as a single modification of either MT-structure or +TIP is believed to cause +TIP dissociation, which is in contrast with the ability of GFP-CLIP-170 and EB3-GFP to bind to the polymerized MT not only immediately at the polymerization front.

We propose that a large number of binding sites for CLIP-170 (and EB3) are formed on the polymerizing MT-end, which slowly disappear. CLIP-170 has a relatively low affinity for these binding sites, resulting in binding times that are much shorter than the overall disappearance of binding sites. Therefore, several binding

reactions can take place on a single binding site, and a single molecule can bind to several binding sites.

Other +TIPs can form another source of binding sites for a given +TIP on the MT end, as most +TIPs are able to bind one another (reviewed in Akhmanova and Hoogenraad, 2005). If fast association and dissociation is the mechanism underlying accumulations of most +TIPs on MT ends, the binding sites generated by an MT-bound +TIP will have a very short life time, in contrast to the (relatively) static binding sites on the MT itself. This will lead to the formation of a “+end raft” (Galjart and Perez, 2003) not so much through prolonged interactions, but rather through a plethora of short-lived interactions between +TIPs, and between +TIPs and the MT, on and in close proximity of the MT end.

Since their discovery about 10 years ago, +TIPs have been shown to be important in diverse processes as mitosis and cell migration. Many +TIPs have been described to influence microtubule dynamics, but how they accomplish it is still poorly understood. One assumption is that +TIPs influence dynamics while being associated with growing microtubules. However, CLIP-170 has been described as a rescue factor that promotes the transition from a shrinking to a growing microtubule (Komarova et al., 2002a). This is puzzling, as CLIP-170 is thought to specifically recognize growing microtubule ends but to lack any affinity for depolymerizing microtubules. A possible explanation for MT-rescue by CLIP-170 might be the formation (or stabilization) of curved tubulin oligomers in the presence of the MT-binding domain of CLIP-170 *in vitro* (Arnal et al., 2004). If these function as “pre-fab” elements that bind to depolymerizing MTs *in vivo*, they could promote rescue. While data presented in Chapter 4 of this thesis argue against CLIP-170 binding to soluble tubulin in the cytoplasm (as no CLIP-170 would be available for MT plus-end binding), high affinity binding of “pre-fab” elements would be possible if these are present in very low concentrations. Based on the data presented in this thesis, one might also envision that few binding sites for CLIP-170 remain along the microtubule lattice. If the depolymerizing microtubules retain few binding sites for CLIP-170, a CLIP-170 molecule that is bound at one of these sites when depolymerization reaches this position, might act as rescue factor. The function of CLIP-170 on polymerizing microtubules may then have less to do with regulating microtubule dynamics and more with providing a “landing platform” for other proteins, for example, dynactin. Such a theory has been proposed for dynactin itself (Vaughan et al., 2002).

Apart from influencing microtubule dynamics, +TIPs have been described to be involved in the attachment of microtubules to other cellular structures (like kinetochores or the plasma membrane). For example, in the absence of CLASP2, migrating cells form fewer stable microtubules (Chapter 3). Stable microtubules are mostly oriented towards the direction of migration, where CLASP2 accumulates in patches at the plasma membrane, locally binds microtubules and thereby stabilizes them. In contrast, CLASP2 does not stabilize microtubules throughout the cytoplasm, where it is not bound to stable structures but behaves like a +TIP. Although these two processes are likely to influence one another, as a microtubule that is tightly bound to another cellular structure is less likely to depolymerize, the short-lived interactions at MT plus-ends alone might not be sufficient to tether MTs

to the kinetochores or other subcellular structures. Data presented in Chapter 3 of this thesis and elsewhere (Akhmanova et al., 2001; Efimov et al., 2007; Lansbergen et al., 2006; Wittmann and Waterman-Storer, 2005) suggest that CLASPs can stabilize a selected subset of microtubules by a common mechanism. Specific CLASP-interaction partners (e.g. LL5beta or GCC185) appear to accumulate at sites within the cell, such as the plasma membrane or the Golgi. The turnover of these proteins is low, that is, they are stably bound. Specific signalling pathways then allow LL5beta and GCC185 to attract CLASPs, which in turn bind and stabilize microtubules. It is striking that CLASPs remain relatively mobile compared to LL5beta and GCC185. In the dynamic world of microtubules high affinity interactions are perhaps not very common and microtubules are tethered by multiple low affinity interactions.

Chapter 6

Summary/Samenvatting

6.1. Summary

The cytoskeleton forms the backbone of cells by providing mechanical stiffness and rails for intracellular transport. Its components are microtubules, actin filaments, and intermediate filaments. Microtubules are hollow tubes with a diameter of 25 nm that are composed of α/β -tubulin heterodimers. Tubulin dimers interact longitudinally in a head-to-tail fashion to form protofilaments, 13 of which interact laterally to form a microtubule. Due to their structured assembly, polarity of tubulin dimers is transferred onto the microtubule, resulting in two distinguishable microtubule ends. Under conditions favoring polymerization in vitro, minus ends of free microtubules grow slower than their plus ends. Microtubules are not static, but switch between phases of growth and shrinkage, this phenomenon is called “dynamic instability”. In vivo, dynamic instability is mainly observed at microtubule plus-ends, which are facing toward the cell periphery. Dynamic instability facilitates rapid rearrangement of the microtubule cytoskeleton and constant probing of the cytoplasm.

The microtubule plus end is an ideal target to influence microtubule dynamics and the interaction between microtubules and other cellular components. +TIPs (plus end tracking proteins) are a group of proteins that specifically recognize growing microtubule plus ends. Many +TIPs promote proper progression through mitosis, play a role in cell polarity, and regulate microtubule dynamics. The mechanisms that allow +TIPs to exert these functions remain unclear, even though the crystal structures of several +TIPs have been solved over the last few years.

An example of a +TIP that has been reported to influence microtubule dynamics is CLASP2. We show in chapter 3 that cells lacking CLASP2 form fewer stable microtubules upon induction of cell migration. Although the lack of CLASP2 has no influence on the migration speed of these cells, it does affect the directionality of migration, leading to a much shorter net migration distance. It is thought that patches of immobilized CLASP2 at the cell edge promote capture of microtubule ends and their subsequent stabilization. We show, that this accumulation is independent of EB1/APC and CLIP-170/IQGAP as upstream signaling factors, but is severely reduced upon depletion of ACF7.

Much effort has been put into understanding the mechanisms by which +TIPs accumulate at microtubule ends, because this is thought to influence the way in which a +TIP can modulate microtubule dynamics. Different models for plus end accumulation have been postulated so far, such as treadmilling, copolymerization and motor mediated transport. For a given +TIP, different methods of accumulation might co-exist depending on the cellular context. We therefore set out to investigate the plus end accumulation of fluorescently tagged CLIP-170 in vivo. We report in chapter 4 that its residence time on plus ends is short, which is compatible with neither the treadmilling nor the copolymerization model. Instead, we propose that CLIP-170 exchanges rapidly on a surplus of binding sites on the plus-end.

6.2. Samenvatting

Het cytoskelet kan worden gezien als het geraamte van eukaryote cellen, omdat het in grote mate verantwoordelijk is voor hun stevigheid en vorm. Ook vormt het de banen langs welke transport binnen de cel plaats vindt. Het cytoskelet bestaat uit microtubuli, microfilamenten en intermediaire filamenten. Microtubuli zijn buizen met een diameter van 25 nm, die uit α/β -tubuline heterodimeren zijn opgebouwd. Tubuline dimeren vormen protofilamenten waarin het α -tubuline van een dimeer aan het β -tubuline van het volgende dimeer gebonden is. Door laterale interactie vormen 13 protofilamenten samen een microtubule. Door deze gestructureerde polymerisatie hebben microtubuli een intrinsieke polariteit, en kan men de twee uiteindes onderscheiden. In omstandigheden die de groei van microtubuli bevorderen, groeit het min-einde minder snel dan het plus-einde. Microtubuli zijn niet statisch, maar schakelen tussen fasen van groei en krimp, wat “dynamische instabiliteit” genoemd wordt. Binnen de cel zijn het voornamelijk plus-einden, die dynamische instabiliteit vertonen. Deze zijn over het algemeen gericht naar de uiteindes van de cel. Dynamische instabiliteit bevordert een snelle herschikking van het microtubuli netwerk en helpt microtubuli om continu het cytoplasma af te tasten.

De plus-einden van microtubuli vormen een ideaal doelwit om de dynamiek van microtubuli te beïnvloeden en hun interactie met andere cellulaire componenten te reguleren. +TIPs (plus-eind bindende eiwitten) zijn een groep van eiwitten die specifiek met de groeiende uiteindes van microtubuli associëren. Van veel +TIPs is beschreven, dat zij een rol spelen bij de celdeling en celpolarisatie, en dat zij de dynamica van microtubuli beïnvloeden. De manieren waarop +TIPs deze functies uitoefenen zijn tot op heden onduidelijk, en dat terwijl de kristalstructuur van meerdere +TIPs recentelijk beschreven is.

Een voorbeeld van een +TIP, waarvan beschreven is dat het de dynamiek van microtubuli beïnvloedt, is CLASP2. Cellen vormen stabiele microtubuli nadat zij aangezet worden tot migratie. Wij laten in hoofdstuk 3 zien, dat dit veel minder het geval is in cellen, die CLASP2 missen. Hoewel de afwezigheid van CLASP2 geen invloed heeft op de migratiesnelheid van deze cellen, heeft het wel een effect op de gerichtheid van de migratie, waardoor de cellen een veel kortere netto afstand afleggen. De gedachte is, dat ophopingen van onbeweeglijke CLASP2 moleculen aan de celrand helpen om microtubuli vast te grijpen en te stabiliseren. Wij laten zien dat de ophoping van CLASP2 moleculen onafhankelijk is van zowel EB1/APC als CLIP-170/IQGAP, maar dat de depletie van ACF7 deze ophopingen sterk vermindert.

Er is tot nu toe al veel moeite gedaan om het mechanisme waarmee +TIPs op plus-einden ophopen te achterhalen, want men denkt dat de manier waarop +TIPs de dynamiek van microtubuli kunnen beïnvloeden afhankelijk is van de manier waarop zij op het plus-eind ophopen. Tot op heden zijn er verschillende modellen gepostuleerd, zoals “treadmilling”, co-polymierisatie, en transport via motor eiwitten. Afhankelijk van de cellulaire omgeving zouden voor een gegeven +TIP verschillende manieren kunnen bestaan, waarop het op het plus-einde ophoopt.

Daarom hebben wij de ophoping van fluorescent gemarkeerd CLIP-170 op plus-eindes binnen de cel bestudeerd. Wij beschrijven in hoofdstuk 4, dat CLIP-170 moleculen maar kort met het plus-einde associëren. Dit is niet in overeenstemming met het treadmilling- of co-polymerisatie-model. In plaats daarvan stellen wij voor, dat er op het plus-einde een overschot aan bindingsplaatsen is, waarop CLIP-170 moleculen snel uitwisselen.

Chapter 7

References

Adams, S. R., Campbell, R. E., Gross, L. A., Martin, B. R., Walkup, G. K., Yao, Y., Llopis, J. and Tsien, R. Y. (2002). New biarsenical ligands and tetracysteine motifs for protein labeling in vitro and in vivo: synthesis and biological applications. *J Am Chem Soc* **124**, 6063-76.

Akhmanova, A. and Hoogenraad, C. C. (2005). Microtubule plus-end-tracking proteins: mechanisms and functions. *Curr Opin Cell Biol* **17**, 47-54.

Akhmanova, A., Hoogenraad, C. C., Drabek, K., Stepanova, T., Dortland, B., Verkerk, T., Vermeulen, W., Burgering, B. M., De Zeeuw, C. I., Grosveld, F. et al. (2001). Clasps are CLIP-115 and -170 associating proteins involved in the regional regulation of microtubule dynamics in motile fibroblasts. *Cell* **104**, 923-35.

Akhmanova, A., Mausset-Bonnefont, A. L., van Cappellen, W., Keijzer, N., Hoogenraad, C. C., Stepanova, T., Drabek, K., van der Wees, J., Mommaas, M., Onderwater, J. et al. (2005). The microtubule plus-end-tracking protein CLIP-170 associates with the spermatid manchette and is essential for spermatogenesis. *Genes Dev* **19**, 2501-15.

Al-Bassam, J., Larsen, N. A., Hyman, A. A. and Harrison, S. C. (2007). Crystal structure of a TOG domain: conserved features of XMAP215/Dis1-family TOG domains and implications for tubulin binding. *Structure* **15**, 355-62.

Amos, L. A. and Schlieper, D. (2005). Microtubules and maps. *Adv Protein Chem* **71**, 257-98.

Arnal, I., Heichette, C., Diamantopoulos, G. S. and Chretien, D. (2004). CLIP-170/tubulin-curved oligomers coassemble at microtubule ends and promote rescues. *Curr Biol* **14**, 2086-95.

Arnal, I., Karsenti, E. and Hyman, A. A. (2000). Structural transitions at microtubule ends correlate with their dynamic properties in *Xenopus* egg extracts. *J Cell Biol* **149**, 767-74.

Arnal, I. and Wade, R. H. (1995). How does taxol stabilize microtubules? *Curr Biol* **5**, 900-8.

Arrio-Dupont, M., Foucault, G., Vacher, M., Devaux, P. F. and Cribier, S. (2000). Translational diffusion of globular proteins in the cytoplasm of cultured muscle cells. *Biophys J* **78**, 901-7.

Asbury, C. L. (2005). Kinesin: world's tiniest biped. *Curr Opin Cell Biol* **17**, 89-97.

Askham, J. M., Vaughan, K. T., Goodson, H. V. and Morrison, E. E. (2002). Evidence that an interaction between EB1 and p150(Glued) is required for the formation and maintenance of a radial microtubule array anchored at the centrosome. *Mol Biol Cell* **13**, 3627-45.

Axelrod, D., Koppel, D. E., Schlessinger, J., Elson, E. and Webb, W. W. (1976). Mobility measurement by analysis of fluorescence photobleaching recovery kinetics. *Biophys J* **16**, 1055-69.

Baas, P. W., Pienkowski, T. P., Cimbalka, K. A., Toyama, K., Bakalis, S., Ahmad, F. J. and Kosik, K. S. (1994). Tau confers drug stability but not cold stability to microtubules in living cells. *J Cell Sci* **107 (Pt 1)**, 135-43.

Bacia, K., Kim, S. A. and Schwille, P. (2006). Fluorescence cross-correlation spectroscopy in living cells. *Nat Methods* **3**, 83-9.

Banan, A., Zhang, L. J., Shaikh, M., Fields, J. Z., Farhadi, A. and Keshavarzian, A. (2004). Theta-isoform of PKC is required for alterations in cytoskeletal dynamics and barrier permeability in intestinal epithelium: a novel function for PKC-theta. *Am J Physiol Cell Physiol* **287**, C218-34.

Banks, D. S. and Fradin, C. (2005). Anomalous diffusion of proteins due to molecular crowding. *Biophys J* **89**, 2960-71.

Baron, U. and Bujard, H. (2000). Tet repressor-based system for regulated gene expression in eukaryotic cells: principles and advances. *Methods Enzymol* **327**, 401-21.

Behnke, O. and Forer, A. (1967). Evidence for four classes of microtubules in individual cells. *J Cell Sci* **2**, 169-92.

Berns, G. S. and Berns, M. W. (1982). Computer-based tracking of living cells. *Exp Cell Res* **142**, 103-9.

Berrueta, L., Kraeft, S. K., Tirnauer, J. S., Schuyler, S. C., Chen, L. B., Hill, D. E., Pellman, D. and Bierer, B. E. (1998). The adenomatous polyposis coli-binding protein EB1 is associated with cytoplasmic and spindle microtubules. *Proc Natl Acad Sci U S A* **95**, 10596-601.

Bieling, P., Laan, L., Schek, H., Munteanu, E. L., Sandblad, L., Dogterom, M., Brunner, D. and Surrey, T. (2007). Reconstitution of a microtubule plus-end tracking system in vitro. *Nature*.

Bienzi, M. (2002). The subcellular destinations of APC proteins. *Nat Rev Mol Cell Biol* **3**, 328-38.

Bilbe, G., Delabie, J., Bruggen, J., Richener, H., Asselbergs, F. A., Cerletti, N., Sorg, C., Odink, K., Tarcsay, L., Wiesendanger, W. et al. (1992). Restin: a novel intermediate filament-associated protein highly expressed in the Reed-Sternberg cells of Hodgkin's disease. *Embo J* **11**, 2103-13.

Blaineau, C., Tessier, M., Dubessay, P., Tasse, L., Crobu, L., Pages, M. and Bastien, P. (2007). A novel microtubule-depolymerizing Kinesin involved in length control of a eukaryotic flagellum. *Curr Biol* **17**, 778-82.

Bode, C. J., Gupta, M. L., Suprenant, K. A. and Himes, R. H. (2003). The two alpha-tubulin isotypes in budding yeast have opposing effects on microtubule dynamics in vitro. *EMBO Rep* **4**, 94-9.

Bolte, S. and Cordelieres, F. P. (2006). A guided tour into subcellular colocalization analysis in light microscopy. *J Microsc* **224**, 213-32.

Bond, J. F., Fridovich-Keil, J. L., Pillus, L., Mulligan, R. C. and Solomon, F. (1986). A chicken-yeast chimeric beta-tubulin protein is incorporated into mouse microtubules in vivo. *Cell* **44**, 461-8.

Bonnet, C., Boucher, D., Lazereg, S., Pedrotti, B., Islam, K., Denoulet, P. and Larcher, J. C. (2001). Differential binding regulation of microtubule-associated proteins MAP1A, MAP1B, and MAP2 by tubulin polyglutamylation. *J Biol Chem* **276**, 12839-48.

Borisy, G. G. and Olmsted, J. B. (1972). Nucleated assembly of microtubules in porcine brain extracts. *Science* **177**, 1196-7.

Brangwynne, C. P., MacKintosh, F. C., Kumar, S., Geisse, N. A., Talbot, J., Mahadevan, L., Parker, K. K., Ingber, D. E. and Weitz, D. A. (2006). Microtubules

can bear enhanced compressive loads in living cells because of lateral reinforcement. *J Cell Biol* **173**, 733-41.

Briggs, M. W. and Sacks, D. B. (2003). IQGAP proteins are integral components of cytoskeletal regulation. *EMBO Rep* **4**, 571-4.

Brock, R., Hink, M. A. and Jovin, T. M. (1998). Fluorescence correlation microscopy of cells in the presence of autofluorescence. *Biophys J* **75**, 2547-57.

Brunner, D. and Nurse, P. (2000). CLIP170-like tip1p spatially organizes microtubular dynamics in fission yeast. *Cell* **102**, 695-704.

Bryan, J. and Wilson, L. (1971). Are cytoplasmic microtubules heteropolymers? *Proc Natl Acad Sci U S A* **68**, 1762-6.

Bu, W. and Su, L. K. (2001). Regulation of microtubule assembly by human EB1 family proteins. *Oncogene* **20**, 3185-92.

Bu, W. and Su, L. K. (2003). Characterization of functional domains of human EB1 family proteins. *J Biol Chem* **278**, 49721-31.

Bulinski, J. C. (2007). Microtubule modification: acetylation speeds anterograde traffic flow. *Curr Biol* **17**, R18-20.

Bulinski, J. C. and Gundersen, G. G. (1991). Stabilization of post-translational modification of microtubules during cellular morphogenesis. *Bioessays* **13**, 285-93.

Bulinski, J. C., Odde, D. J., Howell, B. J., Salmon, T. D. and Waterman-Storer, C. M. (2001). Rapid dynamics of the microtubule binding of ensconsin in vivo. *J Cell Sci* **114**, 3885-97.

Burgess, S. A., Walker, M. L., Sakakibara, H., Knight, P. J. and Oiwa, K. (2003). Dynein structure and power stroke. *Nature* **421**, 715-8.

Burns, R. G. and Surridge, C. (1990). Analysis of beta-tubulin sequences reveals highly conserved, coordinated amino acid substitutions. Evidence that these 'hot spots' are directly involved in the conformational change required for dynamic instability. *FEBS Lett* **271**, 1-8.

Busch, K. E., Hayles, J., Nurse, P. and Brunner, D. (2004). Tea2p kinesin is involved in spatial microtubule organization by transporting tip1p on microtubules. *Dev Cell* **6**, 831-43.

Bussolati, O., Uggeri, J., Belletti, S., Dall'Asta, V. and Gazzola, G. C. (1996). The stimulation of Na,K,Cl cotransport and of system A for neutral amino acid transport is a mechanism for cell volume increase during the cell cycle. *Faseb J* **10**, 920-6.

Campbell, R. E., Tour, O., Palmer, A. E., Steinbach, P. A., Baird, G. S., Zacharias, D. A. and Tsien, R. Y. (2002). A monomeric red fluorescent protein. *Proc Natl Acad Sci U S A* **99**, 7877-82.

Caplow, M. and Fee, L. (2003). Concerning the chemical nature of tubulin subunits that cap and stabilize microtubules. *Biochemistry* **42**, 2122-6.

Caplow, M. and Shanks, J. (1996). Evidence that a single monolayer tubulin-GTP cap is both necessary and sufficient to stabilize microtubules. *Mol Biol Cell* **7**, 663-75.

Carim-Todd, L., Escarceller, M., Estivill, X. and Sumoy, L. (2001). Characterization of human FSD1, a novel brain specific gene on chromosome 19 with paralogy to 9q31. *Biochim Biophys Acta* **1518**, 200-3.

- Carrier, M. F.** (1982). Guanosine-5'-triphosphate hydrolysis and tubulin polymerization. Review article. *Mol Cell Biochem* **47**, 97-113.
- Carvalho, P., Gupta, M. L., Jr., Hoyt, M. A. and Pellman, D.** (2004). Cell cycle control of kinesin-mediated transport of Bik1 (CLIP-170) regulates microtubule stability and dynein activation. *Dev Cell* **6**, 815-29.
- Carvalho, P., Tirnauer, J. S. and Pellman, D.** (2003). Surfing on microtubule ends. *Trends Cell Biol* **13**, 229-37.
- Cassimeris, L.** (1993). Regulation of microtubule dynamic instability. *Cell Motil Cytoskeleton* **26**, 275-81.
- Cassimeris, L.** (2002). The oncoprotein 18/stathmin family of microtubule destabilizers. *Current Opinion in Cell Biology* **14**, 18-24.
- Cassimeris, L., Pryer, N. and Salmon, E.** (1988). Real-time observations of microtubule dynamic instability in living cells 10.1083/jcb.107.6.2223. *J. Cell Biol.* **107**, 2223-2231.
- Cassimeris, L. and Spittle, C.** (2001). Regulation of microtubule-associated proteins. *Int Rev Cytol* **210**, 163-226.
- Chafouleas, J. G., Pardue, R. L., Brinkley, B. R., Dedman, J. R. and Means, A. R.** (1981). Regulation of intracellular levels of calmodulin and tubulin in normal and transformed cells. *Proc Natl Acad Sci U S A* **78**, 996-1000.
- Chalfie, M., Tu, Y., Euskirchen, G., Ward, W. W. and Prasher, D. C.** (1994). Green fluorescent protein as a marker for gene expression. *Science* **263**, 802-5.
- Chang, W., Webster, D. R., Salam, A. A., Gruber, D., Prasad, A., Eiserich, J. P. and Bulinski, J. C.** (2002). Alteration of the C-terminal amino acid of tubulin specifically inhibits myogenic differentiation. *J Biol Chem* **277**, 30690-8.
- Charpillienne, A., Nejmeddine, M., Berois, M., Perez, N., Neumann, E., Hewat, E., Trugnan, G. and Cohen, J.** (2001). Individual rotavirus-like particles containing 120 molecules of fluorescent protein are visible in living cells. *J Biol Chem* **276**, 29361-7.
- Cheezum, M. K., Walker, W. F. and Guilford, W. H.** (2001). Quantitative Comparison of Algorithms for Tracking Single Fluorescent Particles. *Biophysical Journal* **81**, 2378-2388.
- Chen, Y., Muller, J. D., Ruan, Q. and Gratton, E.** (2002). Molecular brightness characterization of EGFP in vivo by fluorescence fluctuation spectroscopy. *Biophys J* **82**, 133-44.
- Chen, Y., Muller, J. D., So, P. T. and Gratton, E.** (1999). The photon counting histogram in fluorescence fluctuation spectroscopy. *Biophys J* **77**, 553-67.
- Chevalier-Larsen, E. and Holzbaur, E. L.** (2006). Axonal transport and neurodegenerative disease. *Biochim Biophys Acta* **1762**, 1094-108.
- Choi, J. H., Bertram, P. G., Drenan, R., Carvalho, J., Zhou, H. H. and Zheng, X. F.** (2002). The FKBP12-rapamycin-associated protein (FRAP) is a CLIP-170 kinase. *EMBO Rep* **3**, 988-94.
- Chretien, D., Fuller, S. D. and Karsenti, E.** (1995). Structure of growing microtubule ends: two-dimensional sheets close into tubes at variable rates. *J Cell Biol* **129**, 1311-28.
- Conklin, E., G. .** (1917). Effects of centrifugal force on the structure and development of the eggs of *Crepidula*. *J. Exp. Zool* **22**, 311-419.

Coquelle, F. M., Caspi, M., Cordelieres, F. P., Dompierre, J. P., Dujardin, D. L., Koifman, C., Martin, P., Hoogenraad, C. C., Akhmanova, A., Galjart, N. et al. (2002). LIS1, CLIP-170's key to the dynein/dynactin pathway. *Mol Cell Biol* **22**, 3089-102.

Coscoy, S., Waharte, F., Gautreau, A., Martin, M., Louvard, D., Mangeat, P., Arpin, M. and Amblard, F. (2002). Molecular analysis of microscopic ezrin dynamics by two-photon FRAP. *Proc Natl Acad Sci U S A* **99**, 12813-8.

Coy, J. F., Wiemann, S., Bechmann, I., Bachner, D., Nitsch, R., Kretz, O., Christiansen, H. and Poustka, A. (2002). Pore membrane and/or filament interacting like protein 1 (POMFIL1) is predominantly expressed in the nervous system and encodes different protein isoforms. *Gene* **290**, 73-94.

Crute, B. E. and Van Buskirk, R. G. (1992). A casein kinase-like kinase phosphorylates beta-tubulin and may be a microtubule-associated protein. *J Neurochem* **59**, 2017-23.

Cui, H., Dong, M., Sadhu, D. N. and Rosenberg, D. W. (2002). Suppression of kinesin expression disrupts adenomatous polyposis coli (APC) localization and affects beta-catenin turnover in young adult mouse colon (YAMC) epithelial cells. *Exp Cell Res* **280**, 12-23.

Culver-Hanlon, T. L., Lex, S. A., Stephens, A. D., Quintyne, N. J. and King, S. J. (2006). A microtubule-binding domain in dynactin increases dynein processivity by skating along microtubules. *Nat Cell Biol* **8**, 264-70.

D'Addario, M., Arora, P. D., Ellen, R. P. and McCulloch, C. A. (2003). Regulation of tension-induced mechanotranscriptional signals by the microtubule network in fibroblasts. *J Biol Chem* **278**, 53090-7.

Danuser, G. and Waterman-Storer, C. M. (2006). Quantitative fluorescent speckle microscopy of cytoskeleton dynamics. *Annu Rev Biophys Biomol Struct* **35**, 361-87.

de la Vega, R. M., Sevilla, R. G., Hermoso, A., Lorenzo, J., Tanco, S., Diez, A., Fricker, L. D., Bautista, J. M. and Aviles, F. X. (2007). Nna1-like proteins are active metallopeptidases of a new and diverse M14 subfamily. *Faseb J* **21**, 851-65.

De Zeeuw, C. I., Hoogenraad, C. C., Goedknegt, E., Hertzberg, E., Neubauer, A., Grosveld, F. and Galjart, N. (1997). CLIP-115, a novel brain-specific cytoplasmic linker protein, mediates the localization of dendritic lamellar bodies. *Neuron* **19**, 1187-99.

Desai, A. and Mitchison, T. J. (1997). Microtubule polymerization dynamics. *Annu Rev Cell Dev Biol* **13**, 83-117.

Diamantopoulos, G. S., Perez, F., Goodson, H. V., Batelier, G., Melki, R., Kreis, T. E. and Rickard, J. E. (1999). Dynamic localization of CLIP-170 to microtubule plus ends is coupled to microtubule assembly. *J Cell Biol* **144**, 99-112.

Dogterom, M., Kerssemakers, J. W., Romet-Lemonne, G. and Janson, M. E. (2005). Force generation by dynamic microtubules. *Curr Opin Cell Biol* **17**, 67-74.

Drabek, K., van Ham, M., Stepanova, T., Draegestein, K., van Horssen, R., Sayas, C. L., Akhmanova, A., Ten Hagen, T., Smits, R., Fodde, R. et al. (2006).

Role of CLASP2 in microtubule stabilization and the regulation of persistent motility. *Curr Biol* **16**, 2259-64.

Dutcher, S. K. (2001). The tubulin fraternity: alpha to eta. *Current Opinion in Cell Biology* **13**, 49-54.

Dzhindzhev, N. S., Rogers, S. L., Vale, R. D. and Ohkura, H. (2005). Distinct mechanisms govern the localisation of Drosophila CLIP-190 to unattached kinetochores and microtubule plus-ends. *J Cell Sci* **118**, 3781-90.

Efimov, A., Kharitonov, A., Efimova, N., Loncarek, J., Miller, P. M., Andreyeva, N., Gleeson, P., Galjart, N., Maia, A. R. R., McLeod, I. X. et al. (2007). Asymmetric CLASP-Dependent Nucleation of Noncentrosomal Microtubules at the trans-Golgi Network. *Developmental Cell* **12**, 917-930.

Eipper, B. A. (1972). Rat brain microtubule protein: purification and determination of covalently bound phosphate and carbohydrate. *Proc Natl Acad Sci U S A* **69**, 2283-7.

Elson, E. L. (2004). Quick tour of fluorescence correlation spectroscopy from its inception. *J Biomed Opt* **9**, 857-64.

Elson, E. L. and Magde, D. (1974). Fluorescence correlation spectroscopy. I. Conceptual basis and theory. *Biopolymers* **13**, 1-27.

Emanuele, M. J., McClelland, M. L., Satinover, D. L. and Stukenberg, P. T. (2005). Measuring the stoichiometry and physical interactions between components elucidates the architecture of the vertebrate kinetochore. *Mol Biol Cell* **16**, 4882-92.

Enderlein, J., Gregor, I., Patra, D., Dertinger, T. and Kaupp, U. B. (2005). Performance of fluorescence correlation spectroscopy for measuring diffusion and concentration. *Chemphyschem* **6**, 2324-36.

Erck, C., Frank, R. and Wehland, J. (2000). Tubulin-tyrosine ligase, a long-lasting enigma. *Neurochem Res* **25**, 5-10.

Erck, C., MacLeod, R. A. and Wehland, J. (2003). Cloning and genomic organization of the TTL gene on mouse chromosome 2 and human chromosome 2q13. *Cytogenet Genome Res* **101**, 47-53.

Erck, C., Peris, L., Andrieux, A., Meissirel, C., Gruber, A. D., Vernet, M., Schweitzer, A., Saoudi, Y., Pointu, H., Bosc, C. et al. (2005). A vital role of tubulin-tyrosine-ligase for neuronal organization. *Proc Natl Acad Sci U S A* **102**, 7853-8.

Erickson, H. P. (1974). Microtubule surface lattice and subunit structure and observations on reassembly. *J Cell Biol* **60**, 153-67.

Etienne-Manneville, S. and Hall, A. (2003). Cdc42 regulates GSK-3beta and adenomatous polyposis coli to control cell polarity. *Nature* **421**, 753-6.

Fabbro, M. and Henderson, B. R. (2003). Regulation of tumor suppressors by nuclear-cytoplasmic shuttling. *Exp Cell Res* **282**, 59-69.

Fawcett, D. (1961). An Atlas of Fine Structure: The Cell, its Organelles and Inclusions: W.B. Saunders Company.

Fawcett, D. and Porter, K. (1954). A study of the fine structure of ciliated epithelia. *J Morphol* **94**, 221-281.

Farla, P., Fersmus, R., Geverts, B. Mari, P.O., Nigg, A. L., Dubink, H. J., Trapman, J. and Houtsmuller, A.B. (2004). The androgen receptor ligand-binding domain stabilizes DNA binding in living cells. *J Struct Biol* **94**, 221-281.

-
- Feit, H., Slusarek, L. and Shelanski, M. L.** (1971). Heterogeneity of tubulin subunits. *Proc Natl Acad Sci U S A* **68**, 2028-31.
- Ferrari, M. E., Bujalowski, W. and Lohman, T. M.** (1994). Co-operative binding of Escherichia coli SSB tetramers to single-stranded DNA in the (SSB)35 binding mode. *J Mol Biol* **236**, 106-23.
- Fischer, D., Mukrasch, M. D., von Bergen, M., Klos-Witkowska, A., Biernat, J., Griesinger, C., Mandelkow, E. and Zweckstetter, M.** (2007). Structural and microtubule binding properties of tau mutants of frontotemporal dementias. *Biochemistry* **46**, 2574-82.
- Folker, E. S., Baker, B. M. and Goodson, H. V.** (2005). Interactions between CLIP-170, Tubulin, and Microtubules: Implications for the Mechanism of CLIP-170 Plus-End Tracking Behavior. *Mol Biol Cell* **16**, 5373-84.
- Fonrose, X., Ausseil, F., Soleilhac, E., Masson, V., David, B., Pouny, I., Cintrat, J. C., Rousseau, B., Barette, C., Massiot, G. et al.** (2007). Parthenolide inhibits tubulin carboxypeptidase activity. *Cancer Res* **67**, 3371-8.
- Fourest-Lieuvain, A., Peris, L., Gache, V., Garcia-Saez, I., Juillan-Binard, C., Lantiez, V. and Job, D.** (2006). Microtubule regulation in mitosis: tubulin phosphorylation by the cyclin-dependent kinase Cdk1. *Mol Biol Cell* **17**, 1041-50.
- Fradkov, A. F., Chen, Y., Ding, L., Barsova, E. V., Matz, M. V. and Lukyanov, S. A.** (2000). Novel fluorescent protein from Discosoma coral and its mutants possesses a unique far-red fluorescence. *FEBS Lett* **479**, 127-30.
- Frixione, E.** (2000). Recurring views on the structure and function of the cytoskeleton: a 300-year epic. *Cell Motil Cytoskeleton* **46**, 73-94.
- Fukata, M., Watanabe, T., Noritake, J., Nakagawa, M., Yamaga, M., Kuroda, S., Matsuura, Y., Iwamatsu, A., Perez, F. and Kaibuchi, K.** (2002). Rac1 and Cdc42 capture microtubules through IQGAP1 and CLIP-170. *Cell* **109**, 873-85.
- Fulton, C. and Simpson, P. A.** (1976). Selective synthesis and utilization of flagellar tubulin: the multi-tubulin hypothesis. In *Cell motility*, (ed. T. Pollard), pp. 987-1005. Cold Spring Harbor Press.
- Gaertig, J., Cruz, M. A., Bowen, J., Gu, L., Pennock, D. G. and Gorovsky, M. A.** (1995). Acetylation of lysine 40 in alpha-tubulin is not essential in Tetrahymena thermophila. *J Cell Biol* **129**, 1301-10.
- Galjart, N.** (2005). CLIPs and CLASPs and cellular dynamics. *Nat Rev Mol Cell Biol* **6**, 487-98.
- Galjart, N. and Perez, F.** (2003). A plus-end raft to control microtubule dynamics and function. *Current Opinion in Cell Biology* **15**, 48-53.
- Gao, Y., Zhong, Z. and Geng, L. M.** (2007). Calibration of probe volume in fluorescence correlation spectroscopy. *Appl Spectrosc* **61**, 956-62.
- Garcia-Parajo, M. F., Segers-Nolten, G. M., Veerman, J. A., Greve, J. and van Hulst, N. F.** (2000). Real-time light-driven dynamics of the fluorescence emission in single green fluorescent protein molecules. *Proc Natl Acad Sci USA* **97**, 7237-42.
- Geuens, G., Gundersen, G. G., Nuydens, R., Cornelissen, F., Bulinski, J. C. and DeBrabander, M.** (1986). Ultrastructural colocalization of tyrosinated and detyrosinated alpha-tubulin in interphase and mitotic cells. *J Cell Biol* **103**, 1883-93.

Gill, S. R., Schroer, T. A., Szilak, I., Steuer, E. R., Sheetz, M. P. and Cleveland, D. W. (1991). Dynactin, a conserved, ubiquitously expressed component of an activator of vesicle motility mediated by cytoplasmic dynein. *J Cell Biol* **115**, 1639-50.

Gittes, F., Mickey, B., Nettleton, J. and Howard, J. (1993). Flexural rigidity of microtubules and actin filaments measured from thermal fluctuations in shape. *J Cell Biol* **120**, 923-34.

Gliksman, N., Skibbens, R. and Salmon, E. (1993). How the transition frequencies of microtubule dynamic instability (nucleation, catastrophe, and rescue) regulate microtubule dynamics in interphase and mitosis: analysis using a Monte Carlo computer simulation. *Mol. Biol. Cell* **4**, 1035-1050.

Gonczy, P., Echeverri, C., Oegema, K., Coulson, A., Jones, S. J., Copley, R. R., Duperon, J., Oegema, J., Brehm, M., Cassin, E. et al. (2000). Functional genomic analysis of cell division in *C. elegans* using RNAi of genes on chromosome III. *Nature* **408**, 331-6.

Goobic, A. P., Tang, J. S. and Acton, S. T. (2005). Image stabilization and registration for tracking cells in the microvasculature. *Ieee Transactions on Biomedical Engineering* **52**, 287-299.

Goodson, H. V., Skube, S. B., Stalder, R., Valetti, C., Kreis, T. E., Morrison, E. E. and Schroer, T. A. (2003). CLIP-170 interacts with dynactin complex and the APC-binding protein EB1 by different mechanisms. *Cell Motil Cytoskeleton* **55**, 156-73.

Gosch, M. and Rigler, R. (2005). Fluorescence correlation spectroscopy of molecular motions and kinetics. *Adv Drug Deliv Rev* **57**, 169-90.

Greber, U. F. and Way, M. (2006). A superhighway to virus infection. *Cell* **124**, 741-54.

Griffin, B. A., Adams, S. R. and Tsien, R. Y. (1998). Specific covalent labeling of recombinant protein molecules inside live cells. *Science* **281**, 269-72.

Griparic, L. and Keller, T. C. (1998). Identification and expression of two novel CLIP-170/Restin isoforms expressed predominantly in muscle. *Biochim Biophys Acta* **1405**, 35-46.

Grohmann, A., Tanneberger, K., Alzner, A., Schneikert, J. and Behrens, J. (2007). AMER1 regulates the distribution of the tumor suppressor APC between microtubules and the plasma membrane. *J Cell Sci*.

Gross, S. P. (2003). Dynactin: coordinating motors with opposite inclinations. *Curr Biol* **13**, R320-2.

Guillaud, L., Bosc, C., Fourest-Lieuvin, A., Denarier, E., Pirollet, F., Lafanechere, L. and Job, D. (1998). STOP proteins are responsible for the high degree of microtubule stabilization observed in neuronal cells. *J Cell Biol* **142**, 167-79.

Gundersen, G. G. and Bulinski, J. C. (1988). Selective stabilization of microtubules oriented toward the direction of cell migration. *Proc Natl Acad Sci U S A* **85**, 5946-50.

Hall, C., Jakus, M. and Schmitt, F. (1946). An investigation of cross striations and myosin filaments in muscle. *Biol Bull* **90**, 32-50.

-
- Hamelin, M., Scott, I. M., Way, J. C. and Culotti, J. G.** (1992). The mec-7 beta-tubulin gene of *Caenorhabditis elegans* is expressed primarily in the touch receptor neurons. *Embo J* **11**, 2885-93.
- Hannak, E. and Heald, R.** (2006). Xorbit/CLASP links dynamic microtubules to chromosomes in the *Xenopus* meiotic spindle. *J Cell Biol* **172**, 19-25.
- Hanson, C. A. and Miller, J. R.** (2005). Non-traditional roles for the Adenomatous Polyposis Coli (APC) tumor suppressor protein. *Gene* **361**, 1-12.
- Hayashi, I. and Ikura, M.** (2003). Crystal structure of the amino-terminal microtubule-binding domain of end-binding protein 1 (EB1). *J Biol Chem* **278**, 36430-4.
- Hayashi, I., Plevin, M. J. and Ikura, M.** (2007). CLIP170 autoinhibition mimics intermolecular interactions with p150Glued or EB1. *Nat Struct Mol Biol* **14**, 980-1.
- Helenius, J., Brouhard, G., Kalaidzidis, Y., Diez, S. and Howard, J.** (2006). The depolymerizing kinesin MCAK uses lattice diffusion to rapidly target microtubule ends. *Nature* **441**, 115-9.
- Henderson, B. R.** (2000). Nuclear-cytoplasmic shuttling of APC regulates beta-catenin subcellular localization and turnover. *Nat Cell Biol* **2**, 653-60.
- Hiller, G. and Weber, K.** (1978). Radioimmunoassay for tubulin: a quantitative comparison of the tubulin content of different established tissue culture cells and tissues. *Cell* **14**, 795-804.
- Hink, M. A., Bisselin, T. and Visser, A. J.** (2002). Imaging protein-protein interactions in living cells. *Plant Mol Biol* **50**, 871-83.
- Hirokawa, N.** (1994). Microtubule organization and dynamics dependent on microtubule-associated proteins. *Curr Opin Cell Biol* **6**, 74-81.
- Hirokawa, N. and Takemura, R.** (2003). Biochemical and molecular characterization of diseases linked to motor proteins. *Trends Biochem Sci* **28**, 558-65.
- Hoetelmans, R. W., Prins, F. A., Cornelese-ten Velde, I., van der Meer, J., van de Velde, C. J. and van Dierendonck, J. H.** (2001). Effects of acetone, methanol, or paraformaldehyde on cellular structure, visualized by reflection contrast microscopy and transmission and scanning electron microscopy. *Appl Immunohistochem Mol Morphol* **9**, 346-51.
- Holy, T. E. and Leibler, S.** (1994). Dynamic instability of microtubules as an efficient way to search in space. *Proc Natl Acad Sci U S A* **91**, 5682-5.
- Honnappa, S., Okhrimenko, O., Jaussi, R., Jawhari, H., Jelesarov, I., Winkler, F. K. and Steinmetz, M. O.** (2006). Key interaction modes of dynamic +TIP networks. *Mol Cell* **23**, 663-71.
- Hoogenraad, C. C., Akhmanova, A., Grosveld, F., De Zeeuw, C. I. and Galjart, N.** (2000). Functional analysis of CLIP-115 and its binding to microtubules. *J Cell Sci* **113** (Pt 12), 2285-97.
- Hoogenraad, C. C., Koekkoek, B., Akhmanova, A., Krugers, H., Dortland, B., Miedema, M., van Alphen, A., Kistler, W. M., Jaegle, M., Koutsourakis, M. et al.** (2002). Targeted mutation of *Cyln2* in the Williams syndrome critical region links CLIP-115 haploinsufficiency to neurodevelopmental abnormalities in mice. *Nat Genet* **32**, 116-27.

Hoogstraten, D., Nigg, A. L., Heath, H., Mullender, L. H., van Driel, R., Hoeijmakers, J. H., Vermeulen, W. and Houtsmuller, A. B. (2002). Rapid switching of TFIIF between RNA polymerase I and II transcription and DNA repair in vivo. *Mol Cell* **10**, 1163-74.

Hook, P. and Vallee, R. B. (2006). The dynein family at a glance. *Journal of Cell Science* **119**, 4369-4371.

Houtsmuller, A. B. and Vermeulen, W. (2001). Macromolecular dynamics in living cell nuclei revealed by fluorescence redistribution after photobleaching. *Histochem Cell Biol* **115**, 13-21.

Howard, J. (2001). *Mechanics of Motor Proteins and the Cytoskeleton*: Sinauer Associates.

Howard, J. and Hyman, A. A. (2003). Dynamics and mechanics of the microtubule plus end. *Nature* **422**, 753-8.

Hubbert, C., Guardiola, A., Shao, R., Kawaguchi, Y., Ito, A., Nixon, A., Yoshida, M., Wang, X. F. and Yao, T. P. (2002). HDAC6 is a microtubule-associated deacetylase. *Nature* **417**, 455-8.

Hulspas, R., Houtsmuller, A. B., Bauman, J.G. and Nanninga, N. (1994). The centrosome moves out of a nuclear indentation in human lymphocytes upon activation. *Exp Cell Res* **215**, 28-32.

Huxley, H. E. (1963). Electron Microscope Studies on the Structure of Natural and Synthetic Protein Filaments from Striated Muscle. *J Mol Biol* **7**, 281-308.

Ibrahim, S. M. (2006). *Quantitative Fluorescence Microscopy of Protein Dynamics in Living Cells*, Ph.D., pp. 261. Rotterdam: Erasmus University.

Ikegami, K., Heier, R. L., Taruishi, M., Takagi, H., Mukai, M., Shimma, S., Taira, S., Hatanaka, K., Morone, N., Yao, I. et al. (2007). Loss of alpha-tubulin polyglutamylation in ROSA22 mice is associated with abnormal targeting of KIF1A and modulated synaptic function. *Proc Natl Acad Sci U S A* **104**, 3213-8.

Imaizumi, T., Jean-Louis, F., Dubertret, M. L., Bailly, C., Cicurel, L., Petchot-Bacque, J. P. and Dubertret, L. (1996). Effect of human basic fibroblast growth factor on fibroblast proliferation, cell volume, collagen lattice contraction: in comparison with acidic type. *J Dermatol Sci* **11**, 134-41.

Inoue, Y. H., do Carmo Avides, M., Shiraki, M., Deak, P., Yamaguchi, M., Nishimoto, Y., Matsukage, A. and Glover, D. M. (2000). Orbit, a Novel Microtubule-associated Protein Essential for Mitosis in *Drosophila melanogaster*. *The Journal of Cell Biology* **149**, 153-166.

Ishiguro, H., Shimokawa, T., Tsunoda, T., Tanaka, T., Fujii, Y., Nakamura, Y. and Furukawa, Y. (2002). Isolation of HELAD1, a novel human helicase gene up-regulated in colorectal carcinomas. *Oncogene* **21**, 6387-94.

Ishikawa, H., Bischoff, R. and Holtzer, H. (1968). Mitosis and intermediate-sized filaments in developing skeletal muscle. *J Cell Biol* **38**, 538-55.

Itoh, T. J. and Hotani, H. (1994). Microtubule-stabilizing activity of microtubule-associated proteins (MAPs) is due to increase in frequency of rescue in dynamic instability: shortening length decreases with binding of MAPs onto microtubules. *Cell Struct Funct* **19**, 279-90.

Janke, C., Rogowski, K., Wloga, D., Regnard, C., Kajava, A. V., Strub, J. M., Temurak, N., van Dijk, J., Boucher, D., van Dorsselaer, A. et al. (2005). Tubulin polyglutamylase enzymes are members of the TTL domain protein family. *Science* **308**, 1758-62.

Janosi, I. M., Chretien, D. and Flyvbjerg, H. (2002). Structural Microtubule Cap: Stability, Catastrophe, Rescue, and Third State. *Biophys. J.* **83**, 1317-1330.

Jimbo, T., Kawasaki, Y., Koyama, R., Sato, R., Takada, S., Haraguchi, K. and Akiyama, T. (2002). Identification of a link between the tumour suppressor APC and the kinesin superfamily. *Nat Cell Biol* **4**, 323-7.

Jordan, M. A., Wendell, K., Gardiner, S., Derry, W. B., Copp, H. and Wilson, L. (1996). Mitotic block induced in HeLa cells by low concentrations of paclitaxel (Taxol) results in abnormal mitotic exit and apoptotic cell death. *Cancer Res* **56**, 816-25.

Juwana, J. P., Henderikx, P., Mischo, A., Wadle, A., Fadle, N., Gerlach, K., Arends, J. W., Hoogenboom, H., Pfreundschuh, M. and Renner, C. (1999). EB/RP gene family encodes tubulin binding proteins. *Int J Cancer* **81**, 275-84.

Kalaidzidis, Y. (2007). Intracellular objects tracking. *Eur J Cell Biol.* **86**, 569-78.

Kalinina, E., Biswas, R., Berezniuk, I., Hermoso, A., Aviles, F. X. and Fricker, L. D. (2007). A novel subfamily of mouse cytosolic carboxypeptidases. *FASEB J* **21**, 836-50.

Karki, S. and Holzbaur, E. L. (1999). Cytoplasmic dynein and dynactin in cell division and intracellular transport. *Curr Opin Cell Biol* **11**, 45-53.

Katsetos, C. D., Herman, M. M. and Mork, S. J. (2003). Class III beta-tubulin in human development and cancer. *Cell Motil Cytoskeleton* **55**, 77-96.

Kavallaris, M., Burkhart, C. A. and Horwitz, S. B. (1999). Antisense oligonucleotides to class III beta-tubulin sensitize drug-resistant cells to Taxol. *Br J Cancer* **80**, 1020-5.

Kellogg, D. R., Moritz, M. and Alberts, B. M. (1994). The centrosome and cellular organization. *Annu Rev Biochem* **63**, 639-74.

Kerssemakers, J. W., Munteanu, E. L., Laan, L., Noetzel, T. L., Janson, M. E. and Dogterom, M. (2006). Assembly dynamics of microtubules at molecular resolution. *Nature* **442**, 709-12.

Khan, I. A. and Luduena, R. F. (1996). Phosphorylation of beta III-tubulin. *Biochemistry* **35**, 3704-11.

Kikkawa, M., Ishikawa, T., Nakata, T., Wakabayashi, T. and Hirokawa, N. (1994). Direct visualization of the microtubule lattice seam both in vitro and in vivo. *J Cell Biol* **127**, 1965-71.

Kim, S. A. and Schwille, P. (2003). Intracellular applications of fluorescence correlation spectroscopy: prospects for neuroscience. *Curr Opin Neurobiol* **13**, 583-90.

Kimura, H. and Cook, P. R. (2001). Kinetics of core histones in living human cells: little exchange of H3 and H4 and some rapid exchange of H2B. *J Cell Biol* **153**, 1341-53.

- Kinoshita, K., Noetzel, T. L., Arnal, I., Drechsel, D. N. and Hyman, A. A.** (2006). Global and local control of microtubule destabilization promoted by a catastrophe kinesin MCAK/XKCM1. *J Muscle Res Cell Motil* **27**, 107-14.
- Kita, K., Wittmann, T., Nathke, I. S. and Waterman-Storer, C. M.** (2006). Adenomatous polyposis coli on microtubule plus ends in cell extensions can promote microtubule net growth with or without EB1. *Mol Biol Cell* **17**, 2331-45.
- Kline-Smith, S. L. and Walczak, C. E.** (2000). Microtubules in orbit. *J Cell Biol* **149**, 5-6.
- Klonis, N., Rug, M., Harper, I., Wickham, M., Cowman, A. and Tilley, L.** (2002). Fluorescence photobleaching analysis for the study of cellular dynamics. *Eur Biophys J* **31**, 36-51.
- Kodama, A., Karakesisoglou, I., Wong, E., Vaezi, A. and Fuchs, E.** (2003). ACF7: an essential integrator of microtubule dynamics. *Cell* **115**, 343-54.
- Komarova, Y., Lansbergen, G., Galjart, N., Grosveld, F., Borisy, G. G. and Akhmanova, A.** (2005). EB1 and EB3 Control CLIP Dissociation from the Ends of Growing Microtubules. *Mol Biol Cell* **16**, 5334-45.
- Komarova, Y. A., Akhmanova, A. S., Kojima, S., Galjart, N. and Borisy, G. G.** (2002a). Cytoplasmic linker proteins promote microtubule rescue in vivo. *J Cell Biol* **159**, 589-99.
- Komarova, Y. A., Vorobjev, I. A. and Borisy, G. G.** (2002b). Life cycle of MTs: persistent growth in the cell interior, asymmetric transition frequencies and effects of the cell boundary. *J Cell Sci* **115**, 3527-39.
- Koning, R. I., Zovko, S., Barcena, M., Oostergetel, G. T., Koerten, H. K., Galjart, N., Koster, A. J. and Mommaas, A. M.** (2007). Cryo electron tomography of vitrified fibroblasts: Microtubule plus ends in situ. *J Struct Biol*. In press
- Korenbaum, E. and Rivero, F.** (2002). Calponin homology domains at a glance. *Journal of Cell Science* **115**, 3543-3545.
- Kreplak, L. and Fudge, D.** (2007). Biomechanical properties of intermediate filaments: from tissues to single filaments and back. *Bioessays* **29**, 26-35.
- Koster, M., Frahm, T. and Hauser, H.** (2005). Nucleocytoplasmic shuttling revealed by FRAP and FLIP technologies. *Curr Opin Biotechnol* **16**, 28-34.
- Kroboth, K., Newton, I. P., Kita, K., Dikovskaya, D., Zumbrunn, J., Waterman-Storer, C. M. and Nathke, I. S.** (2007). Lack of adenomatous polyposis coli protein correlates with a decrease in cell migration and overall changes in microtubule stability. *Mol Biol Cell* **18**, 910-8.
- Kwok, B. H. and Kapoor, T. M.** (2007). Microtubule flux: drivers wanted. *Curr Opin Cell Biol* **19**, 36-42.
- L'Hernault, S. W. and Rosenbaum, J. L.** (1985). Chlamydomonas alpha-tubulin is posttranslationally modified by acetylation on the epsilon-amino group of a lysine. *Biochemistry* **24**, 473-8.
- Lace, G. L., Wharton, S. B. and Ince, P. G.** (2007). A brief history of tau: the evolving view of the microtubule-associated protein tau in neurodegenerative diseases. *Clin Neuropathol* **26**, 43-58.
- Langford, K. J., Askham, J. M., Lee, T., Adams, M. and Morrison, E. E.** (2006). Examination of actin and microtubule dependent APC localisations in living mammalian cells. *BMC Cell Biol* **7**, 3.

Lansbergen, G. and Akhmanova, A. (2006). Microtubule plus end: a hub of cellular activities. *Traffic* **7**, 499-507.

Lansbergen, G., Grigoriev, I., Mimori-Kiyosue, Y., Ohtsuka, T., Higa, S., Kitajima, I., Demmers, J., Galjart, N., Houtsmuller, A. B., Grosveld, F. et al. (2006). CLASPs Attach Microtubule Plus Ends to the Cell Cortex through a Complex with LL5[beta]. *Developmental Cell* **11**, 21-32.

Lansbergen, G., Komarova, Y., Modesti, M., Wyman, C., Hoogenraad, C. C., Goodson, H. V., Lemaitre, R. P., Drechsel, D. N., van Munster, E., Gadella, T. W., Jr. et al. (2004). Conformational changes in CLIP-170 regulate its binding to microtubules and dynactin localization. *J Cell Biol* **166**, 1003-14.

Lawrence, C. J., Dawe, R. K., Christie, K. R., Cleveland, D. W., Dawson, S. C., Endow, S. A., Goldstein, L. S. B., Goodson, H. V., Hirokawa, N., Howard, J. et al. (2004). A standardized kinesin nomenclature. *The Journal of Cell Biology* **167**, 19-22.

Lee, W. L., Oberle, J. R. and Cooper, J. A. (2003). The role of the lissencephaly protein Pac1 during nuclear migration in budding yeast. *J Cell Biol* **160**, 355-64.

Lele, T., Wagner, S. R., Nickerson, J. A. and Ingber, D. E. (2006). Methods for measuring rates of protein binding to insoluble scaffolds in living cells: histone H1-chromatin interactions. *J Cell Biochem* **99**, 1334-42.

Lele, T. P. and Ingber, D. E. (2006). A mathematical model to determine molecular kinetic rate constants under non-steady state conditions using fluorescence recovery after photobleaching (FRAP). *Biophys Chem* **120**, 32-5.

Lemos, C. L., Sampaio, P., Maiato, H., Costa, M., Omel'yanchuk, L. V., Liberal, V. and Sunkel, C. E. (2000). Mast, a conserved microtubule-associated protein required for bipolar mitotic spindle organization. *Embo J* **19**, 3668-82.

Levy, J. R., Sumner, C. J., Caviston, J. P., Tokito, M. K., Ranganathan, S., Ligon, L. A., Wallace, K. E., LaMonte, B. H., Harmison, G. G., Puls, I. et al. (2006). A motor neuron disease-associated mutation in p150Glued perturbs dynactin function and induces protein aggregation. *The Journal of Cell Biology* **172**, 733-745.

Li, H., DeRosier, D. J., Nicholson, W. V., Nogales, E. and Downing, K. H. (2002a). Microtubule structure at 8 Å resolution. *Structure* **10**, 1317-28.

Li, S., Finley, J., Liu, Z. J., Qiu, S. H., Chen, H., Luan, C. H., Carson, M., Tsao, J., Johnson, D., Lin, G. et al. (2002b). Crystal structure of the cytoskeleton-associated protein glycine-rich (CAP-Gly) domain. *J Biol Chem* **277**, 48596-601.

Liao, G., Nagasaki, T. and Gundersen, G. G. (1995). Low concentrations of nocodazole interfere with fibroblast locomotion without significantly affecting microtubule level: implications for the role of dynamic microtubules in cell locomotion. *J Cell Sci* **108 (Pt 11)**, 3473-83.

Lin, H., de Carvalho, P., Kho, D., Tai, C. Y., Pierre, P., Fink, G. R. and Pellman, D. (2001). Polyploids require Bik1 for kinetochore-microtubule attachment. *J Cell Biol* **155**, 1173-84.

Lippincott-Schwartz, J. and Patterson, G. H. (2003). Development and use of fluorescent protein markers in living cells. *Science* **300**, 87-91.

Lippincott-Schwartz, J., Snapp, E. and Kenworthy, A. (2001). Studying protein dynamics in living cells. *Nat Rev Mol Cell Biol* **2**, 444-56.

Louie, R. K., Bahmanyar, S., Siemers, K. A., Votin, V., Chang, P., Stearns, T., Nelson, W. J. and Barth, A. I. (2004). Adenomatous polyposis coli and EB1 localize in close proximity of the mother centriole and EB1 is a functional component of centrosomes. *J Cell Sci* **117**, 1117-28.

Lowe, J., Li, H., Downing, K. H. and Nogales, E. (2001). Refined structure of alpha beta-tubulin at 3.5 Å resolution. *J Mol Biol* **313**, 1045-57.

Lu, Q. and Luduena, R. F. (1994). In vitro analysis of microtubule assembly of isotypically pure tubulin dimers. Intrinsic differences in the assembly properties of alpha beta II, alpha beta III, and alpha beta IV tubulin dimers in the absence of microtubule-associated proteins. *J Biol Chem* **269**, 2041-7.

Luduena, R. F. (1993). Are tubulin isotypes functionally significant. *Mol Biol Cell* **4**, 445-57.

Luduena, R. F. (1998). Multiple forms of tubulin: different gene products and covalent modifications. *Int Rev Cytol* **178**, 207-75.

Maccioni, R. B. and Cambiazo, V. (1995). Role of microtubule-associated proteins in the control of microtubule assembly. *Physiol Rev* **75**, 835-64.

Maekawa, H. and Schiebel, E. (2004). CLIP-170 family members: a motor-driven ride to microtubule plus ends. *Dev Cell* **6**, 746-8.

Maes, T., Barcelo, A. and Buesa, C. (2002). Neuron navigator: a human gene family with homology to unc-53, a cell guidance gene from *Caenorhabditis elegans*. *Genomics* **80**, 21-30.

Magde, D., Elson, E. and Webb, W. W. (1972). Thermodynamic Fluctuations in a Reacting System - Measurement by Fluorescence Correlation Spectroscopy. *Physical Review Letters* **29**, 705.

Magde, D., Elson, E. and Webb, W. W. (1974). Fluorescence correlation spectroscopy. II. An experimental realization. *Biopolymers* **13**, 29-61.

Maiato, H., Fairley, E. A., Rieder, C. L., Swedlow, J. R., Sunkel, C. E. and Earnshaw, W. C. (2003). Human CLASP1 is an outer kinetochore component that regulates spindle microtubule dynamics. *Cell* **113**, 891-904.

Maiti, S., Haupts, U. and Webb, W. W. (1997). Fluorescence correlation spectroscopy: diagnostics for sparse molecules. *Proc Natl Acad Sci USA* **94**, 11753-7.

Manabe, R., Whitmore, L., Weiss, J. M. and Horwitz, A. R. (2002). Identification of a novel microtubule-associated protein that regulates microtubule organization and cytokinesis by using a GFP-screening strategy. *Curr Biol* **12**, 1946-51.

Mandelkow, E. and Mandelkow, E. M. (2002). Kinesin motors and disease. *Trends Cell Biol* **12**, 585-91.

Mandelkow, E. M., Schultheiss, R., Rapp, R., Muller, M. and Mandelkow, E. (1986). On the surface lattice of microtubules: helix starts, protofilament number, seam, and handedness. *J Cell Biol* **102**, 1067-73.

Margolin, G., Gregoret, I. V., Goodson, H. V. and Alber, M. S. (2006). Analysis of a mesoscopic stochastic model of microtubule dynamic instability. *Phys Rev E Stat Nonlin Soft Matter Phys* **74**, 041920.

Martin, R., Walther, A. and Wendland, J. (2004). Deletion of the dynein heavy-chain gene DYN1 leads to aberrant nuclear positioning and defective hyphal development in *Candida albicans*. *Eukaryot Cell* **3**, 1574-88.

Martinez-Lopez, M. J., Alcantara, S., Mascaro, C., Perez-Branguli, F., Ruiz-Lozano, P., Maes, T., Soriano, E. and Buesa, C. (2005). Mouse neuron navigator 1, a novel microtubule-associated protein involved in neuronal migration. *Mol Cell Neurosci* **28**, 599-612.

Matus, A. (1990). Microtubule-associated proteins. *Curr Opin Cell Biol* **2**, 10-4.

Matz, M. V., Fradkov, A. F., Labas, Y. A., Savitsky, A. P., Zarsisky, A. G., Markelov, M. L. and Lukyanov, S. A. (1999). Fluorescent proteins from nonbioluminescent Anthozoa species. *Nat Biotechnol* **17**, 969-73.

McNally, F. J. (1996). Modulation of microtubule dynamics during the cell cycle. *Curr Opin Cell Biol* **8**, 23-9.

McNally, K., Audhya, A., Oegema, K. and McNally, F. J. (2006). Katanin controls mitotic and meiotic spindle length. *J Cell Biol* **175**, 881-91.

Medina, M. A. and Schwille, P. (2002). Fluorescence correlation spectroscopy for the detection and study of single molecules in biology. *Bioessays* **24**, 758-64.

Meijering, E., Smal, I. and Danuser, G. (2006). Tracking in molecular bioimaging. *Ieee Signal Processing Magazine* **23**, 46-53.

Meijering, E., Smal, I., Dzyubachyk, O. and Olivo-Marin, J.-C. (2008). Time-Lapse Microscopy Imaging. In *Microscope Image Processing*, (eds Q. Wu, F. Merchant and K. Castleman). Elsevier Academic Press.

Merrill, R. A., Plum, L. A., Kaiser, M. E. and Clagett-Dame, M. (2002). A mammalian homolog of unc-53 is regulated by all-trans retinoic acid in neuroblastoma cells and embryos. *Proc Natl Acad Sci USA* **99**, 3422-7.

Merzlyak, E. M., Goedhart, J., Shcherbo, D., Bulina, M. E., Shcheglov, A. S., Fradkov, A. F., Gaintzeva, A., Lukyanov, K. A., Lukyanov, S., Gadella, T. W. et al. (2007). Bright monomeric red fluorescent protein with an extended fluorescence lifetime. *Nat Methods* **4**, 555-7.

Meseth, U., Wohland, T., Rigler, R. and Vogel, H. (1999). Resolution of fluorescence correlation measurements. *Biophys J* **76**, 1619-31.

Miller, D. M., 3rd, Desai, N. S., Hardin, D. C., Piston, D. W., Patterson, G. H., Fleenor, J., Xu, S. and Fire, A. (1999). Two-color GFP expression system for *C. elegans*. *Biotechniques* **26**, 914-8, 920-1.

Miller, L. W. and Cornish, V. W. (2005). Selective chemical labeling of proteins in living cells. *Curr Opin Chem Biol* **9**, 56-61.

Mimori-Kiyosue, Y., Grigoriev, I., Lansbergen, G., Sasaki, H., Matsui, C., Severin, F., Galjart, N., Grosveld, F., Vorobjev, I., Tsukita, S. et al. (2005). CLASP1 and CLASP2 bind to EB1 and regulate microtubule plus-end dynamics at the cell cortex. *J Cell Biol* **168**, 141-53.

Mimori-Kiyosue, Y., Shiina, N. and Tsukita, S. (2000). Adenomatous polyposis coli (APC) protein moves along microtubules and concentrates at their growing ends in epithelial cells. *J Cell Biol* **148**, 505-18.

Mimori-Kiyosue, Y. and Tsukita, S. (2003). "Search-and-capture" of microtubules through plus-end-binding proteins (+TIPs). *J Biochem (Tokyo)* **134**, 321-6.

Mishima, M., Maesaki, R., Kasa, M., Watanabe, T., Fukata, M., Kaibuchi, K. and Hakoshima, T. (2007). Structural basis for tubulin recognition by cytoplasmic linker protein 170 and its autoinhibition. *Proc Natl Acad Sci USA* **104**, 10346-51.

Mitchison, T. and Kirschner, M. (1984). Dynamic instability of microtubule growth. *Nature* **312**, 237-42.

Molodtsov, M. I., Ermakova, E. A., Shnol, E. E., Grishchuk, E. L., McIntosh, J. R. and Ataullakhanov, F. I. (2005). A molecular-mechanical model of the microtubule. *Biophys J* **88**, 3167-79.

Moore, A. and Wordeman, L. (2004). The mechanism, function and regulation of depolymerizing kinesins during mitosis. *Trends Cell Biol* **14**, 537-546.

Morrison, E. E. (2007). Action and interactions at microtubule ends. *Cell Mol Life Sci.* **64**, 307-17.

Muller, J. D. (2004). Cumulant analysis in fluorescence fluctuation spectroscopy. *Biophys J* **86**, 3981-92.

Murphy, D. B. and Borisy, G. G. (1975). Association of high-molecular-weight proteins with microtubules and their role in microtubule assembly in vitro. *Proc Natl Acad Sci USA* **72**, 2696-700.

Nagasaki, T. and Gundersen, G. G. (1996). Depletion of lysophosphatidic acid triggers a loss of oriented detyrosinated microtubules in motile fibroblasts. *J Cell Sci* **109 (Pt 10)**, 2461-9.

Nakagawa, H., Koyama, K., Murata, Y., Morito, M., Akiyama, T. and Nakamura, Y. (2000). EB3, a novel member of the EB1 family preferentially expressed in the central nervous system, binds to a CNS-specific APC homologue. *Oncogene* **19**, 210-6.

Nakamura, M., Zhou, X. Z. and Lu, K. P. (2001). Critical role for the EB1 and APC interaction in the regulation of microtubule polymerization. *Curr Biol* **11**, 1062-7.

Nathke, I. (2004). APC at a glance. *J Cell Sci* **117**, 4873-4875.

Niethammer, P., Bastiaens, P. and Karsenti, E. (2004). Stathmin-Tubulin Interaction Gradients in Motile and Mitotic Cells. *Science* **303**, 1862-1866.

Nogales, E. and Wang, H. W. (2006). Structural intermediates in microtubule assembly and disassembly: how and why? *Curr Opin Cell Biol* **18**, 179-84.

Nogales, E., Wolf, S. G. and Downing, K. H. (1998). Structure of the alpha beta tubulin dimer by electron crystallography. *Nature* **391**, 199-203.

North, B. J., Marshall, B. L., Borra, M. T., Denu, J. M. and Verdin, E. (2003). The human Sir2 ortholog, SIRT2, is an NAD⁺-dependent tubulin deacetylase. *Mol Cell* **11**, 437-44.

Oakley, C. E. and Oakley, B. R. (1989). Identification of gamma-tubulin, a new member of the tubulin superfamily encoded by mipA gene of *Aspergillus nidulans*. *Nature* **338**, 662-4.

Olmsted, J. B. (1981). Tubulin pools in differentiating neuroblastoma cells. *J Cell Biol* **89**, 418-23.

-
- Oosawa, F.** (1970). Size distribution of protein polymers. *J Theor Biol* **27**, 69-86.
- Oshima, R. G.** (2007). Intermediate filaments: A historical perspective. *Exp Cell Res* **313**, 1981-1994.
- Osoegawa, K., Tatenno, M., Woon, P. Y., Frengen, E., Mammoser, A. G., Catanese, J. J., Hayashizaki, Y. and de Jong, P. J.** (2000). Bacterial artificial chromosome libraries for mouse sequencing and functional analysis. *Genome Res* **10**, 116-28.
- Ovechkina, Y. and Wordeman, L.** (2003). Unconventional motoring: an overview of the Kin C and Kin I kinesins. *Traffic* **4**, 367-75.
- Palazzo, A. F., Joseph, H. L., Chen, Y. J., Dujardin, D. L., Alberts, A. S., Pfister, K. K., Vallee, R. B. and Gundersen, G. G.** (2001). Cdc42, dynein, and dynactin regulate MTOC reorientation independent of Rho-regulated microtubule stabilization. *Curr Biol* **11**, 1536-41.
- Panda, D., Miller, H. P., Banerjee, A., Luduena, R. F. and Wilson, L.** (1994). Microtubule dynamics in vitro are regulated by the tubulin isotype composition. *Proc Natl Acad Sci USA* **91**, 11358-62.
- Panda, D., Miller, H. P. and Wilson, L.** (2002). Determination of the Size and Chemical Nature of the Stabilizing "Cap" at Microtubule Ends Using Modulators of Polymerization Dynamics. *Biochemistry* **41**, 1609-1617.
- Pankov, R., Endo, Y., Even-Ram, S., Araki, M., Clark, K., Cukierman, E., Matsumoto, K. and Yamada, K. M.** (2005). A Rac switch regulates random versus directionally persistent cell migration. *J Cell Biol* **170**, 793-802.
- Peeters, P. J., Baker, A., Goris, I., Daneels, G., Verhasselt, P., Luyten, W. H., Geysen, J. J., Kass, S. U. and Moechars, D. W.** (2004). Sensory deficits in mice hypomorphic for a mammalian homologue of unc-53. *Brain Res Dev Brain Res* **150**, 89-101.
- Pereira, A. L., Pereira, A. J., Maia, A. R., Drabek, K., Sayas, C. L., Hergert, P. J., Lince-Faria, M., Matos, I., Duque, C., Stepanova, T. et al.** (2006). Mammalian CLASP1 and CLASP2 cooperate to ensure mitotic fidelity by regulating spindle and kinetochore function. *Mol Biol Cell* **17**, 4526-42.
- Perez, F., Diamantopoulos, G. S., Stalder, R. and Kreis, T. E.** (1999). CLIP-170 highlights growing microtubule ends in vivo. *Cell* **96**, 517-27.
- Peris, L., Thery, M., Faure, J., Saoudi, Y., Lafanechere, L., Chilton, J. K., Gordon-Weeks, P., Galjart, N., Bornens, M., Wordeman, L. et al.** (2006). Tubulin tyrosination is a major factor affecting the recruitment of CAP-Gly proteins at microtubule plus ends. *J Cell Biol* **174**, 839-49.
- Peters, R. A.** (1930). Surface structure in the integration of cell activity. *Trans. Faraday Soc.* **26**, 797-809.
- Phair, R. D. and Misteli, T.** (2000). High mobility of proteins in the mammalian cell nucleus. *Nature* **404**, 604-9.
- Pierre, P., Scheel, J., Rickard, J. E. and Kreis, T. E.** (1992). CLIP-170 links endocytic vesicles to microtubules. *Cell* **70**, 887-900.
- Piperno, G., LeDizet, M. and Chang, X. J.** (1987). Microtubules containing acetylated alpha-tubulin in mammalian cells in culture. *J Cell Biol* **104**, 289-302.

Pluta, M. (1994). Nomarski's DIC microscopy: a review. In *Phase Contrast and Differential Interference Contrast Imaging Techniques and Applications*, vol. 1846, pp. 10-25. SPIE.

Pollard, T. D. and Korn, E. D. (1973). Electron microscopic identification of actin associated with isolated amoeba plasma membranes. *J Biol Chem* **248**, 448-50.

Potma, E. O., de Boeij, W. P., Bosgraaf, L., Roelofs, J., van Haastert, P. J. and Wiersma, D. A. (2001). Reduced protein diffusion rate by cytoskeleton in vegetative and polarized dictyostelium cells. *Biophys J* **81**, 2010-9.

Prasher, D. C., Eckenrode, V. K., Ward, W. W., Prendergast, F. G. and Cormier, M. J. (1992). Primary structure of the *Aequorea victoria* green-fluorescent protein. *Gene* **111**, 229-33.

Qian, H. and Elson, E. L. (1990). Distribution of molecular aggregation by analysis of fluctuation moments. *Proc Natl Acad Sci USA* **87**, 5479-83.

Qian, H. and Elson, E. L. (1991). Analysis of confocal laser-microscope optics for 3-D fluorescence correlation spectroscopy. *Appl. Opt.* **30**, 1185.

Raynaud-Messina, B. and Merdes, A. (2007). Gamma-tubulin complexes and microtubule organization. *Curr Opin Cell Biol* **19**, 24-30.

Reed, N. A., Cai, D., Blasius, T. L., Jih, G. T., Meyhofer, E., Gaertig, J. and Verhey, K. J. (2006). Microtubule acetylation promotes kinesin-1 binding and transport. *Curr Biol* **16**, 2166-72.

Reits, E. A. and Neefjes, J. J. (2001). From fixed to FRAP: measuring protein mobility and activity in living cells. *Nat Cell Biol* **3**, E145-7.

Rickard, J. E. and Kreis, T. E. (1990). Identification of a novel nucleotide-sensitive microtubule-binding protein in HeLa cells. *J Cell Biol* **110**, 1623-33.

Rickard, J. E. and Kreis, T. E. (1991). Binding of pp170 to microtubules is regulated by phosphorylation. *J Biol Chem* **266**, 17597-605.

Riehemann, K. and Sorg, C. (1993). Sequence homologies between four cytoskeleton-associated proteins. *Trends Biochem Sci* **18**, 82-3.

Rigler, R., Mets, U., Widengren, J. and Kask, P. (1993). Fluorescence correlation spectroscopy with high count rates and low background, analysis of translational diffusion. *Eur Biophys J* **22**, 169-175.

Rogers, S. L., Rogers, G. C., Sharp, D. J. and Vale, R. D. (2002). *Drosophila* EB1 is important for proper assembly, dynamics, and positioning of the mitotic spindle. *J Cell Biol* **158**, 873-84.

Roper, K., Gregory, S. L. and Brown, N. H. (2002). The 'spectraplakins': cytoskeletal giants with characteristics of both spectrin and plakin families. *J Cell Sci* **115**, 4215-25.

Rozsa, G., Szent-Gyorgyi, A. and Wyckoff, R. W. G. (1950). The fine structure of myofibrils. *Exp Cell Res* **1**, 194-205.

Runge, M. S., Detrich, H. W., 3rd and Williams, R. C., Jr. (1979). Identification of the major 68,000-dalton protein of microtubule preparations as a 10-nm filament protein and its effects on microtubule assembly in vitro. *Biochemistry* **18**, 1689-98.

Sadegh Zadeh, K., Elman, H. C., Montas, H. J. and Shirmohammadi, A. (2007). A finite element model for protein transport in vivo. *Biomed Eng Online* **6**, 24.

Sage, D., Neumann, F. R., Hediger, F., Gasser, S. M. and Unser, M. (2005). Automatic tracking of individual fluorescence particles: Application to the study of chromosome dynamics. *Ieee Trans Image Process* **14**, 1372-1383.

Sammak, P. J. and Borisy, G. G. (1988). Direct observation of microtubule dynamics in living cells. *Nature* **332**, 724-6.

Samso, M. and Koonce, M. P. (2004). 25 Angstrom resolution structure of a cytoplasmic dynein motor reveals a seven-member planar ring. *J Mol Biol* **340**, 1059-72.

Sandblad, L., Busch, K. E., Tittmann, P., Gross, H., Brunner, D. and Hoenger, A. (2006). The Schizosaccharomyces pombe EB1 homolog Mal3p binds and stabilizes the microtubule lattice seam. *Cell* **127**, 1415-24.

Savage, C., Xue, Y., Mitani, S., Hall, D., Zakhary, R. and Chalfie, M. (1994). Mutations in the Caenorhabditis elegans beta-tubulin gene mec-7: effects on microtubule assembly and stability and on tubulin autoregulation. *J Cell Sci* **107 (Pt 8)**, 2165-75.

Saxton, W., Stemple, D., Leslie, R., Salmon, E., Zavortink, M. and McIntosh, J. (1984). Tubulin dynamics in cultured mammalian cells. *J. Cell Biol.* **99**, 2175-2186.

Sbalzarini, I. F. and Koumoutsakos, P. (2005). Feature point tracking and trajectory analysis for video imaging in cell biology. *J Struct Biol* **151**, 182-95.

Scheel, J., Pierre, P., Rickard, J. E., Diamantopoulos, G. S., Valetti, C., van der Goot, F. G., Haner, M., Aebi, U. and Kreis, T. E. (1999). Purification and analysis of authentic CLIP-170 and recombinant fragments. *J Biol Chem* **274**, 25883-91.

Schek, H. T., 3rd, Gardner, M. K., Cheng, J., Odde, D. J. and Hunt, A. J. (2007). Microtubule Assembly Dynamics at the Nanoscale. *Curr Biol*.

Schiebel, E. (2000). gamma-tubulin complexes: binding to the centrosome, regulation and microtubule nucleation. *Curr Opin Cell Biol* **12**, 113-8.

Schliwa, M. and van Blerkom, J. (1981). Structural interaction of cytoskeletal components. *The Journal of Cell Biology* **90**, 222-235.

Schmidt, W. J. (1939). Doppelbrechung der Kernspindel und Zugfasertheorie der Chromosomenbewegung *Chromosoma* **1**, 253-264

Schroeder, T. E. (1973). Actin in dividing cells: contractile ring filaments bind heavy meromyosin. *Proc Natl Acad Sci USA* **70**, 1688-92.

Schroer, T. A. (2004). Dynactin. *Annu Rev Cell Dev Biol* **20**, 759-79.

Schulze, E., Asai, D. J., Bulinski, J. C. and Kirschner, M. (1987). Posttranslational modification and microtubule stability. *J Cell Biol* **105**, 2167-77.

Schulze, E. and Kirschner, M. (1987). Dynamic and stable populations of microtubules in cells. *J. Cell Biol.* **104**, 277-288.

Schulze, E. and Kirschner, M. (1988). New features of microtubule behaviour observed in vivo. *Nature* **334**, 356-9.

Schuyler, S. C. and Pellman, D. (2001). Microtubule "plus-end-tracking proteins": The end is just the beginning. *Cell* **105**, 421-4.

Schwille, P., Meyer-Almes, F. J. and Rigler, R. (1997). Dual-color fluorescence cross-correlation spectroscopy for multicomponent diffusional analysis in solution. *Biophys J* **72**, 1878-86.

Seiffert, S. and Oppermann, W. (2005). Systematic evaluation of FRAP experiments performed in a confocal laser scanning microscope. *J Microsc* **220**, 20-30.

Seksek, O., Biwersi, J. and Verkman, A. S. (1997). Translational diffusion of macromolecule-sized solutes in cytoplasm and nucleus. *J Cell Biol* **138**, 131-42.

Sept, D., Baker, N. A. and McCammon, J. A. (2003). The physical basis of microtubule structure and stability. *Protein Sci* **12**, 2257-2261.

Serohijos, A. W., Chen, Y., Ding, F., Elston, T. C. and Dokholyan, N. V. (2006). A structural model reveals energy transduction in dynein. *Proc Natl Acad Sci USA* **103**, 18540-5.

Serrano, L., Diaz-Nido, J., Wandosell, F. and Avila, J. (1987). Tubulin phosphorylation by casein kinase II is similar to that found in vivo. *J Cell Biol* **105**, 1731-9.

Shaner, N. C., Campbell, R. E., Steinbach, P. A., Giepmans, B. N., Palmer, A. E. and Tsien, R. Y. (2004). Improved monomeric red, orange and yellow fluorescent proteins derived from *Discosoma* sp. red fluorescent protein. *Nat Biotechnol* **22**, 1567-72.

Sharp, D. J., Mennella, V. and Buster, D. W. (2005). KLP10A and KLP59C: the dynamic duo of microtubule depolymerization. *Cell Cycle* **4**, 1482-5.

Shcherbo, D., Merzlyak, E. M., Chepurnykh, T. V., Fradkov, A. F., Ermakova, G. V., Solovieva, E. A., Lukyanov, K. A., Bogdanova, E. A., Zarsisky, A. G., Lukyanov, S. et al. (2007). Bright far-red fluorescent protein for whole-body imaging. *Nat Methods* **4**, 741-6.

Shelanski, M. L., Gaskin, F. and Cantor, C. R. (1973). Microtubule assembly in the absence of added nucleotides. *Proc Natl Acad Sci USA* **70**, 765-8.

Shimomura, O., Johnson, F. H. and Saiga, Y. (1962). Extraction, purification and properties of aequorin, a bioluminescent protein from the luminous hydromedusa, *Aequorea*. *J Cell Comp Physiol* **59**, 223-39.

Silverstein, A. M. (2004). Labeled antigens and antibodies: the evolution of magic markers and magic bullets. *Nat Immunol* **5**, 1211-7.

Slep, K. C., Rogers, S. L., Elliott, S. L., Ohkura, H., Kolodziej, P. A. and Vale, R. D. (2005). Structural determinants for EB1-mediated recruitment of APC and spectraplakins to the microtubule plus end. *J Cell Biol* **168**, 587-98.

Slep, K. C. and Vale, R. D. (2007). Structural Basis of Microtubule Plus End Tracking by XMAP215, CLIP-170, and EB1. *Molecular Cell* **27**, 976-991.

Sloboda, R. D. and Rosenbaum, J. L. (1979). Decoration and stabilization of intact, smooth-walled microtubules with microtubule-associated proteins. *Biochemistry* **18**, 48-55.

Smal, I., Draegestein, K., Galjart, N., Niessen, W. and Meijering, E. (2007). Rao-Blackwellized marginal particle filtering for multiple object tracking in molecular bioimaging. *Inf Process Med Imaging* **20**, 110-21.

Smits, R., Kielman, M. F., Breukel, C., Zurcher, C., Neufeld, K., Jagmohan-Changur, S., Hofland, N., van Dijk, J., White, R., Edelmann, W. et al. (1999).

Apc1638T: a mouse model delineating critical domains of the adenomatous polyposis coli protein involved in tumorigenesis and development. *Genes Dev* **13**, 1309-21.

Song, Y. H. and Mandelkow, E. (1993). Recombinant kinesin motor domain binds to beta-tubulin and decorates microtubules with a B surface lattice. *Proc Natl Acad Sci USA* **90**, 1671-5.

Sonnenberg, A. and Liem, R. K. (2007). Plakins in development and disease. *Exp Cell Res* **313**, 2189-203.

Sprague, B. L., Pego, R. L., Stavreva, D. A. and McNally, J. G. (2004). Analysis of binding reactions by fluorescence recovery after photobleaching. *Biophys J* **86**, 3473-95.

Stein, P. A., Toret, C. P., Salic, A. N., Rolls, M. M. and Rapoport, T. A. (2002). A novel centrosome-associated protein with affinity for microtubules. *J Cell Sci* **115**, 3389-402.

Stepanova, T., Slemmer, J., Hoogenraad, C. C., Lansbergen, G., Dortland, B., De Zeeuw, C. I., Grosveld, F., van Cappellen, G., Akhmanova, A. and Galjart, N. (2003). Visualization of microtubule growth in cultured neurons via the use of EB3-GFP (end-binding protein 3-green fluorescent protein). *J Neurosci* **23**, 2655-64.

Strelkov, S. V., Herrmann, H. and Aebi, U. (2003). Molecular architecture of intermediate filaments. *Bioessays* **25**, 243-51.

Su, L. K., Burrell, M., Hill, D. E., Gyuris, J., Brent, R., Wiltshire, R., Trent, J., Vogelstein, B. and Kinzler, K. W. (1995). APC binds to the novel protein EB1. *Cancer Res* **55**, 2972-7.

Su, L. K. and Qi, Y. (2001). Characterization of human MAPRE genes and their proteins. *Genomics* **71**, 142-9.

Suzuki, K. and Koike, T. (2007). Mammalian Sir2-related protein (SIRT) 2-mediated modulation of resistance to axonal degeneration in slow Wallerian degeneration mice: a crucial role of tubulin deacetylation. *Neuroscience* **147**, 599-612.

Svedberg, T. and Inouye, K. (1911). Eine neue Methode zur Prufung der Gultigkeit des Boyle-Gay-Lussacschen Gesetzes fur Kolloide Losungen. *Z. Phys. Chem.* **77**, 145-190.

Swaminathan, R., Hoang, C. P. and Verkman, A. S. (1997). Photobleaching recovery and anisotropy decay of green fluorescent protein GFP-S65T in solution and cells: cytoplasmic viscosity probed by green fluorescent protein translational and rotational diffusion. *Biophys J* **72**, 1900-7.

Tanenbaum, M. E., Galjart, N., van Vugt, M. A. and Medema, R. H. (2006). CLIP-170 facilitates the formation of kinetochore-microtubule attachments. *Embo J* **25**, 45-57.

Thazhath, R., Liu, C. and Gaertig, J. (2002). Polyglycylation domain of beta-tubulin maintains axonemal architecture and affects cytokinesis in Tetrahymena. *Nat Cell Biol* **4**, 256-9.

Thompson, N. L. (1991). Fluorescence correlation spectroscopy. In *Topics in Fluorescence Spectroscopy*, (ed. J. R. Lakowicz), pp. 337-378: Plenum Press.

Thompson, N. L., Lieto, A. M. and Allen, N. W. (2002). Recent advances in fluorescence correlation spectroscopy. *Curr Opin Struct Biol* **12**, 634-41.

Tirnauer, J. S. and Bierer, B. E. (2000). EB1 Proteins Regulate Microtubule Dynamics, Cell Polarity, and Chromosome Stability. *J. Cell Biol.* **149**, 761-766.

Tirnauer, J. S., Grego, S., Salmon, E. D. and Mitchison, T. J. (2002). EB1-microtubule interactions in *Xenopus* egg extracts: role of EB1 in microtubule stabilization and mechanisms of targeting to microtubules. In *Mol Biol Cell*, vol. 13, pp. 3614-26.

Tran, A. D., Marmo, T. P., Salam, A. A., Che, S., Finkelstein, E., Kabarriti, R., Xenias, H. S., Mazitschek, R., Hubbert, C., Kawaguchi, Y. et al. (2007). HDAC6 deacetylation of tubulin modulates dynamics of cellular adhesions. *J Cell Sci* **120**, 1469-79.

Trichet, V., Ruault, M., Roizes, G. and De Sario, A. (2000). Characterization of the human tubulin tyrosine ligase-like 1 gene (TTLL1) mapping to 22q13.1. *Gene* **257**, 109-17.

Tsien, R. Y. (1998). The green fluorescent protein. *Annu Rev Biochem* **67**, 509-544.

Tsvetkov, A. S., Samsonov, A., Akhmanova, A., Galjart, N. and Popov, S. V. (2007). Microtubule-binding proteins CLASP1 and CLASP2 interact with actin filaments. *Cell Motil Cytoskeleton* **64**, 519-530.

Vale, R. D., Soll, D. R. and Gibbons, I. R. (1989). One-dimensional diffusion of microtubules bound to flagellar dynein. *Cell* **59**, 915-25.

van Buren, V., Odde, D. J. and Cassimeris, L. (2002). Estimates of lateral and longitudinal bond energies within the microtubule lattice. *Proc Natl Acad Sci USA* **99**, 6035-40.

van den Boom, V., Kooistra, S. M., Boesjes, M., Geverts, B., Houtsmuller, A. B., Monzen, K., Komuro, I., Essers, J., Drenth-Diephuis, L.J. and Eggen, B. J. (2007). UTF1 is a chromatin-associated protein involved in ES cell differentiation. *J Cell Biol* **26**, 437-48.

van Dijk, J., Rogowski, K., Miro, J., Lacroix, B., Edde, B. and Janke, C. (2007). A targeted multienzyme mechanism for selective microtubule polyglutamylation. *Mol Cell* **26**, 437-48.

Vaughan, K. T. (2004). Surfing, regulating and capturing: are all microtubule-tip-tracking proteins created equal? *Trends Cell Biol* **14**, 491-6.

Vaughan, K. T., Tynan, S. H., Faulkner, N. E., Echeverri, C. J. and Vallee, R. B. (1999). Colocalization of cytoplasmic dynein with dynactin and CLIP-170 at microtubule distal ends. *J Cell Sci* **112** (Pt 10), 1437-47.

Vaughan, P. S., Miura, P., Henderson, M., Byrne, B. and Vaughan, K. T. (2002). A role for regulated binding of p150(Glued) to microtubule plus ends in organelle transport. *J Cell Biol* **158**, 305-19.

Verhey, K. J. and Gaertig, J. (2007). The Tubulin Code. *Cell Cycle* **6**, 2152-60.

Visser, A. J. W. G. and Hink, M. A. (1999). New Perspectives of Fluorescence Correlation Spectroscopy. *J Fluoresc* **9**, 81-87.

von Hippel, P. H. and Berg, O. G. (1989). Facilitated target location in biological systems. *J Biol Chem* **264**, 675-8.

- Vukojevic, V., Pramanik, A., Yakovleva, T., Rigler, R., Terenius, L. and Bakalkin, G.** (2005). Study of molecular events in cells by fluorescence correlation spectroscopy. *Cell Mol Life Sci* **62**, 535-50.
- Wachsmuth, M., Weidemann, T., Muller, G., Hoffmann-Rohrer, U. W., Knoch, T. A., Waldeck, W. and Langowski, J.** (2003). Analyzing intracellular binding and diffusion with continuous fluorescence photobleaching. *Biophys J* **84**, 3353-63.
- Wang, H. W. and Nogales, E.** (2005). Nucleotide-dependent bending flexibility of tubulin regulates microtubule assembly. *Nature* **435**, 911-5.
- Wang, Z., Shah, J. V., Berns, M. W. and Cleveland, D. W.** (2006). In vivo quantitative studies of dynamic intracellular processes using fluorescence correlation spectroscopy. *Biophys J* **91**, 343-51.
- Waterman-Storer, C. M., Karki, S. B., Kuznetsov, S. A., Tabb, J. S., Weiss, D. G., Langford, G. M. and Holzbaur, E. L.** (1997). The interaction between cytoplasmic dynein and dynactin is required for fast axonal transport. *Proc Natl Acad Sci USA* **94**, 12180-5.
- Watson, P. and Stephens, D. J.** (2006). Microtubule plus-end loading of p150(Glued) is mediated by EB1 and CLIP-170 but is not required for intracellular membrane traffic in mammalian cells. *J Cell Sci* **119**, 2758-67.
- Weidemann, T., Wachsmuth, M., Tewes, M., Rippe, K. and Langowski, J.** (2002). Analysis of Ligand Binding by Two-Colour Fluorescence Cross-Correlation Spectroscopy. **3**, 49-61.
- Weisbrich, A., Honnappa, S., Jaussi, R., Okhrimenko, O., Frey, D., Jelesarov, I., Akhmanova, A. and Steinmetz, M. O.** (2007). Structure-function relationship of CAP-Gly domains. *Nat Struct Mol Biol* **14**, 959-67.
- Weisenberg, R. C.** (1972). Microtubule formation in vitro in solutions containing low calcium concentrations. *Science* **177**, 1104-5.
- Weiss, M.** (2004). Challenges and artifacts in quantitative photobleaching experiments. *Traffic* **5**, 662-71.
- Welte, M. A.** (2004). Bidirectional Transport along Microtubules. *Curr Biol* **14**, R525-37.
- Wen, Y., Eng, C. H., Schmoranzler, J., Cabrera-Poch, N., Morris, E. J., Chen, M., Wallar, B. J., Alberts, A. S. and Gundersen, G. G.** (2004). EB1 and APC bind to mDia to stabilize microtubules downstream of Rho and promote cell migration. *Nat Cell Biol* **6**, 820-30.
- Westermann, S. and Weber, K.** (2003). Post-translational modifications regulate microtubule function. *Nat Rev Mol Cell Biol* **4**, 938-47.
- Whipple, R. A., Cheung, A. M. and Martin, S. S.** (2007). Detyrosinated microtubule protrusions in suspended mammary epithelial cells promote reattachment. *Exp Cell Res* **313**, 1326-36.
- Widengren, J., Mets, U. and Rigler, R.** (1995). Fluorescence correlation spectroscopy of triplet states in solution: a theoretical and experimental study. *J Phys Chem* **99**, 13368-13379.
- Widengren, J., Mets, U. and Rigler, R.** (1999). Photodynamic properties of green fluorescent proteins investigated by fluorescence correlation spectroscopy. *Chem Phys* **250**, 171-186.

- Winder, S. J. and Ayscough, K. R.** (2005). Actin-binding proteins. *J Cell Sci* **118**, 651-654.
- Wittmann, T. and Waterman-Storer, C. M.** (2005). Spatial regulation of CLASP affinity for microtubules by Rac1 and GSK3beta in migrating epithelial cells. *J Cell Biol* **169**, 929-39.
- Wood, J. D., Landers, J. A., Bingley, M., McDermott, C. J., Thomas-McArthur, V., Gleadall, L. J., Shaw, P. J. and Cunliffe, V. T.** (2006). The microtubule-severing protein Spastin is essential for axon outgrowth in the zebrafish embryo. *Hum Mol Genet* **15**, 2763-71.
- Wordeman, L.** (2005). Microtubule-depolymerizing kinesins. *Curr Opin Cell Biol* **17**, 82-88.
- Wozniak, M. J., Milner, R. and Allan, V.** (2004). N-terminal kinesins: many and various. *Traffic* **5**, 400-10.
- Wu, X., Bowers, B., Rao, K., Wei, Q. and Hammer, J. A., 3rd.** (1998). Visualization of melanosome dynamics within wild-type and dilute melanocytes suggests a paradigm for myosin V function In vivo. *J Cell Biol* **143**, 1899-918.
- Wu, X. S., Tsan, G. L. and Hammer, J. A., 3rd.** (2005). Melanophilin and myosin Va track the microtubule plus end on EB1. *J Cell Biol* **171**, 201-7.
- Xouri, G., Squire, A., Dimaki, M., Geverts, B., Verveer, P. J., Taraviras, S., Nishitani, H., Houtsmuller, A. B., Bastiaens, P. I. and Lygerou, Z.** (2007). Cdt1 associates dynamically with chromatin throughout G1 and recruits Geminin onto chromatin. *EMBO J* **26**, 1303-14.
- Yan, X., Habedanck, R. and Nigg, E. A.** (2006). A complex of two centrosomal proteins, CAP350 and FOP, cooperates with EB1 in microtubule anchoring. *Mol Biol Cell* **17**, 634-44.
- Yang, T. T., Cheng, L. and Kain, S. R.** (1996). Optimized codon usage and chromophore mutations provide enhanced sensitivity with the green fluorescent protein. *Nucleic Acids Res* **24**, 4592-3.
- Yin, H., You, L., Pasqualone, D., Kopski, K. M. and Huffaker, T. C.** (2002). Stu1p is physically associated with beta-tubulin and is required for structural integrity of the mitotic spindle. *Mol Biol Cell* **13**, 1881-92.
- Yvon, A. M., Wadsworth, P. and Jordan, M. A.** (1999). Taxol suppresses dynamics of individual microtubules in living human tumor cells. *Mol Biol Cell* **10**, 947-59.
- Zhang, D., Rogers, G. C., Buster, D. W. and Sharp, D. J.** (2007). Three microtubule severing enzymes contribute to the "Pacman-flux" machinery that moves chromosomes. *J Cell Biol* **177**, 231-42.
- Zhang, J., Li, S., Fischer, R. and Xiang, X.** (2003a). Accumulation of cytoplasmic dynein and dynactin at microtubule plus ends in *Aspergillus nidulans* is kinesin dependent. *Mol Biol Cell* **14**, 1479-88.
- Zhang, Y., Li, N., Caron, C., Matthias, G., Hess, D., Khochbin, S. and Matthias, P.** (2003b). HDAC-6 interacts with and deacetylates tubulin and microtubules in vivo. *Embo J* **22**, 1168-79.
- Zhou, F. Q., Zhou, J., Dedhar, S., Wu, Y. H. and Snider, W. D.** (2004). NGF-induced axon growth is mediated by localized inactivation of GSK-3beta and functions of the microtubule plus end binding protein APC. *Neuron* **42**, 897-912.

Curriculum vitae

Name: Katharina Asja Drägestein

Date of birth: 27 May 1978

Place of birth: Berlin, Germany

Education

1996-2002: Biochemistry (Dipl.)
University of Hannover, Germany

2002: thesis project "Interaction Partners of the Y-box protein YB1"
Max-Delbrück-Zentrum (MDC), Berlin-Buch, Germany, group of
Prof. Dörken

2004-2007: ErasmusMC, Rotterdam, The Netherlands
Department of Cell Biology, Ph.D. program
Supervisors: Dr. N. Galjart and Prof. Dr. F. Grosveld

Publications

Drabek, K., van Ham, M., Stepanova, T., **Draegestein, K.**, van Horssen, R., Sayas, C. L., Akhmanova, A., Ten Hagen, T., Smits, R., Fodde, R., Grosveld, F. and Galjart, N. Role of CLASP2 in microtubule stabilization and the regulation of persistent motility. (2006) *Curr Biol* 16, 2259-64.

Smal, I., **Draegestein, K.**, Galjart, N., Niessen, W., and Meijering, E. Rao-Blackwellized Marginal Particle Filtering for Multiple Object Tracking in Molecular Bioimaging. *Information Processing in Medical Imaging - IPMI 2007* (Kerkrade, The Netherlands, July 2-6, 2007), N. Karssenmeijer and B. Lelieveldt (eds.), *Lecture Notes in Computer Science*, vol. 4584, Springer-Verlag, Berlin, 2007, pp. 110-121.

Smal, I., **Draegestein, K.**, Galjart, N., Niessen, W., and Meijering, E. Particle Filtering for Multiple Object Tracking in Dynamic Fluorescence Microscopy Images: Application to Microtubule Growth Analysis. *IEEE Transaction on Medical Imaging*, to appear

Dragestein, K. A., van Cappellen, W. A., van Haren, J., Tsibidis, G. D., Akhmanova, A., Knoch, T. A., Grosveld, F. and Galjart, N. Dynamic Behavior of GFP-CLIP-170 Reveals Fast Protein Turnover on Microtubule Plus-Ends. (2008) *J Cell Biol*, in press

Dankwoord

Beste Niels... je zag het ruim 4 jaar geleden wel zitten om met mij in zee te gaan. Dank je wel voor je vertrouwen in mij en de vrijheden die ik had! Ik heb er iedere keer weer van genoten om samen lekker te discussiëren, en theorieën te ontwikkelen, torpederen, verwerpen, bevestigen, veranderen,... De poetsvrouw zal nooit vergeten dat het “Katha’s klokje” is... en ik zal nooit vergeten dat jij wist hoe belangrijk dat klokje voor me was. Nu dat ik weg ben krijgt je neus ook weer rust, zonder “vieze thee”.

De grote vraag van de dinsdag middag was “Is er werkbespreking bij Frank?” en “Heeft al iemand gebeld?”. Jammer genoeg was de antwoord op de eerste vraag niet altijd “Ja!”, want het informele inter-groeps-gesprek bij jou op de bank was iedere keer weer gezellig en nuttig. Je hebt een ontzettend talent om door te blijven vragen – waardoor zelfs mijn eigen onderzoek voor mij vaak (nog) duidelijker werd. Ik zal je whiteboard-tafel met ingebouwde lamp gaan missen... en nooit te weten komen wat CLASP in de longontwikkeling doet of dat eigenlijk wel zo belangrijk is. Dank je wel dat je ff mijn secretaresse was.

Ik weet nog hoe ik voor het eerst het lab binnen kwam om met Niels te praten... het voelde gewoon goed... niet “jeder gegen jeden” maar “samen zijn we sterker”... Bedankt lab 710/1030 voor de teamspirit, de zoetheit tijdens de werkbesprekingen, de internationale snoepjes, de “Wednesday Dutch Day” with the “bouwvakkersdecolleté”, de vrijdag-middag muziek keuze,...

Jeff, mijn “drugsmaatje” (dank je wel, Frank) – kunnen de DE-dames er tegen dat het niet meer “een Heavenly Hazel, en een Mellow Morning” is? Dank je wel voor al het meedenken, kloneren, verbeteren, samen resultaten bespreken... gewoon ervoor dat jij jij bent! Ik ben blij, dat jij mijn paranymf wilt zijn. Als jouw tijd er aan zit te komen weet je me wel te vinden!

Keys - je “gekke vijf minuten” hebben me vaak van binnen laten grijnsen. Wat gaat er met het lab1030-video gebeuren als jij er niet meer bent? Het kan alleen maar slechter worden...

Ksenia – you rather looked at the “bigger picture” (=mouse), I preferred the details (=microscope), but we complemented one another well. Thanks for the opportunity to join the CLASP-project.

Ik zou zo door kunnen gaan en nog een heel boekje met “dank jullie wel’etjes” kunnen vullen, maar voordat dat af zou komen zijn jullie al lang met pensioen. Dus in het kort: Suz – dank je wel voor onderdak voor de gestrande reizigster, Marja – bedankt voor je uitleg in het begin, Marco – altijd vrolijk en helpend, Helen – so quiet, but still waters run deep, Michael – met het nieuwste surf-video van de Maasvlakte, Ana – who listens patiently to all my rabbit-stories, Laura – thanks for all advice and the “Spanish sunshine” you spread in the lab, Nanda – je was een “wandelande protocol-database” en hebt heel veel stilte achter gelaten toen je naar boven verhuizde, en alle anderen – dank jullie wel ervoor dat jullie zo zijn als jullie zijn.

De uren achter de mic die dit boekje pas mogelijk hebben gemaakt dreigden vaak frustratie te worden omdat iets het weer eens niet deed – maar dan was er gelukkig het belletje naar Gert die bijna altijd een oplossing op afstand wist te bedenken (of zo snel mogelijk langskwam om het te fixen). Ik zal het missen om bij

jou het kantoor binnen te lopen om het over experimenten, resultaten of “god en de wereld” te hebben.

Marieke en Jasperina, jullie zijn de beste secretaresses die er zijn. Dankj je wel Marieke voor je geduld met mijn chaos. Als een bestelling mis dreigde te lopen was “ff Melle bellen” vaak al voldoende om het alsnog te regelen. Zonder de dames uit de spoelkeuken zouden heel wat metro-ritten saaier zijn geweest, en zonder de “computer-guys” waren we nog steeds alle data kwijt. Gelukkig – ik hoefte het niet zonder jullie te doen.

Wat is een lab-leven dat alleen maar om en op het lab draait... Lieve familie van Jeff, het was gezellig op de “Privé-camping in Tiel”... En zonder de sneeuwstorm op Terschelling met Jan Jos was het een boekje zonder cover geworden...

Heel soms kom je mensen tegen met wie het gewoon meteen “klikt” en dan hoef je niet meer veel te zeggen om elkaar te begrijpen. Martijn, ik ben blij dat wij het microscoop-hok, de literatuurbesprekingen en de liefde voor konijnen hebben gedeeld – en ik verheug me erop samen met jou te promoveren.

D&D’ers... samen te hakken, de onbekende wereld van “de sok” te ontdekken, met planken de beesten uit de lucht te slaan... gelukkig had ik niet alleen het promotie-avontuur te beleven.

Poot van de Rainy en likje van de zwarte duivel – Lies en Floor, ik heb weer meer tijd voor jullie!

Marije, Carla, Renske en de anderen – bedankt voor het meedenken!

Ohne Euch stünde ich nicht wo ich heute stehe. Ich bin so froh, dass ich damals keine Fahrkarte zum Mond gekauft habe. Evi und Papi – Danke für alles! Lesterschwein – ich lieb dich trotzdem immer.

Schat... als ik jou niet had en de grote aardappelen, dan moest ik altijd de kleine eten. Dank je, dat je me zo goed “gevoerd” hebt.

Last but not least... bedankt lieve NS voor de stremmingen die het mij de afgelopen jaren mogelijk hebben gemaakt om tussen Leiden en Rotterdam door half Nederland te reizen – ik zal het niet missen.

